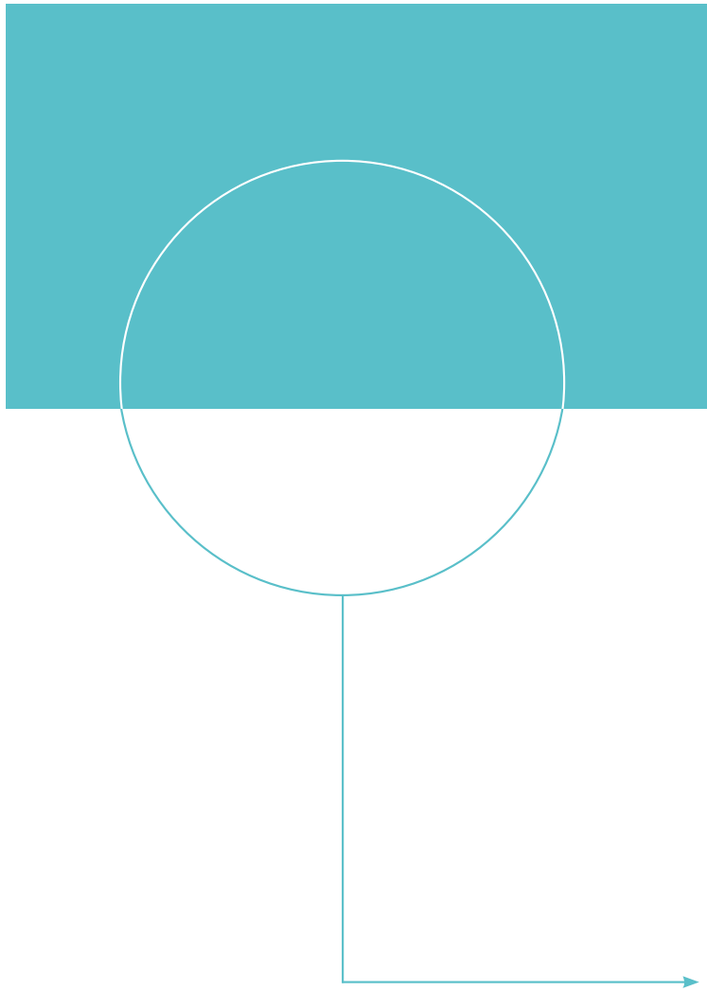

Master's thesis

2022

Ida Svendsen

NTNU
Norwegian University of
Science and Technology
Faculty of Engineering
Department of Civil and Environmental Engineering

Ida Svendsen

Tailings Dam Monitoring and the Prediction of Tailings Dam Failures

An Investigation of Tailings Dam Monitoring and an Early Warning Approach Towards Tailings Dam Failures

February 2022

NTNU
Norwegian University of
Science and Technology

NTNU
Norwegian University of
Science and Technology

NTNU
Norwegian University of
Science and Technology

Tailings Dam Monitoring and the Prediction of Tailings Dam Failures

An Investigation of Tailings Dam Monitoring and an Early Warning Approach Towards Tailings Dam Failures

Ida Svendsen

Geotechnics and Geohazards
Submission date: February 2022
Supervisor: Steinar Nordal (NTNU)
Co-supervisor: Luca Piciullo (NGI) Malte Vøge (NGI)

Norwegian University of Science and Technology
Department of Civil and Environmental Engineering

Abstract

Waste materials produced by mining activities (tailings) can be collected in artificial ponds delimited by earth embankments (tailings dams). In case of tailings dam failure, the consequences are often catastrophic for the surrounding communities and livelihoods as this rupture may release large amounts of tailings and mining wastewater that moves downstream. Furthermore, the mining by-products cause, in many cases, a devastating impact on the surrounding environments and ecosystem. As an increased trend of tailing dam failure has been observed in the last decade, there is an urgent demand from the industry as well as the civil society and the investor community to gain a broader understanding of the risks posed by tailing facilities. Furthermore, efficient techniques to monitor and predict the failure of tailing dams are also crucial.

This study investigates how the satellite remote sensing interferometric synthetic aperture radar (InSAR) technique can be used to monitor tailings dams and the applicability of the inverse velocity method to predict failures. InSAR data have been used to map surface displacement in two case studies: the Feijao tailings dam in Brazil and the Cadia tailings dam in Australia. In the case of the Feijao dam, both the Small Baseline and Persistent Scatter techniques were applied to process displacement time-series from the satellite data. For the Cadia dam, data processing was carried out using the SqueeSAR algorithm.

The inverse velocity method uses surface displacement measurement points to predict a time of failure. For the Feijao dam InSAR dataset, the inverse velocity method was applicable to different periods presenting an evident increase in the displacement rate. However, it was difficult to retrieve any reliable indication of failure. Contrary to the Feijao dam, the results from the Cadia dam shows a significantly accelerating deformation with time, and by applying the inverse velocity method a predicted time of failure can be retrieved in good agreement with the actual one.

Preface

The master thesis is written as a part of the two-year master's degree program in Geotechnics and Geohazards at the Norwegian University of Science and Technology (NTNU). Completing the masters-program results in a Master of Science in Engineering from the Faculty of Engineering. The thesis has been carried out in cooperation with the Norwegian Geotechnical Institute (NGI), and their support has been outstanding.

The thesis is written entirely by myself with support from supervisors and family. Furthermore, it completes my long path of studies that started with a degree in Peace- and Conflict Studies ten years ago and awoke a continuously interest for geohazards and how to prevent those from happening.

The thesis has given me insight to a man-made hazard I knew little about from before. It has been extremely interesting, and I have enjoyed the learning process all the way. This has certainly increased my knowledge in several fields that I will bring with me in my professional life.

Several people have helped me in the process of writing and improving my thesis. A special thanks goes to Steinar Nordal (NTNU) that has provided me with wise and mind-opening questions and comments. I am very thankful to Luca Piciullo at NGI that gave me the research topic and guided me all the way by continuously following up my process and results. I also want to express my thankfulness towards Malte Vöge at NGI who in several occasions used time to explain and discuss the numerical analysis of my study. Finally, I am most thankful to my husband and my two children that stood by me during the last six months and supported me even though I have been working full-time and dedicated most of my spare-time to the thesis.

Table of Contents

List of Figures

List of Tables

List of Equations

List of Abbreviations

BHP	Broken Hill Proprietary Company Limited
c-LMA	Long-term Moving Average
c-SMA	Short-term Moving Average
EOA	End of Acceleration
ESA	European Space Agency
InSAR	Interferometry Synthetic Aperture Radar
ICOLD	The International Commission on Large Dams
LOS	Line-of-Sight
NASA	National Aeronautics and Space Administration
NTNU	Norwegian University of Science and Technology
NGI	Norwegian Geotechnical Institute
NVE	Norwegian Water Resources and Energy Directorate
OOA	Onset of Acceleration
PS	Persistent Scatter
QGIS	Quantum Geographic Information System
SAR	Synthetic Aperture Radar
SBAS	Small Baseline and Subset
UNEP	United Nations Environment Programme
US EPA	United States Environmental Protection Agency

1 Introduction

For the last decades, the incidents of tailings dams failure have increased significantly. Tailings dams failure often has catastrophic consequences for the surrounding communities and livelihoods as its rupture may release large amounts of mining wastewater that moves downstream. Furthermore, the mining by-products do in many cases, cause a devastating impact on the surrounding environments and ecosystem. Tailing dams failure will continue to occur in the near future. There is an urgent demand from the industry, civil society, and investor communities to understand how to reduce the risk posed by tailings dams failures (Armstrong et al., 2019; Owen et al., 2020; Rico et al., 2008).

To avoid devastating consequences of tailings dams failures, the monitoring of tailings dams is crucial. However, traditional monitoring methods have in several cases shown to be faulty (Grebby et al., 2021). Tailings dams consist of large geotechnical structures and traditional point-based monitoring techniques will only monitor parameters in a specific section of the dam. Therefore, these techniques may not record the overall movement of a dam. In 2019, the lack of reliable monitoring resulted in the disastrous failure of Córrego do Feijão tailings dam where over 250 people died. The ground measurement did not record any signs of instability or anomalies (Robertson et al., 2019), thus there were no warnings on the upcoming failure.

To secure the monitoring of tailings dams, satellite data has in recent years been incorporated in tailings dam monitoring to detect potential deformation. With the ability to monitor ground deformation over large areas, the Interferometry Synthetic Aperture Radar (InSAR) technique has shown to be a complementary tool to the traditional in-situ monitoring instruments. Additionally, the InSAR technique is frequently used within the slope stability community when performing early warning analysis of unstable slopes. Based on this, it is of interest to understand if the InSAR might be used for an early warning system in tailings dams as well. The inverse velocity method is a well-known tool to predict slope failures where relatively slow deformation occurs. The inverse velocity method uses surface displacement over time to calculate surface displacement velocity, and the inverse velocity is then applied to estimate an eventual failure. As the method is time-dependent it will not register a sudden collapse of a tailings dam. Tailings dams vary significantly in their characteristics and behave unpredictably compared to natural slopes, thus the method is still being tested to understand its usefulness.

Some authors (Gama et al., 2020; Grebby et al., 2021; Thomas et al, 2019; Voge et al., 2021) have applied the inverse velocity method in well-known tailings dam failure cases and showed significant results, but little effort has been put into understanding how the method applies to periods of no failure or during cyclic behavior of a tailings dam. This calls for a widened understanding of how the method applies on tailings dams that presenting periods of increased displacement even though a failure did not occur. A better understanding of how the inverse velocity method applies in tailings dam context might contribute to reduce the risk of future failures.

1.1 Research question

This study investigates how the inverse velocity method monitors and predicts tailings dam failures. The data used for the inverse velocity method was collected with the InSAR technique, which provides information about the ground deformation direction and rate. The following questions will guide the research:

1. *Is the Inverse Velocity Method, based on InSAR data, reliable for predicting Tailings dam failure?*

   1.1 How can the Inverse Velocity method be applied to predict Tailings dams failure?
   1.3 What are the limitations of the Inverse Velocity Method when using SAR data?

1.2 Contributors

The research questions were through discussions established with the support of the supervisors. The elaboration of the introduction and background was done through a literature review by the author, where the supervisors contributed with input on relevant literature. Based on the collaboration with, and contribution from Norwegian Geotechnical Institute (NGI), it was possible to select relevant case studies for this research. NGI provided Synthetic Aperture Radar (SAR) data for the potential case studies and discussed which case studies would be most appropriate for this study. The images processed with InSAR methods were in the first case study realized by NGI, and shared with the author. For the second case study, the company TRE Altamira did the data processing, and the InSAR data was shared with NGI and then with the author.

1.3 Limitations

There are some limitations to the study. First of all, the author could potentially have processed the InSAR data herself. However, due to the limited amount of time and limited access to current software, this data was provided by NGI. Secondly, supplementing the case used in this study with an additional one containing a dam that has not yet failed could have been relevant. Due to limited access to data this was not possible. Thirdly, the method used for this study, presented by Carla et al. (2017a) in *"Guidelines on the use of inverse velocity method as a tool for setting alarm thresholds and forecasting landslides and structure collapses.",* contains an alternative equation for filtering the data namely the exponential smoothing function, that is not taken into usage. The moving average equation taken into use demonstrates satisfactory results and is therefore considered good enough for the aim of this study. Finally, one could also question if another approach towards the inverse velocity method could be more relevant. After the literature research and dialog with supervisors, there was an agreement that the method presented by Carla et al. (2017a) was most appropriate for this study.

.

1.4 Structure

The thesis is divided into six chapters.

The first chapter is the introduction and research question.

The second chapter consists of an introduction to tailings dams and tailing dams failure. The chapter also touches upon the theoretical background of SAR and the inverse velocity method.

The third chapter explains the method used to gather and process the data in each case study.

The fourth chapter presents the case studies and the results for each case study.

Chapter five discusses the results, how they answer the research question, and limitations and benefits to the method.

The last chapter covers concluding remarks and suggestions for further research.

2 Background and theory

This first part of this chapter aims to give a general overview of tailings dams, their expansion worldwide, the construction types, and the tailings composition. Further on, the chapter explains different causes of tailings dams failure. The second part of the chapter introduces the monitoring of tailings dams and the theoretical aspects of the remote synthetic apparatus radar (SAR) and the InSAR technique. Finally, the chapter touch upon the theoretical aspects of the inverse velocity method.

2.1 Tailings dams

Tailings dams are large structures where the waste material generated through mining operations is stored. The waste material is often referred to as tailings and is defined as "a common by-product of the process of extracting valuable minerals and metals from mined ore" (Global Tailings Review, 2022) (UNEP, 2017).

There are several steps taken when mining ore and afterwards storing the residuals. First, the mined rock is processed to separate the minerals and the metals (step 1, figure 1). Then the rock is finely crushed and blended with water and needed chemicals to separate the minerals and metals from the rest (step 2, figure 1). After separating the minerals from the crushed rock, the remaining waste are tailings (step 3, figure 1). The tailings are processed and stored as dry or wet material. Thus, the storage of wet tailings is within a tailings dam facility (step 4, figure 1) (Global Tailings Review, 2020).

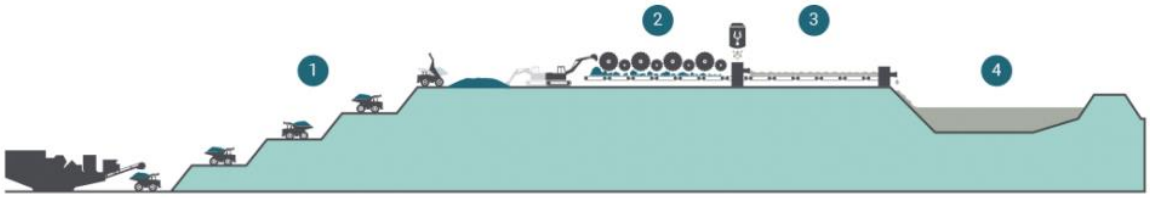

Figure 1: The process of retrieving minerals or metals from tailings (Global Tailings Review, 2022).

According to the Global Tailings Portal[1], as many as 1862 tailings dams exist worldwide, located at 761 different mine sites, and owned by 106 different mining companies. Figure 2 demonstrates the global distribution of the tailings dams.

[1] "The Global Tailings Portal, launched in January 2020, is a free, searchable database with detailed information on more than 1,800 mine tailings dams around the world." (Global Tailings Portal, 2019).

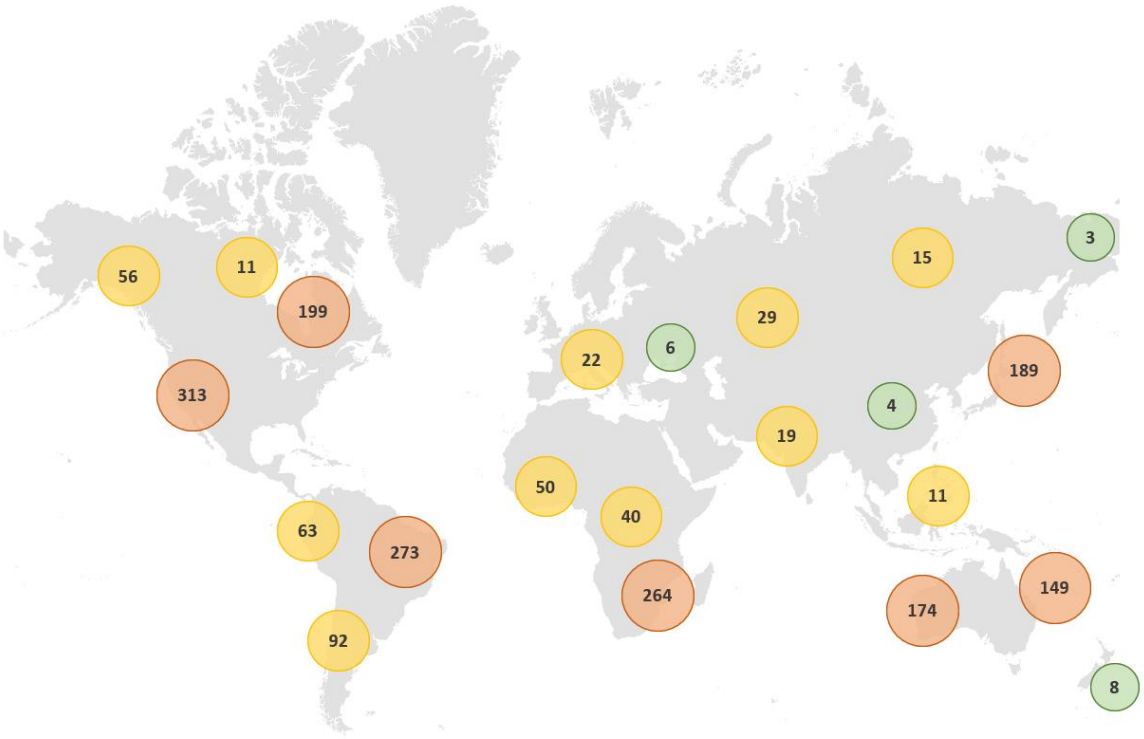

Figure 2: Global distribution of tailings storage facilities, modified from Global Tailings Portal (2019).

The largest amount of tailings dam is in the western and south-western parts of the United States and the eastern part of Canada. Furthermore, the northern part of Brazil and the southern part of Africa also account for numerous tailings dams. The western part of Australia and Japan also present a high number of tailings dams facilities.

2.1.1 Tailings dam design

Identifying the most proper design for a tailings dam depends on multiple factors such as the type of the mined mineral, the topography, the amount of precipitation, seismic activity, and the geographical location of the mining (Global Tailings Review, 2020; Owen et al., 2020).

During the construction of the tailings dam, locally available materials such as waste rock and the proper tailings are often used (Kossof et al., 2014). When constructing a tailings dam, there are three main designs: the upstream, downstream, and centerline designs (BHP, 2019). The name refers to which direction the embankment crest moves in relation to the starter dam. During the dam construction, several raises construct the embankment wall that secures the tailings.

For the upstream dam construction, the new parts of the tailings dam, also called embankment, are built on top of each other in an upstream direction. Initially, the construction builds a starter dam, and then the tailings are stored in the facility. The new section rests on the tailings impounded in the previous stage. In general, this type of construction uses much time since the tailings have to dry and stabilize before raising the next step of the embankment. The upstream dam construction is the most popular embankment construction for tailings dam as it has a much lower cost than the other methods (small amount of building material required). However, the upstream dam is

considered the most insecure way of constructing the embankment. The water level within the tailing dam often becomes critical and might cause piping (further explained in chapter 2.2.1). Piping might cause implications to the dam stability (BHP, 2019; Kossof et al., 2014; WISE Uranium, 2022). Figure 3 illustrate a simplified figure of the upstream method.

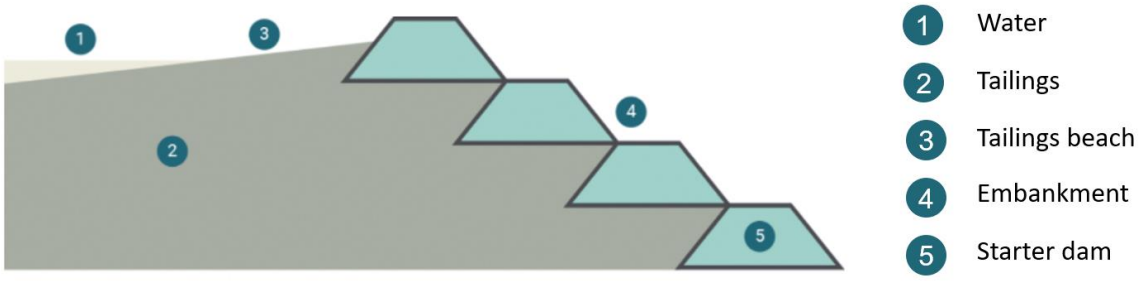

Figure 3: Upstream tailings dam construction (Global Tailings Review, 2020).

The downstream construction builds in a downstream direction. The construction begins with a starter dam, and each new embankment raises on the top of the downstream slope of the previous section. After building the starter dam, tailings are discharged into the dam. The upstream starter dam and embankments have an impervious layer in the upstream direction. This design is considered much safer in terms of slope stability than the upstream design. The downstream dam was designed for areas with seismic activity and a large amount of precipitation. (BHP, 2019; Global Tailings Review, 2020). Figure 4 illustrate a simplified figure of the upstream method.

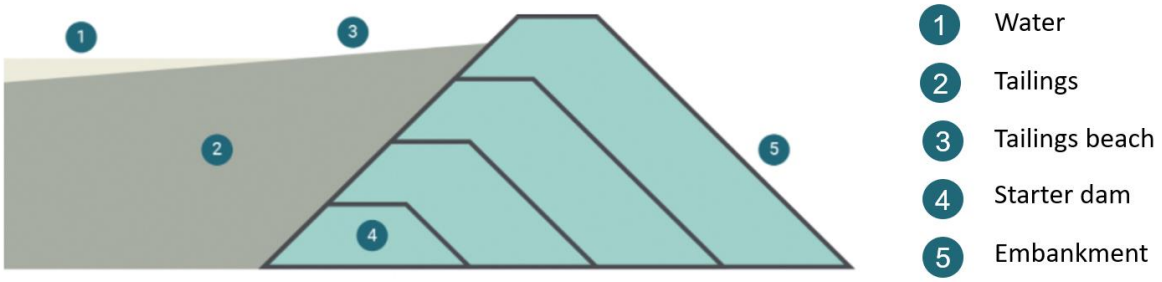

Figure 4: Downstream tailings dam construction (Global Tailings Review, 2020)

The centerline construction is a combination of the downstream and the upstream design. In some cases, internal drainage improves stability by reducing the hydraulic gradient. The dam is constructed vertically from the starter dam, and the dam crest always continues in the same position (Global Tailings Review, 2020). Figure 5 illustrate a simplified figure of the upstream method.

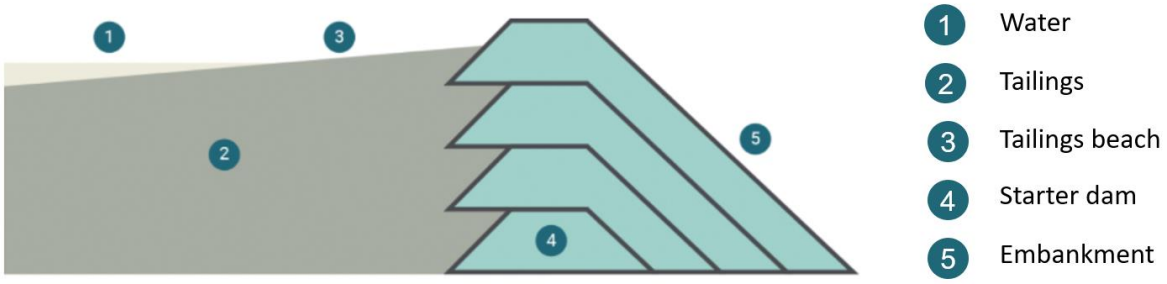

Figure 5: Centerline tailings dam construction (Global Tailings Review, 2020).

Additionally to the three dam designs mentioned above, other types of methods are used to store tailings for smaller tailings dams. Those methods includes single-stage dams that are raised in one stage. In-pit storage refers to backfilling an open pit that is not in use anymore. Dry stack storage consists of placing the dry stack in a location it can be spread out and compacted. This is done after filtering the waste material, though the water content is very low (Twin Metal, 2022)

From the 1862 tailings dams identified at the Global Tailings Portal, table 1 shows the distribution of the different designs. The table shows that the upstream method accounts for most of the constructions.

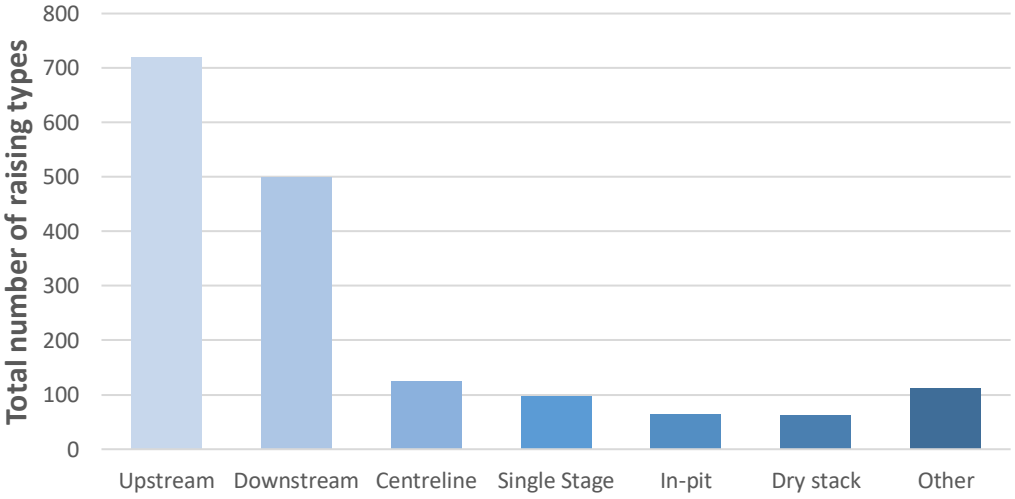

Table 1: Global distribution of tailings dam construction (Global Tailings Portal, 2019).

2.1.2 Tailings dam residuals

Tailing dams differ from other dams, such as embankment dams where water is stored, as they contain waste and residues from mining activities. The waste material stored in a tailings dam might be solid or liquid, thus as a combination, it becomes a slurry substance (BHP, 2019; ICOLD, 2001). Tailings often consist of granular and unsaturated material. The density might differ from loose to dense, which depends on the void ratio, or in other words, the ratio of the volume of space between the soil particles and the volume of soil (Jeffries et al., 2019). When saturated, tailings might leave the particles suspended in water and obtain a fluid behavior that easily flows out at large distances (EPA, 1994).

The tailings properties vary significantly and depend on several factors such as the moister content, the processing method, and the properties and mineralogy of the mined material

(UNEP, 2017). Some of the most hazardous waste types present in tailings dams are sulfide, heavy metals (containing arsenic, chromium, cadmium, cobalt, copper, and others), cyanide, radioactive, phosphate, and bitumen. These hazardous materials are of significant concern as the hazardous substances might cause catastrophic consequences to the surrounding nature and environments. Many large environmental disasters have occurred due to tailings dam spillage and failure. An example of this is the Mount Polley mine in Canada that released 25 million cubic meters into a river lying close by. Another case is the Catoca mine in Angola that breached in July 2021, leading to massive spill in the rivers nearby and polluting drinking water in downstream communities. The main reason for pollution is often related to tailings dam failure, leakage, or seepage (Rana et al., 2021; UNEP, 2017, Wise Uranium, 2021). However, the contamination might also happen through the air. An example is the tailings of aluminum extraction, also called red mud, containing small particles ranging between 2 to 200 micra's. When released to the environment, one of the primary sources of pollution is dry material during the filtering process that blows with the wind to all open surfaces around the tailings storage facility (Indian Minister of Environment Forest and Climate Change, 2021).

This study does not aim to give a comprehensive overview of all chemical residuals that the tailing releases; however, there are two particular aspects worth mentioning. Firstly, as modern society demands an increased amount of minerals and metals to produce goods, ore extraction has increased significantly during the last two decades. The extraction has resulted in a significant decrease in the ore grade[2]. The ore grade has decreased by 25 percent in 10 years (Calvo et al., 2016). This raises concern as the continuous demand for minerals and metals results in mineral deposits with lower ore grades, and consequently the tailing waste increases (Bowker & Chambers, 2016; Calvo et al., 2016; Kossof et al., 2014; Owen et al., 2020; UNEP, 2016)

Secondly, the chemical and physical properties of the tailings will vary during the life cycle of a tailings dam. The chemical properties might change over time and generate different compounds or chemical compositions. One example is Sulphide waste, where the oxidation of the residue will form acid sulfate-rich drainage. The operator should know about the long-term consequences of the tailings; however, unexpected consequences might also appear. An example is the Córrego do Feijão iron ore dam, which caused one of history's most significant tailings dam catastrophes. One of the potential causes of the tailings dam failure was that the oxidation of the iron-ore produced bonding between the particles. The bonding resulted in stiff tailings that were very susceptible to undrained conditions (Robertson et al., 2019).

2.1.3 Tailings Dam Failure

In 2001 The International Commission on Large Dams (ICOLD) released a comprehensive and groundbreaking report on the causes of tailings dam failures and how the failures in many cases arre avoidable. The comprehensive "Tailings Dams: Risk of Dangerous Occurrences" reports concluded that it would have been possible to prevent many tailings dams accidents. Lack of continuous control over the whole life-cycle of a dam and safe storage facilities has led to evitable disasters (ICOLD, 2001; UNEP 2017). Another aspect of the technical competence concerns the lifespan of the tailings dam. Tailings dams are

[2] The ore grade is the concentration of ore in mineable ore deposits, measured in weight or volume (Encyclopedia, 2021).

often raised in several steps over a long period since increasing waste will demand more space and a larger structure.

Furthermore, the construction time might vary over so many years that this will influence the initial design of the tailings dam (Davies, 2002). In several cases, the long construction time of tailings dams has led to an underestimation of the risk and future impact of the final construction of a dam. Hence, poor management and practices increase the risk of a potential failure towards the surrounding communities and environment (UNEP, 2017).

In the ICOLD report more than 220 tailings dams failures were studied, and the report concludes that many of the mistakes are repeated in various cases. A common consensus highlighted an urgent demand to reform and establish management terms and regulations (ICOLD, 2001; UNEP 2017). Authors such as Norbert Morgenstern, who has conducted more than 15 extensive revisions of tailings dams during the last 30 years, have emphasized the need for a better engineering understanding and guidelines for tailings dams (Morgenstern, 2018).

Even though the mining industry has gone through significant efforts to improve the failure situation, the severeness of tailings dam failure has continued to increase (Bowker & Chambers, 2015; Owen et al., UNEP, 2017). Even though there is a decrease in the amount of tailings dams failures, almost 50 % of all recorded "serious" and "very serious" tailings dam failures have occurred from 1990 and forward (figure 6). This refers to failures that have caused a significant impact on the "environmental security beyond the mine site" (Bowker & Chambers, 2017). The increase of severe tailings dam failures has led to a growing concern on tailings dam failure worldwide and in Europe. Recent incidents have gained much coverage in the media as the consequences have caused loss of life and environmental spills, and contaminated surroundings with devastating impacts. In particular, two recent tailings dam failures have gained much attention, namely the Corrego de Feijao iron ore mine and the Samarco iron ore mine in Brazil in 2019 and 2015. More than 250 people died (Armstrong, 2019; Owen et al., 2020; Morgenstern et al., 2016).

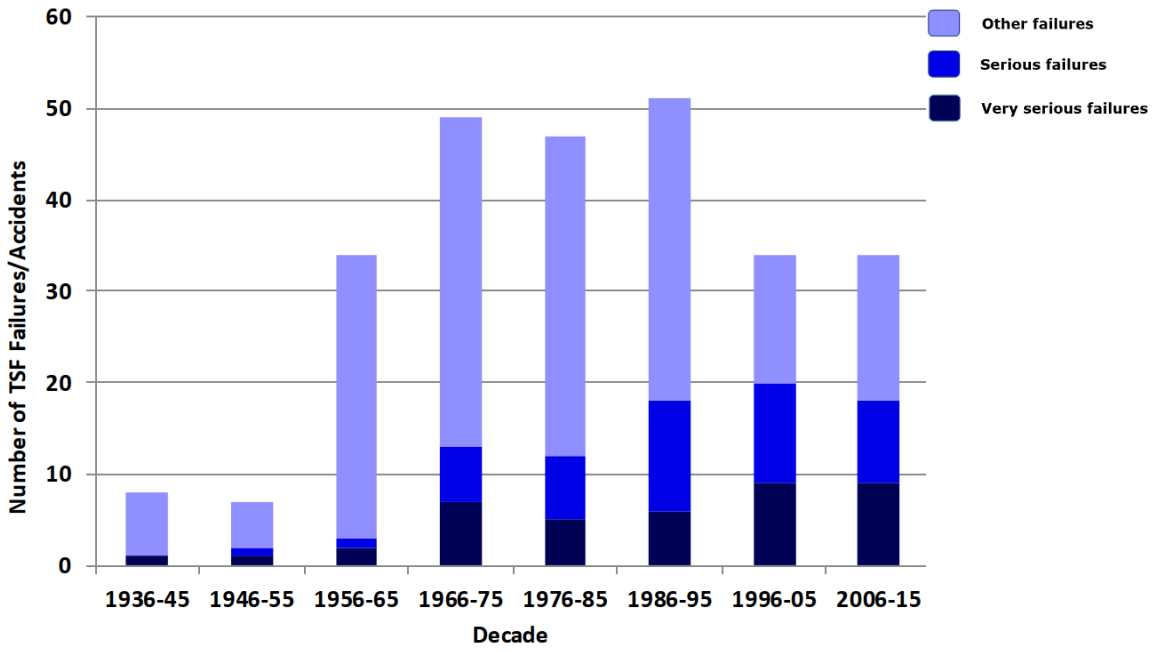

Figure 6: Severeness of tailings dam failures, modified from Bowker & Chambers (2017).

Since tailing dams will be used and constructed in the future, mitigation is essential. There is an emerging need to prevent tailings dam failure rather than "reacting after the fact" (Rico et al., 2008). Furthermore, climate change brings changes in the weather pattern and extreme weather events will bring challenges to tailings dams in the coming years. Additionally, the decrease in the purity of the material demands more significant amounts of tailings to extract the same amount of ore grade. Consequently, there will be a large volume of tailings from mine activity that needs storage in a sustainable way (UNEP, 2017).

2.2 Causes of Tailings dam failure

To better understand how to prevent and monitor dam failure, the causes of the dam failure should be understood. In many cases, the failure of a tailings dam is not dependent on only one cause. Instead, a series of causes might trigger the failure (Owen et al., 2020; UNEP, 2017). The susceptibility of a tailings dam should also be taken into account, referring to the likelihood of being harmed by a specific factor. The susceptibility of tailings dams will influence how exposed the dam is to a failure. Five key factors are by Rico et al. (2008) identified as the reason why tailing dam might be more susceptible to failure or damage than other geotechnical structures being that: 1, embankments are formed by locally collected fills; 2, dams are raised with solid material that has a much higher outlet of liquid waste than typical construction material as concrete; 3, there is a lack of regulation on specific design criteria; 4, there is a lack of stability requirements regarding continuous monitoring control during emplacement, construction and operation of a tailing dam; 5, the high cost of maintenance works for tailings dams after the closure of mining activities results in a deficiency in the control and monitoring of dams with ceased activity (Rico et al., 2008).

Several authors have identified the leading causes of failure. Additionally, multiple studies have gathered all available information on tailings dam failures. Some of the studies to mention are the ICOLD report (2001), the US Committee on Large Dam (1994), Rico et al. (2008), Bowker and Chamber (2015), and the UNEP report in 2017. More than this, the

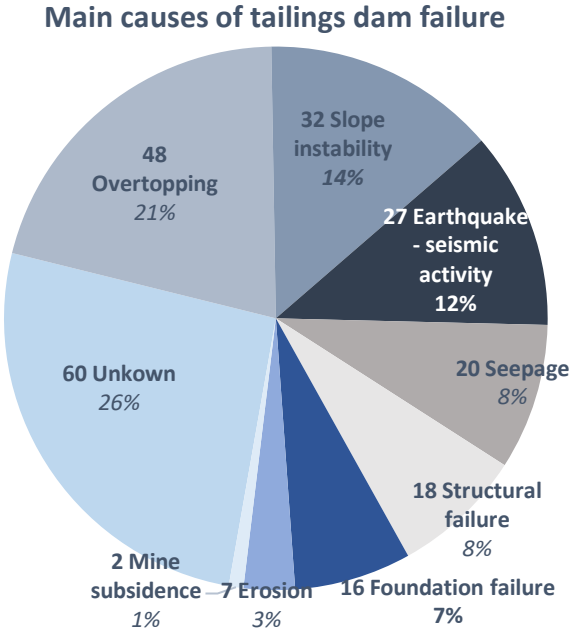

Table 2: Causes of tailings dam failure, modified from UNEP (2017) with data from Wise-Uranium (2022).

site Wise Uranium contains a register of all the major tailings dams failure since 1961 (WISE Uranium, 2022). The data presented by UNEP in the "Mine Tailings Storage: Safety Is No Accident" (2017) gives an overview of all tailings dam failures from 1915 to 2016. The registered information on the site Wise-Uranium filled in information about tailings dam failures from 2017 to 2022. This information was added to the original chart produced by UNEP (2017). A total of 230 tailings dam failures occurred from 1915 to 2022, and Table 2 demonstrate the distribution of the corresponding causes. The definition of the causes of failures corresponds to the definition given by UNEP (2017) given in Table 3.

Cause of Failure	Definition given by UNEP (2017)
Unknown	*Many of the older dam failures that were not sufficiently documented may fall into this category.*
Overtopping	*Water flowing over the top of a dam. Tailings dams are made of erodible material, and overtopping will cause erosion.*
Slope instability	*A constant load that causes deformation, to the point at which a dam partially or completely fails.* *Often caused by partial saturation of areas of the dam that are designed to remain dry.*
Earthquake - seismic activity	*Dams are designed to withstand earthquakes, but if the earthquake is larger than that which was anticipated, the structure can be destroyed by the shaking.*
Seepage	*Erosion of dam material due to water passing through areas of the dam that are designed to remain dry.*
Structural failure	*Design errors or failure of a designed component to function as designed.* *Failed decants (which drain water from the impoundments) are a common cause*
Foundation failure	*Failure related to building the dam on a surface that does not provide sufficient support for the weight of the dam. An example is a layer of clay under a dam.*
Erosion	*Simple erosion of a dam face, typically due to precipitation runoff that is not repaired*
Mine subsidence	*If the dam or impoundment is built above an underground mine, collapse of the underground mine workings can lead to the release of the impounded tailings.*

Table 3: Main causes of tailings dam failure from UNEP (2017) and Wise-Uranium (2022).

2.2.1 Seepage

The hydrological conditions in tailings dams are among the most common reasons for failure, including failures caused by overtopping, slope instability, erosion, or seepage. Seepage occurs as the water stored in a tailings dam will flow down in the tailings, through the cracks and layers, and if possible, through the embankment. The seepage rate might accelerate and lead to internal erosion of the dam material, and eventually, slope instability might lead to failure. This process is in many cases referred to as piping (US EPA, 1994; Klohn, 1979).

To avoid significant seepage within the tailings dam, the so-called spigotted beach, or as demonstrated in figure 5, the tailings beach, is essential. This part of the tailings dam consists of fine materials and should function as an impervious barrier. The ideal conditions involve a wide tailings beach, as this will increase the length of the seepage path and consequently lower the phreatic line, as demonstrated in figure 7a. However, if the water table close to the tailings beach increase and the tailings beach narrows significantly, the seepage will increase, and the phreatic line will be higher, as demonstrated in figure 7b (Klohn, 1979).

The figure below demonstrates how the hydraulic conductivity (*k*) conditions a favourable or unfavourable phreatic level in an upstream construction. Hydraulic conductivity refers to how easily water might move through soil or rock. In an upstream dam with favourable conditions, the hydraulic conductivity would be highest above the phreatic level (*k1*) and easily let the water flow down through the tailings (*k2*). However, the tailings dam located close to the pond should have lower permeability (*k3*), so the pond water will not flow into the tailings (figure 7a). On the other hand, an unfavourable condition occurs when the phreatic level rises, and the hydraulic gradient in the embankment (*k1*) is lower than the gradient in the tailings (*k2*). (Robertson et al., 2019). This creates a higher pore pressure, which lowers the tailings' shear strength and generates a hydrostatic pressure from the tailings towards the embankment.

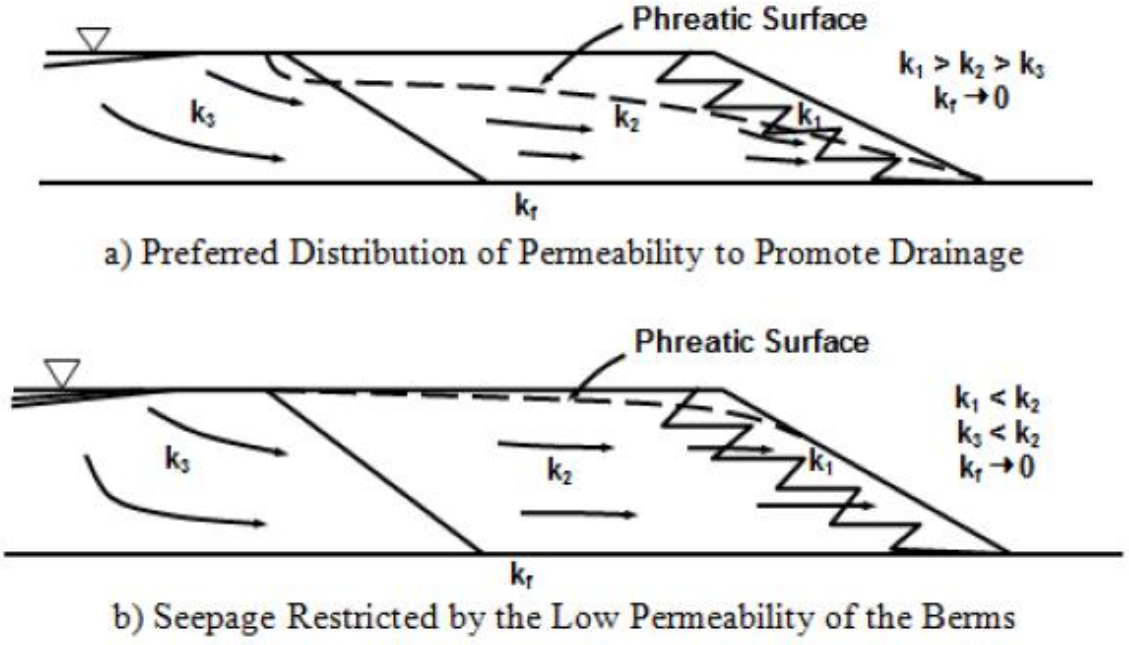

Figure 7: Favorable and unfavorable distribution of the phreatic level in an upstream tailings dam (Robertson et al., 2019)

2.2.2 Earthquakes

Earthquakes can damage dams by shaking. The upstream method is especially prone to earthquakes, and the method is recommended not to be used in areas where there is a risk of earthquakes. A particular phenomenon that earthquakes might cause is static liquefaction. Liquefaction might also be caused by applying high stress towards the tailings, and the mechanism of this phenomenon is explained in section 2.2.4 on slope stability.

The downstream method has oppositely to the upstream method shown to be tolerating against earthquakes. Also, the dams have withstood very strong shaking conditions by

using clayey soil to fill the dam embankment, and there are no reports of tailings dam failures (ICOLD, 2001). By compacting the embankment material to a high density, the risk of liquefaction due to the seismic activity minimizes (US EPA, 1994).

2.2.3 Foundation failure and structural failure

Foundation failure happens when the dam fails due to a weak layer in the foundation under the embankment. Several examples have shown how tailings dams built on clay layers might cause a slippery layer below the embankment. With enough load or water, the clay layer might shear and cause a failure of the dam. The Aznalcôllar tailings dam in Spain was built on soils that overlayed marl's in-situ rock. The marl had a pre-formed slip surface, which caused an approximate 45 meters breach of the tailings dam. Foundation failure can, in most cases, relate to a lack of understanding of the geological and geotechnical conditions of the site. This lack of understanding often relies on inadequate investigation prior to construction or wrongly interpretation of the site condition by the dam designer (ICOLD, 2001; Rico et al., 2018). As pointed out by Morgenstern (2018) there is a deficiency in engineering practices which in many cases might cause failure. Therefore, good geotechnical practice is fundamental to discover potential weak and thin layers that might increase the susceptibility towards shear stress. Noteworthy is also that the permeability of the foundation is crucial for the stability of a tailings dam. However, a too permeable layer might increase the chance of piping in the foundation. On the other hand, a layer with low permeability might cause a rise of the water table, and consequently, the poor pressure will increase, which again might lower the shear strength of the structure (Kossof et al., 2014).

Mistakes in the dam design are often the reason for dam failure. As already mentioned in the previous section, errors in the dam design depend on a correct understanding of the geotechnical and geological site investigation. More than this, the structural characteristics of a tailings dam rely on the construction material, the construction type, and the dimensioning of the dam (Bowker & Chamber, 2015).

2.2.4 Slope instability

Most of the causes of failure already mentioned in this chapter somehow influence the stability of the slope. When a failure occurs, it has, in the end, to do with how the resisting forces in a slope withstand the driving forces. Some of the factors that influence the slope stability are internal or external erosion, seepage, the foundation characteristics, earthquakes, and to a certain degree, the dam's design because this might not be adequate. However, this section will briefly highlight how a slope fails due to changes in the strength of the tailings.

The tailings strength resists a load (or stress) before they start to shear. This capacity is usually referred to as effective stress and is a function of the overburden stress and the water pressure present in the pores between the soil particles. If the water saturates the pores between the particles, this will lower the overburden stress towards the soil particles and reduce the shear strength. Hence, increasing the pore water pressure will reduce the shear strength of the soil and decrease the resistance to withstand stress (Robertson et al., 2019).

When the soil is shearing, it will contract or dilate in volume, depending on if the shearing is due to unloading or loading. If the soil is contracting, this might cause an internal collapse of the soil particles. The contraction will also result in a rapid rise of the water pressure, consequently decreasing the effective stress and a loss of the shear strength. This process

is referred to as liquefaction as the water between the soil particles will leave the soil particles in a liquid state (Robertson et al., 2019; US EPA, 1994). Put straight forward, during static liquefaction, the soil shear and will lose the solid properties to behave like a liquid (Kossoff et al., 2014). Flow liquefaction is a well-known phenomenon in sensitive clay; however, liquefaction is also common in tailings due to lose saturated material that quickly contracts under load (Robertson et al., 2019).

Some of the triggering factors for flow liquefaction are rapid loading due to construction or dumping of new tailings deposits or cyclic loading due to earthquakes or blasting. Other triggering factors are such as rise in pore water pressure, loss of suction and shear strength above the water lever in unsaturated zones due to precipitation, and strain (or internal creep) that might develop over time due to constant load (Robertson et al., 2019).

2.2.5 Erosion

There are mainly two locations at the dam that are especially prone to erosion, namely the dam face and the embankment abutments, located at the bottom of the dam with a supporting function (US EPA, 1994). Erosion might occur on the dam face when runoff water flows down the slope and remove material, and with high discharge, the erosion might increase. There are also erosion records on the foot of embankments, such as the Mojkovac mine in Montenegro. The tailings dam failed in 1992 as the Tara River, alongside the tailings dam, rose during floods and eroded the toe of the dam (ICOLD, 2001).

2.2.6 Overtopping

Overtopping occurs when the water ponded in a tailings dam flow over the top of the dam. Overtopping might happen if the water is not removed fast enough from the water pond. A decanting tower/pipe typically removes the water pond as the water flows into the tower. Additionally, evaporation or pumps also removes water. Several factors can cause the rise of pond water. One primary concern is the default behaviour of the decants tower, due to destruction of the outlet of the decants pipe, or debris blockage of the decants pipe (ICOLD, 2001). The water level might also rise due to heavy and extreme precipitation and potentially cause overtopping. After the overtopping occur, the water might erode the top of the embankment and the surface of the embankment (US EPA, 1994). More than this, the water moving downward in the tailings might cause seepage, erosion and additionally, the water might saturate the tailings. Saturation of the tailings increases the weight, and saturation of the soil or sand might reduce the shear strength. All these factors would reduce the slope stability of the tailings dam and lead to failure in the worst case. A well-known case of overtopping is the Merriespruit tailings dam, which failed in 1994 after heavy rainfall. The accident released more than 600,000 m^3 of tailings (Lyu et al., 2019).

2.3 Monitoring techniques

Monitoring techniques of tailings dams provide insight into the phreatic surface level, pore pressure, seepage, and potential deformation. Tools used for the monitoring includes inclinometers, piezometers, earth pressure cells, seismic sensors, wire extensometers, ground-based radars, and additional geodesic instruments (Adamo et al., 2020). The traditional monitoring techniques mentioned above are often costly time consuming, and they demand thoroughly visual inspections. Even though the instruments are reliable and accurate, early signals of potential rupture might not be detected as the field measurement is limited to a specific sector of the structure (Gama et al., 2020). Prior to the failure of the Corrego de Feijao dam, none of the monitoring instruments indicated any warning signal of the upcoming failure (Robertson et al., 2019)

In recent years, earth observation tools have been integrated into the monitorization of tailings dams. Satellite-based radar interferometry (InSAR) has become a well-known tool to observe surface displacement and is frequently used when studying earth deformation and managing hazards. There is no other monitoring tool that has the potential to cover such a large area in such a comprehensive way (Rosen, 2021). Based on the widespread coverage of the SAR data, it complements the point-based in-situ measurements tools (Grebby et al., 2021). Furthermore, the InSAR method has been incorporated to monitor tailings dams to develop cost-effective means and potentially assess early-warning movement alerts (Grebby et al., 2021).

With an emerging amount of SAR imagery (both free of charge and purchased), the potential to retrieve information on surface displacement is constantly improving (Cigna and Tapete, 2021). The temporal resolution is decreasing. With free images, such as Sentinel-1, the revisiting time is 6 to 12 days (ESA, 2021; Hussain et al., 2021). The spatial resolution is also fundamental, as it defines the accuracy of the data collected. The meters per pixel indicate how good the accuracy is, and with good resolution, InSAR can measure changes under 1 millimeter with a swath (coverage) of hundreds of kilometers (Rosen, 2021). The ability to acquire surface data during the day- and night-time, independently of cloud cover, enables monitoring entities and scientific communities to collect a large amount of data concerning topics such as seismic deformation, volcanic activity, and ground movement (Biggs and Wright, 2020; Rosen, 2021).

Despite the usefulness and importance of the method, the InSAR method should not be simplified and taken for granted in slope stability monitoring as it is restricted to slow rates of deformations. If there is a sudden collapse or a brittle failure, the failure might happen faster than the revisiting time of the satellite. Therefore, the data needs to be used to complement in-situ measurement tools as the ground-based tools contain crucial information (Grebby et al., 2021).

2.3.1 Syntethic Aperture Radar (SAR)

Satellites acquire two different types of images, namely optical and radar images. The optical sensor functions as a very large camera and captures optical images from the earth's surface. The optical sensor is a passive radar. They do not emit any radiation themselves; instead, they capture the images through the visible part of the electromagnetic spectrum reflected from sunlight (Petorelli et al., 2018; NASA 2021). As demonstrated in figure 8, the optical sensor manages to capture the wavelengths between

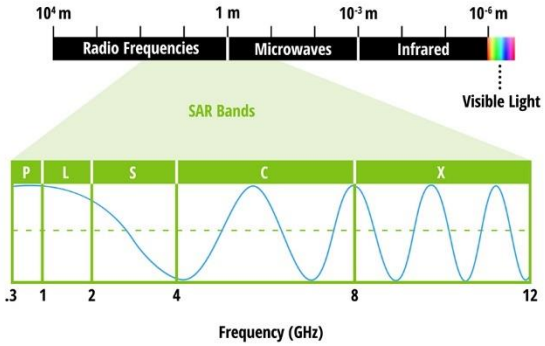

Figure 8: The frequency and wavelength of the electromagnetic spectrum (NASA, 2021).

10^{-3} and 10^{-6} meters and includes the near-infrared short-wave infrared in its spectrum while it is orbiting worldwide. However, the radar sensors are often referred to as the active sensors, as data is collected by emitting microwaves signals through the Synthetic Aperture

Radar (SAR) towards the earth, which is then reflected (also referred to as backscattered or echo) by the obstacles on the surface. The information brought back with the microwaves is based on the amplitude and the phase of the signal. The amplitude is the intensity of the radar response. At the same time, the phase refers to the delay of the signal and is proportional to the signal's travel distance from the sensor to the surface and back divided by the transmitted wavelength. Hence, the delay of the backscattered signal is equal to the change of the transmitted and received signal, namely the phase change (Ferretti et al., 2007). Rough surfaces will reflect a large amount of the signal to the antenna, while flat surfaces reflect away the signal, and less signal will return to the antenna (NASA, 2021). As the antenna moves along the earth's surface, it emits and receives microwaves signals to record the surface characteristics (Ferreti et al., 2014)

The spatial resolution of the radar data is proportional to the length of the antenna and the wavelength emitted by the sensor. This proportion means that to obtain an image with, for example, a spatial resolution of 10 m, the wavelength emitted by the radar would be about 5 cm, and the antenna required would need to be more than 4000 meters long, which is impossible. Thus, a solution to this has been that the SAR collects data with a shorter segment, and as the antenna moves, it joins the segments to simulate a large antenna. Based on this, the microwaves emitted and received by the SAR images range between 3 and 30 cm (NASA, 2021)

As illustrated by figure 9 the satellites follow a predefined Line-Of-Sight (LOS) and continuously move along the same orbit.

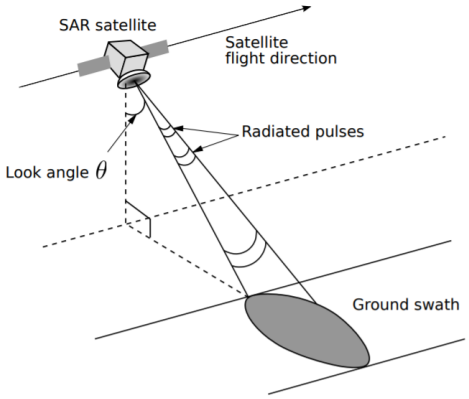

Figure 9: The satellites flight direction and acquisition mechanism (Lauknes, 2010)

A satellite that travels in a descending orbit refers to a satellite that travels from north to south. Naturally, when an orbit moves in the ascending direction, it travels from south to north. Figure 10 demonstrates how the descending and ascending orbits vary. The acquisition of SAR data will repeat over the same areas (Ferretti et al, 2014). The access to several images over the same area makes it possible to apply the SAR interferometry technique (InSAR).

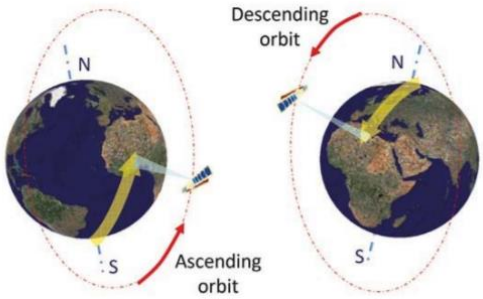

Figure 10: Ascending and descending direction of the satellite orbit (Ferreti et al., 2014).

2.3.2 Interferometric SAR

Interferometric SAR uses two complex radar SAR satellite images from the same area to reveal phase changes between the images. Change detections are temporal phenomena and depend on data acquisition over a specific area at two different times t_o and t_1 (Lauknes, 2010), Figure 11 demonstrates how a possible surface deformation relates to the interferometric phase change term ΔR_d to detect ground deformation.

The different SAR images need to be processed before producing a SAR interferometric. Shortly explained, this processing contains the import of the raw data, the removal of irrelevant phase components, and the coregistration of the images, so the pixels in one of the images are adjusted to overlay the other image. The processing happens through different software, such as SNAP.

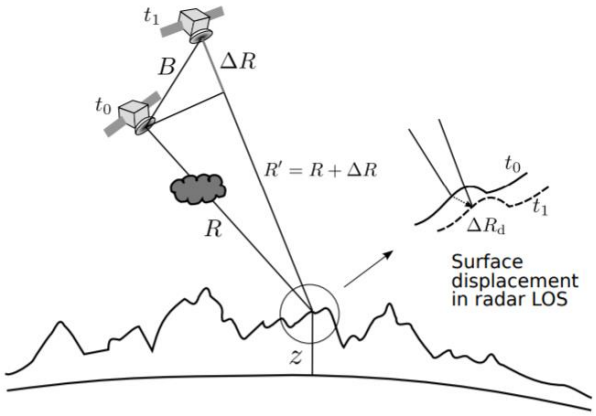

Figure 11: Detection of surface displacement between two SAR images acquired over the same location at different times (Lauknes, 2010)

From the processed images, it is possible to estimate the phase change. The following equation can explain the interferometric phase change;

$$\Delta\phi = \frac{4\pi}{\lambda}\frac{B_\perp}{Rsin\theta}z + \frac{4\pi}{\lambda}\Delta R_d + \Delta\phi_{APS} + \Delta\phi_{decorr}$$

$\Delta\phi$ - interferometric phase change

λ - radar wavelength

$B_\perp$ - the distance between two orbits

R – range distance

θ – incident angle

z - altitude

ΔR_d – possible surface displacement

$\Delta\phi_{APS}$ – the difference in atmospheric path delay

$\Delta\phi_{decorr}$ – noise contributions

Note that the first term of the equation above needs to be removed to study the surface displacement. This is normally done by using a digital elevation model (Lauknes, 2010).

Instead of having just two images to detect surface displacement, it is possible to integrate a time series of several images over a period. This is referred to as multi-interferometry and has evolved significantly during the last two decades. Limitations of having just two images are disturbing effects such as atomic effects, geometric decorrelations, or surface deformation over time. Limitations like these can be mitigated with the time series of InSAR since time-series focus on entire data stacks that consist of multiple interferograms. Large data stacks enable the user to observe temporal displacement over many years. Additionally, it is possible to apply spatial and temporal filters to diminish phase contributions that disturb the data (Ferretti, 2014; Lauknes, 2010; Rouyet, 2015).

The signal sent back during SAR acquisitions is represented through each image pixel and can be referred to as scattering. Different scattering mechanisms can be expected from a pixel under study. A single scatter point can be defined as a "scatter that dominates the scattering from the resolution cell" (Lauknes, 2010). Figure 12 shows how one scatter point might represent the whole cell or dominate other scatter points. The distributed scattering mechanism represents the "coherent summation of all individual small scatters within the resolution cell" (Lauknes, 2010). The persistent scatters often corresponds to man-made or natural objects such as buildings or a rock (Ferreti, 2014; Lauknes, 2010)

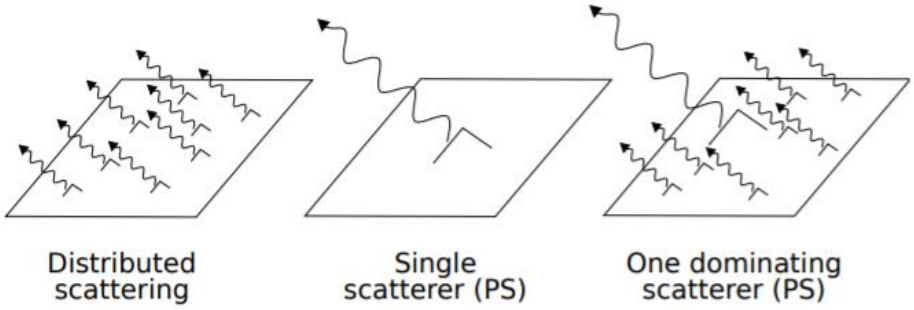

Figure 12: Different Surface scattering mechanisms modified from Lauknes (2010).

There are two main categories within the time-series InSAR methods which mainly are distinguished based on the different scattering mechanisms.

The first is the Persistent Scatters (PS) technique. The PS technique mainly identifies stable reflectors (scatters), also referred to as Persistent Scatters, in the SAR interferometric time series. An initial image is used as the master scene and applies as a reference to all other images. Individual scatter points are used to analyze the temporal phase evolution and

detect eventual phase changes between the collected images and the master scene image (Ferreti, 2014; Lauknes, 2010; Rouyet, 2015; Voge et al., 2021).

The second category refers to as Small Baseline (SB) technique. Instead of having a unique master scene as a reference for the interferograms, pairs of collected images generate many interferograms in consecutive order. The idea of this approach is that instead of having point-wise coherent scatters, baseline interferograms are averaged and compared. The method relies on the distributed scattering mechanism and will give the best results when analyzing natural environments with few strong scatter points (Lauknes, 2010; Rouyet, 2015; Ferreti, 2014).

2.4 The Inverse Velocity Method

Superficial displacement is the most evident sign of slope instability and is considered a crucial indicator of slope failure. The surface displacement velocity can easily be retrieved from the difference of displacement divided on time. In recent years it has become popular within the field of slope failure studies to apply the inverse velocity method as an early-warning system, as the method in some cases might be used to predict future slope failures (Carla et al., 2017, Intrieri et al., 2019).

Velocity is defined as the rate a single particle, or object, change its position over time. As the velocity increases, the slope of the movement increases, and the velocity is constantly accelerating. When the velocity of the surface displacement starts to accelerate, this might indicate the beginning of a failure. Theoretically, constant acceleration would mean that the velocity would be infinite, which is obviously not the case during a slope failure. Immediately after a slope fails, the surface displacement will stop. However, the relation

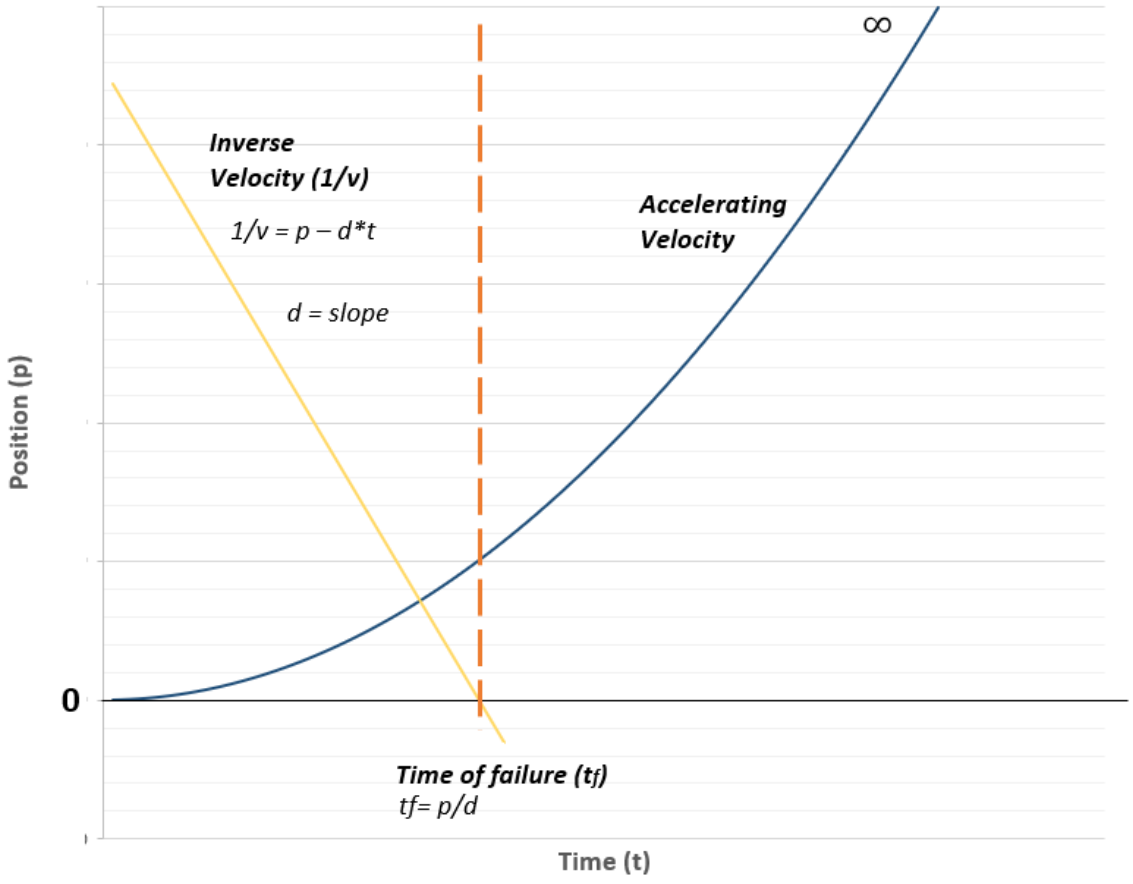

Figure 13: The relation between the inverse velocity method and the acceleration of velocity.

between acceleration, time, and position can indicate when the velocity will start to accelerate. Figure 13 demonstrate the relation between the inverse velocity and the acceleration. The time of failure is predicted when the acceleration increases exponential.

The inverse velocity method was first presented by Fukozono., T (1985) in the article "A New Method for Predicting the Failure of a Slope". By inverting the velocity and time graph, the method predicts the approximate time of failure of a slope. A trend-line is drawn by plotting the inverse velocity of surface displacement against time, and as it intersects with the x-axis, the time of failure is predicted (Fukuzono, 1985).

Fukozono emphasized that the surface displacement curve is divided into three forms, namely linear, convex, and concave. Their shape varies depending on the relationship between the acceleration of surface displacement and velocity just before failure (Fukuzono, 1985). Equation 2-1 is given by Fukozono (1985) to predict the failure time;

$$V^{-1} = [A(\alpha - 1)]^{\frac{1}{\alpha}-1}(t_f - t)^{\frac{1}{\alpha}-1}$$

Equation 2-1: The inverse velocity equation (Fukozono, 1985).

whereas A and α depends on the slope characteristics and are considered as constants. These parameters were established by laboratory testing. α is estimated to be concave when α>2, convex when α<2 and linear when α =2. Fukuzono proposed the linear trend to fit the prediction of failure the best. It would provide an approximate estimation of the failure time (Fukuzono, 1985; Rose & Hungr, 2007), as demonstrated in figure 14.

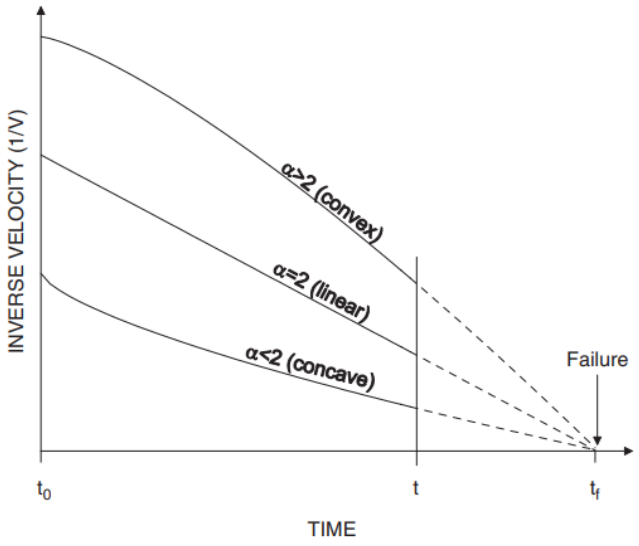

Figure 14: Inverse-Velocity versus time relationship presented by Fukuzono (1985), plotted by Rose & Hung (2007).

The method presented by Fukozono was theoretically established through laboratory experiments, and the triggering factor was artificially rainfall (Fukuzono, 1985). The method is suggested to be a powerful tool when predicting slope failure as the curve tend to become linear close to the final stage of failure and is somehow easier to extrapolate then hyperbolic curves, which generally represent the acceleration deformation close to

failure (Rose & Hungr, 2007, Carlá et al., 2017a). Several studies (Carlà et al., 2017a, 2017b, 2019; 2020; Grebby et al., 2021) have back-analyzed the inverse velocity trend-line and demonstrated how the method could be used to observe accelerating trends the weeks or days before the slope failure.

2.4.1 Challenges with the method

Despite the usefulness of the inverse velocity method, there are several limitations encountered that might influence the accuracy and the reliability of the predicted time of failure (tf). To start with, universal laws related to slope failure do not generally consider the nature of the slope and the physical mechanisms properties of the material. As already explained, the inverse velocity method was established through laboratory tests, where the conditions were constant and controlled. In reality, these constant and controlled conditions seldomly exist. In contrast, the field's conditions are often influenced by local slope movement, variation in mechanical properties, and periodically changing factors (such as human activities, rainfall, groundwater, etc.) that influence the displacement rate (Carlá et al., 2017b). Another essential aspect is that the method assumes that the inverse velocity at failure is infinite, which never occurs in a slope. The velocity of failure will vary depending on slope angle, rock types, mechanism of failure, and volume (Carla et al., 2017a). Furthermore, when the data for the inverse velocity depends on SAR images, the method is limited to failures that occur due to rather slow deformation. The data acquired depends on the revisiting time of the satellite, and would therefor not be able to predict or capture a brittle failure or a sudden collapse (Grebby et al., 2021).

Carla et al., (2017b) argue that the method should be used with caution as the failure-time prediction must be interpreted as general and that the margin of error can vary from hours to days. Rose & Hungr (2007) present the same argument in their study of open-pit mines. They further emphasize that the trend line should be continuously re-evaluated to include potential trend changes and changes observed in the field. Other kinds of limitations that are evident are related to field monitoring and instrumental usage. There might be disturbances in the field, or the temporal resolution is of major importance when estimating the displacement time from satellite imagery. The revisiting time of commercial satellite data often varies 5-6 days. Consequently, the movement might not be captured in the final stage before a slope failure.

2.4.2 Identifying where to apply the inverse velocity method

Carla et al. (2017a) feature the importance of correctly processing the inverse-velocity time series to deal with some of the limitations mentioned above. They further refer to two types of disturbing effects: "instrumental noise" corresponds to the monitoring instrument, and the "natural noise" refers to all other factors that cause discrepancy to the theoretical linear behavior. Their comprehensive study aims to understand how the noise affects the reliability of the time of failure (Tf). In conclusion, they establish some guidelines for a more coherent utilization of the Inverse velocity method. Briefly summarized, their findings conclude that noise might delay the identification of the onset acceleration (OOA); however, using a long-term and short-term smoothening moving average can detect significant changes in the raw data set to identify the OOA. The most prominent smoothing function, demonstrated in equation 1, can be considered a simple moving average where the average of the 3-measurement point (short-time simple moving average) and >7 measurement points (long-time simple moving average) are drawn. Observing both of the smoothening curves in the same graph makes it possible to identify where the short-term moving average (c-SMA) line crosses the long-term moving average (c-LMA) line. Where

the c-SMA crosses above the C-LMA, there is an uptrend, something that indicates an OOA. If oppositely, the c-SMA trend line crosses below the c-LMA, a negative trend is identified corresponding to an end of the acceleration (EOA). The method presented by Carla et al. (2017a), namely the crossover rule, defines an onset of the acceleration and consequently signals from where the inverse velocity method should be applied. Figure 15 gives an example of how to identify the crossover points. After identifying the OOA, the user would eventually be able to forecast the time of the failure window by applying the inverse velocity method on both moving averages trend lines.

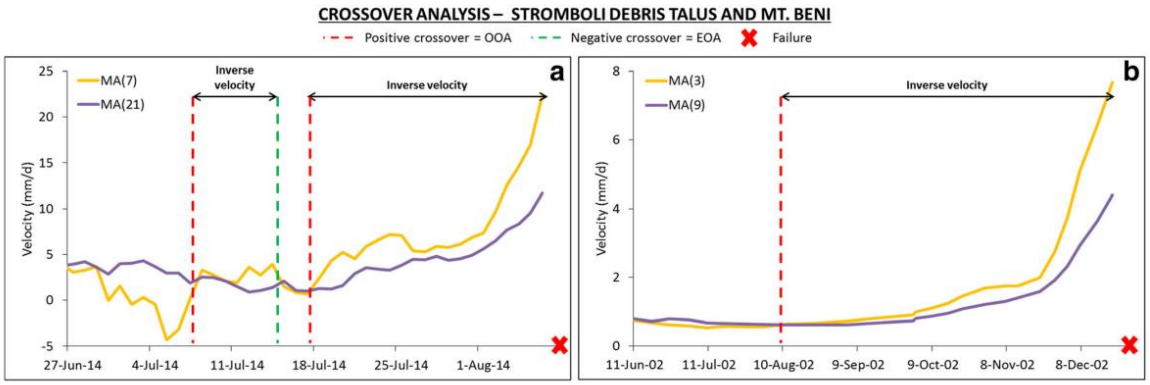

Figure 15: Crossover analysis for Stromboli Debris Talus and Mt. Benti (Carla et al., 2017a).

To remove noise and smoothen the curve, the moving average displacement is calculated through equation 2-2;

$$\bar{V} = \frac{V_t + V_{t-1} + \cdots + V_{t-(n-1)}}{n}$$

Equation 2-2: The moving average equation (Carla et al., 2017a).

Where n = 3 or 7 for the short-term moving average, and n = 9 or 21 for the long-term moving average.

3 Methodology

The chapter explains the selection of case studies, the collection of data, and the data processing. The chapter also explains how the Inverse Velocity Method applies in each case.

3.1 Selection of case studies

In order to select the most relevant cases for this study, the following three criteria has been used;

- The case must contain a tailings dam failure occurred with a long-term deformation before the date of failure;
- The case needs to provide sufficient access to SAR images over the area of interest;
- The displacement curve retrieved from the surface displacement data should indicate acceleration along the timeline.

Two prominent case studies fulfilled these criteria's. Case study one is the Córrego do Feijão mine located in the Brumandiho municipality, south of Minas Gerais, Brazil. The Córrego do Feijão tailings dam failure is a famous case, as the failure was unpredictable and caused many casualties. Numerous authors have also studied the case, and multiple investigations have applied the inverse velocity method (Gama et al., 2020; Grebby et al., 2021). NGI delivered data that extends from 2015 until 2019, when the failure occurred. This data has made it possible to observe the deformation of the dam over a more extended period than previous studies that have used data from 2017 and 2018 (Gama et al., 2020; Grebby et al., 2021).

The second case study is the Cadia mine located in southwestern Australia. This case study differs from the Córrego do Feijão mine, as ground deformation indicated the failure, and it was possible to implement mitigation measurements. The data in the Cadia mine extends from the beginning of 2017 until March 2018.

The flowchart in figure 16, gives a general overview of the data collection and processing.

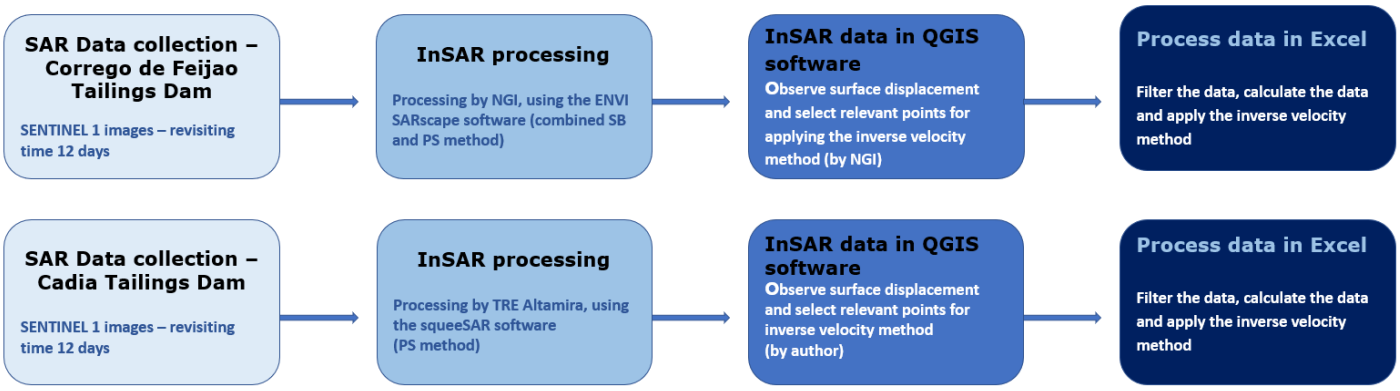

Figure 16: Flowchart of the methodology for each case study.

3.2 SAR data Collection

In the period from May 2015 until January 2019, 108 Sentinel-1 images were collected by NGI for the Córrego do Feijão Dam. The LOS of the radar is down-slope, and the orbit generates a 45-degree angle towards the northern part of the dam (Voge et al., 2021).

Between January 2017 and September 2019, thirty-four Sentinel 1 images were acquired by TRE Altamira over the Cadia Tailings Dam.

Sentinel-1 consists of Sentinel – 1A and Sentinel – 1B sharing the same orbital plane, and when both are acquiring data over an area of interest, the revisiting time is six days. However, in the data collection for the Córrego do Feijão Dam and Cadia Dam, the revisiting time of Sentinel-1 is 12 days since the mission only provides descending acquisitions over this specific area. The spatial resolution of Sentinel-1 in the area covered is 20 meters in the satellite flight direction and 5 meters in the crossing direction (Voge et al., 2021).

3.3 Processing of Data

This section explains the processing of the data. The section will not go deep into InSAR processing. For an in-depth understanding, it is referred to the European Space Agency Guideline for SAR Interferometry Processing and Interpretation (ESA, 2019).

3.3.1 InSAR processing

For the data provided in the Córrego do Feijão Dam case study, the SAR data was processed, and the interferograms were produced using the ENVI SARscape program provided by L3HARRIS Geospatial. The interferometric stacking analysis provided by SARscape uses the SBAS and PS techniques to estimate surface displacement. For the Feijao Dam case study, a combination of the SBAS and PS techniques was the most prominent as they showed to be complementary in the sense that they covered both spatial and accumulated deformation (Gama et al., 2020; Voge et al., 2021).

Regarding the Cadia Dam, TRE Altamira used a program developed by themselves, namely SqueeSAR. SqueeSAR is based on the PSI technique and uses a multi-image dataset. By identifying stable reflectors (permanent scatters), the SqueeSAR program surface displacement with millimeter accuracy. The results of the SqueeSAR processing provide average velocity maps and time series of displacement for specific measurement points (TRE Altamira, 2022). For a visual understanding, see figure 20.

3.3.2 Quantum GIS

Quantum GIS (QGIS) is an Open-Source Geographic Information System. In this study, the program investigated which deformation points would would be most interesting when applying the Inverse Velocity Method. By installing the QGIS PS Time Series Viewer plugin, it is possible to visualize and access the displacement time-series extracted through the SARscape or SqueeSAR Softwares. When processing the InSAR data with any of the used softwares, the results provide measurement points that show average velocity over time. QGIS displays the measurement points and makes it easy to retrieve information on where the significant deformation occurred. Figure 17 follows an example of how QGIS displays the data for the Cadia dam.

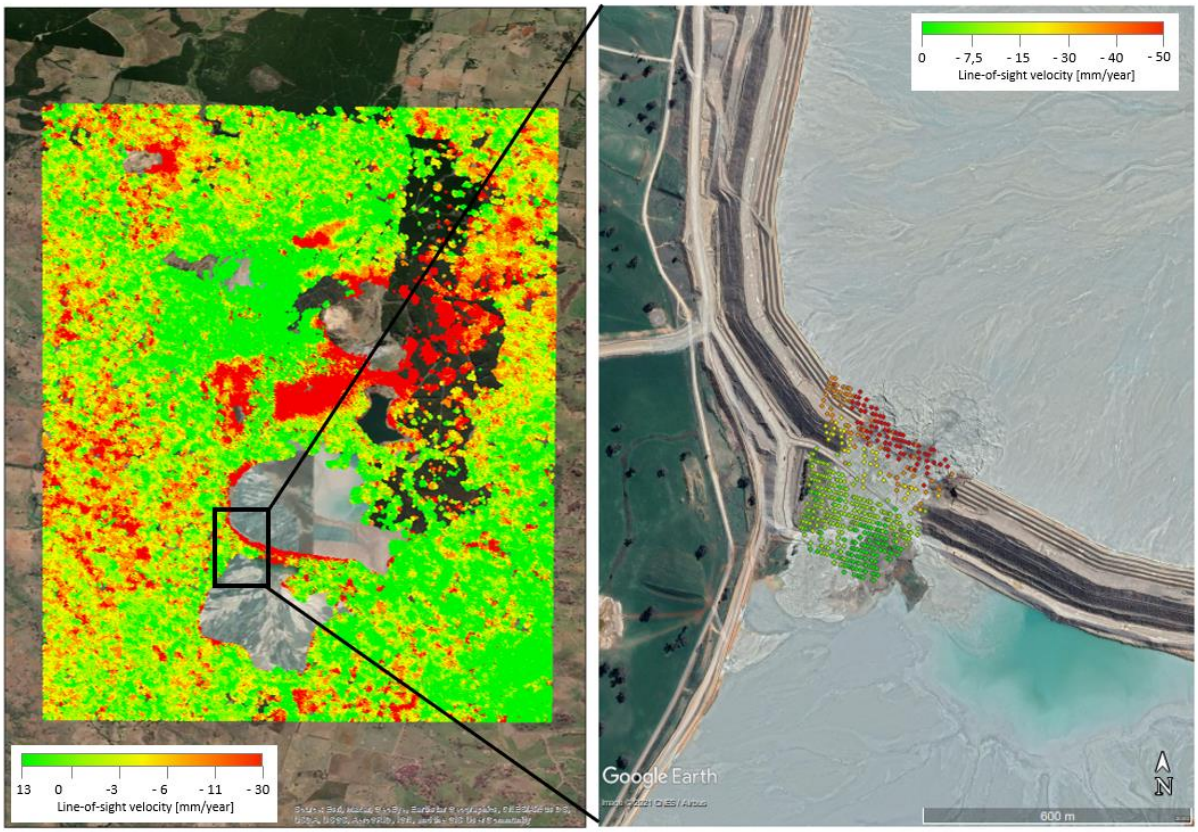

Figure 18: Example on how the QGIS displays the different measurement points in relation to the surface velocity over time.

Observing the average velocity of displacement on different parts of the tailings dams makes it possible to indicate the surface displacement. In QGIS, this is done by using the PS Time Series Viewer in several parts of the dam and then exporting the data to excel to calculate the mean velocity. In both case studies, deformation in relation to time has been observed in three parts of the dam; the crest, the slope, and the foot. The different estimations make it possible to retrieve the plot that might be most relevant for the inverse velocity method—referring to a plot that indicates significant acceleration along the time.

3.3.3 Excel – preparing the data

Before applying the inverse velocity method and calculating the moving average presented by Carla et al. (2017a), the data was separated and filtered in four ways to compare and retrieve the best-fitted results. Figure 17 intends to give a general overview of the filter applied to the dataset before calculating the velocity.

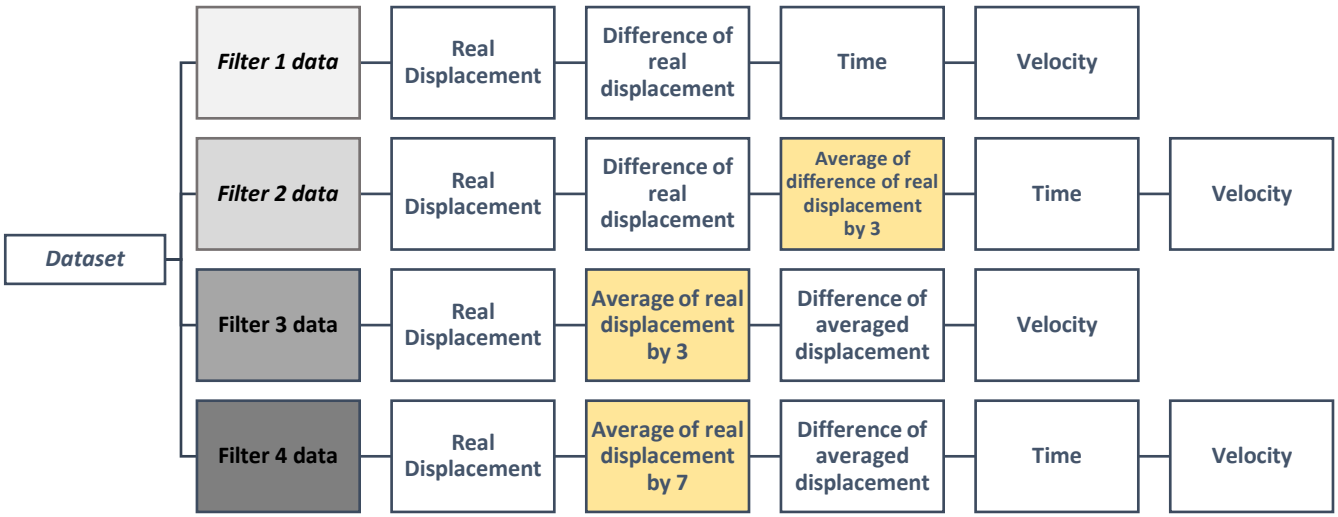

Figure 17: Flowchart on how the data was filtered in excel before applying the moving average.

Filter 1 data; no filters were applied to the data, and all the processing / smoothening steps were performed using the raw data.

Filter 2 data; the real displacement was used; however, the difference of displacement was filtered with an average of 3 points.

Filter 3 data; the real displacement measurement points were averaged by 3, giving a mean displacement before calculating the difference of displacement.

Filter 4 data; equal to dataset 3, the averaged value of 7 real displacement measurement points was also calculated. This was not used for the moving average. However, it was used when smoothen the velocity and the inverse velocity.

Furthermore, to present the velocity in a positive direction in accordance with the method presented by Carla et al. (2017a), the velocity has been multiplied with -1 in excel.

3.3.4 Excel – applying the inverse velocity method

After calculating the velocity, the moving average was estimated. Where n = 3 or 7 for the short-term moving average and n = 9 or 21 for the long-term moving average. Additionally to the moving averages suggested by Carla et al. (2017a), other short- and long-term moving averages have been experimented to understand if there would be other combinations that could improve the identification of the OOA and EOA. The moving averages were compared and used to identify visible points of OOA and EOA (the background of this is given in chapter 2.4.2).

Finally, different velocity data estimated the inverse velocities to be able to analyze and compare the best prediction of a failure compared to the real-time failure. First, the inverse velocity was plotted with the moving average values according to the method presented by Carla et al. (2017a). After this, the inverse velocity was also plotted using Filter 1, 2, 3, and 4 data, though without using the moving average values. Figure 18 provides a brief overview of how the process was conducted by the author

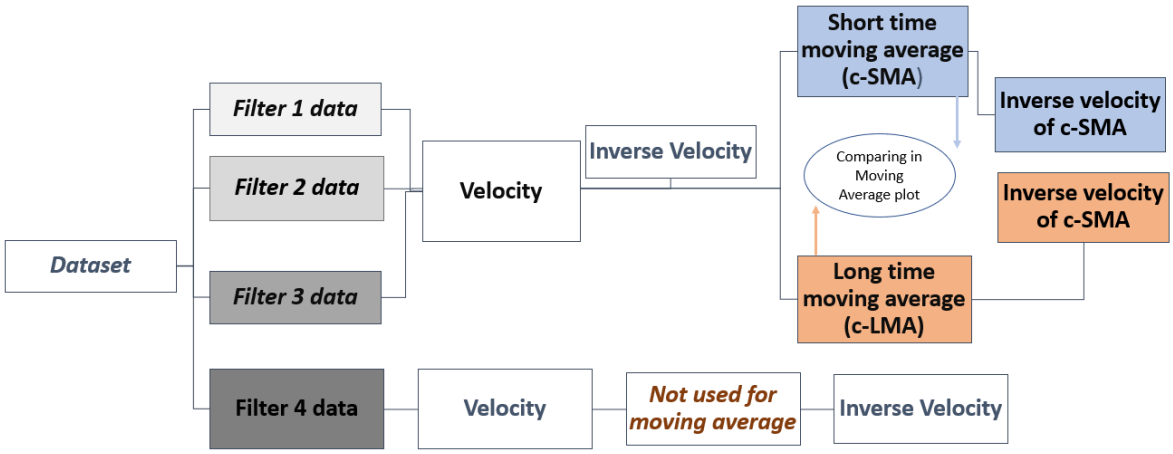

Figure 18: Flowchart on how the inverse velocity was applied to the moving average and the filter data.

4 Result

4.1 The Córrego do Feijão tailings dam case study

The Córrego do Feijão mine is located in the southern part of the Minas Gerais state in Brazil. It is often referred to by the municipality's name, namely Brumadinho. The mine extracted iron-ore, and in 2018, the mine produced 8.5 million tons. Dam-1 was raised between 1976 and 2013 through 15 stages and 10 raises (figure 19) and was used to store the iron-ore tailings. The Dam had a crest length of over 700 meters, and the Dam had a maximum height of 86 meters. Dam-1 was in operation until 2016, when it ceased (Gama et al., 2020; Robertson et al., 2019).

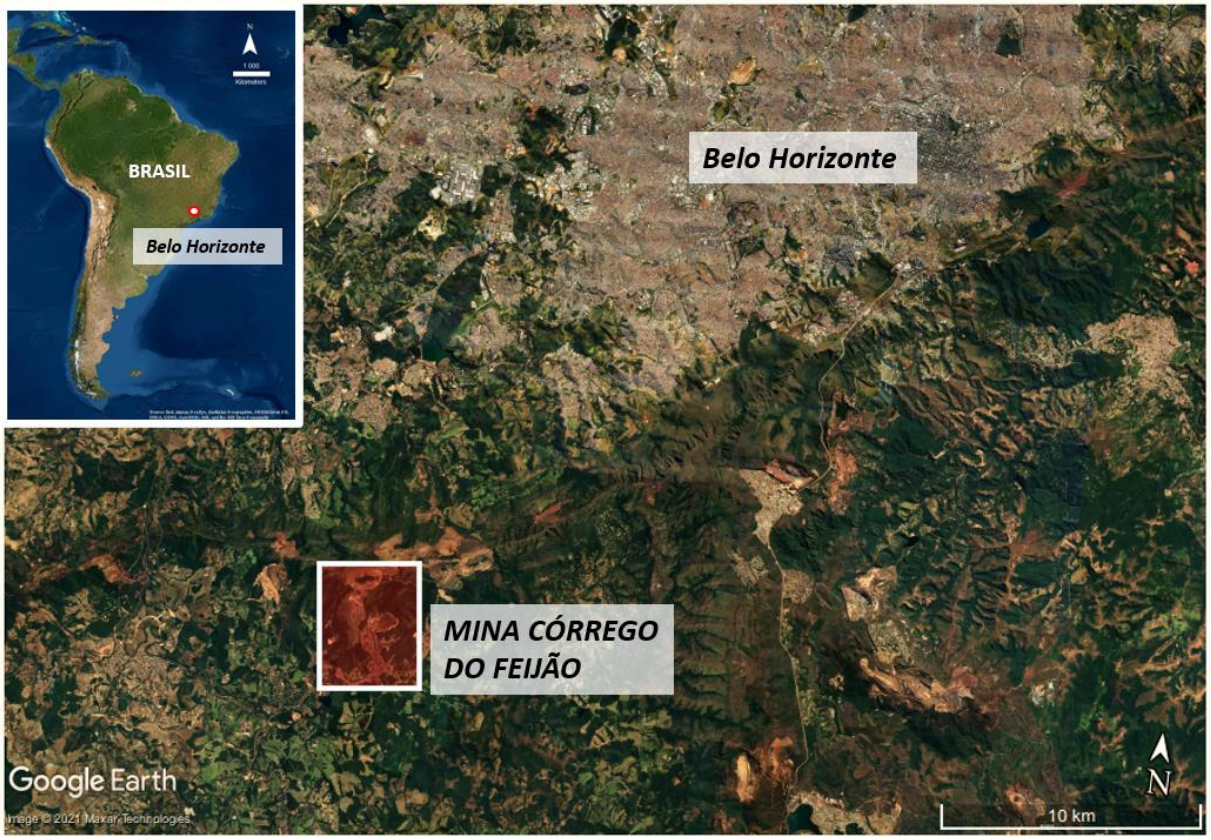

Figure 19: Geographical location of the Córrego do Feijão mine.

On the 25th of January 2019, the Burmandinho tailings dam breached. The mudflow released from the tailing Dam had devastating consequences for the downstream communities as a 30 meters high wave was generated and swept through everything that was in its way until it reached the Paraoeba River located at the edge of Brumadinho. The failure resulted in more than 250 deaths. From LiDAR detection, it was possible to detect as much as 9.7 million cubic meters of material that took part in the failure (Gama et al., 2020; Robertson et al., 2019; Silva et al., 2020). The dam prior and post failure can be observed in figure 20.

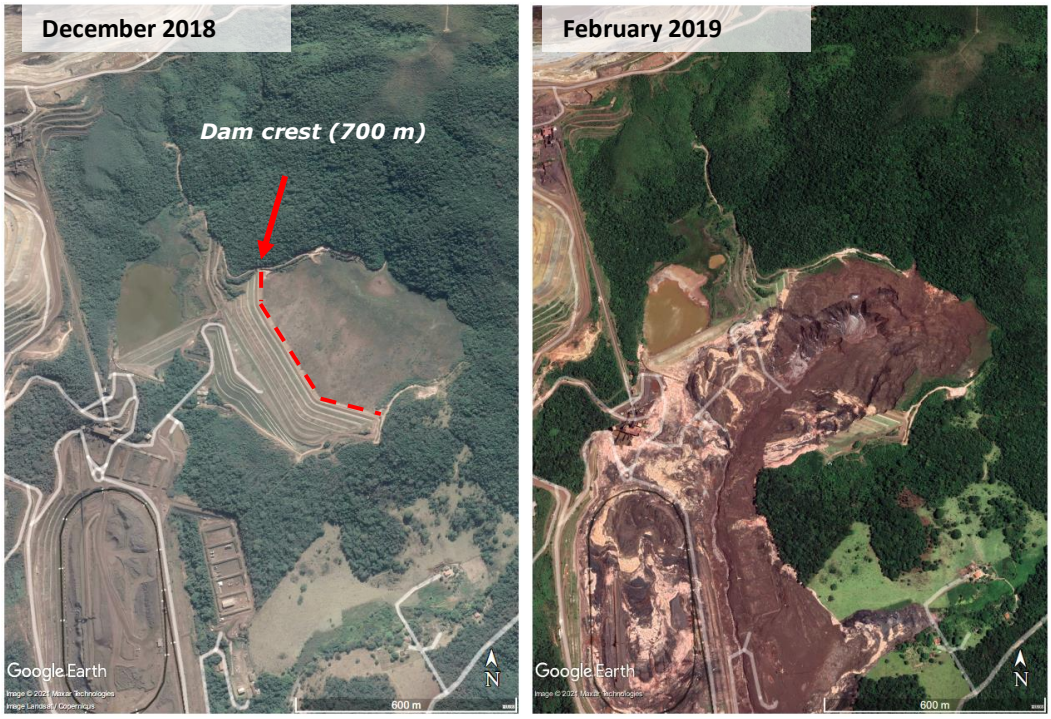

Figure 20: Córrego do Feijão tailings dam before and after failure.

The Burmandinho tailings dam failure is one of the most devastating tailings dam disasters in history and is, therefore, a well-studied case. Multiple authors investigated the reasons for the collapse (Gama et al., 2020; Grebby et al., 2021; Robertson et al., 2019; Silva et al., 2020; Voge et al., 2021). A comprehensive report was also published almost a year after the embankment collapsed, where an expert panel identified several potential factors that could have caused or influenced the failure (Robertson et al., 2019). The failure occurred as a flow liquefaction. Although the Dam was extensively monitored, with several types of in-situ instruments, there were no signs of distress or deformation prior to the failure. However, the study of post-failure indicates slow deformation in the dam face, where measurements show that the deformation corresponds to under 36 millimeters per year (Robertson et al., 2019). Several authors (Gama et al., 2020; Grebby et al., 2021; Voge et al., 2021) have tried to optimize the deformation calculation through available Sentinel-1 satellite images by utilizing different processing techniques.

4.1.1 Potential triggering factors

In their extensive report, the Expert Panel pointed out that the deformations observed through InSAR are consistent with a long-term settlement of the Dam and would therefore solely not indicate a potential failure (Robertson et al., 2019). Thus, the report indicates that complex conditions were present in the Dam prior to the failure. Below is a brief explanation of these conditions.

- The upstream construction of the Dam was initially very steep; however, a setback of the embankment early in the construction phase should have dealt with this. The setback is demonstrated in figure 21. As a result of the setback, the pond came closer to the dam crest, resulting in a high phreatic line.

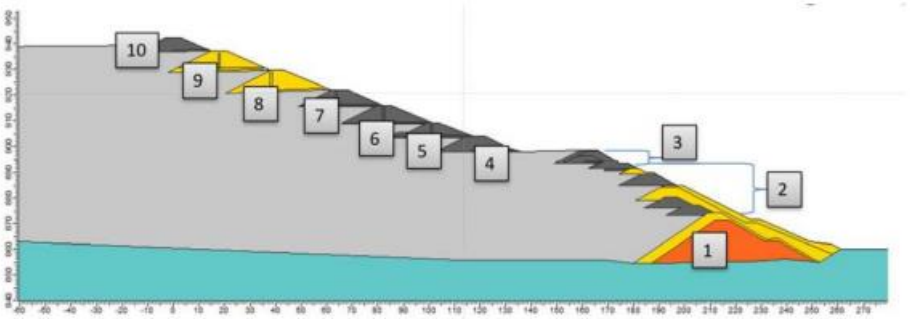

Table 1: Dam I Construction Details[7]

Stage	Year	Raising ID	Top Elevation (m msl)	Height max (m)	Project Design Firm	Construction Company
1	1976	Starter Dam (first)	874	18	Christoph Erb	Emtel
2	1982	Second	877	21	Tecnosan	Tercam
3	1983		879	23		Unknown
4	1984		884	28		Construtora Sul Minas
5	1986		889	33		Unknown
6	1990		891.5	35.5		Unienge Com. e Constr. Ltda.
7	1991	Third	895	39	Chammas Engenharia	Construtora Sul Minas
8	1993		899	43		Unknown
9	1995	Fourth	905	49	Tecnosolo	CMS Constr. S.A.
10	1998	Fifth	910	54		U & M
11	2000	Sixth	916.5	60.5		Constr. Dragagem Paraopeba
12	2003	Seventh	922.5	66.5		Construtora Impar Ltda.
13	2004	Eighth	929.5	73.5		Integral
14	2008	Ninth	937.0	81.0	Geoconsultoria	Integral
15	2013	Tenth	942.0	86.0	Geoconsultoria	Salum Enga

Figure 21: The construction stages of the Córrego do Feijãos tailings dam modified from Robertson et al. (2019).

- Poor drainage and the interbedded layers of coarse and fine tailing material resulted in a high water level in the Dam. During the fourth rising stage of the construction, seepage occurred on the face of the Dam. The seepage indicated unsafe conditions. The upper part of the Dam (stages 8, 9, 10, figure 25) consisted of fine material with low permeability, which resulted in saturated layers. Consequently, the material close to the embankment, below the water lever, was weak. Other authors (Grebby et al., 2021; Silva et al., 2020) have also investigated how deformation within the Dam-1 is affected by rainfall. More precisely, Silva et al. (2020) demonstrate how seepage erosion, or piping, clearly influences the stability of the slope. Though, the expert panel did not identify seepage as a triggering mechanism for the failure (Robertson et al., 2019).
- Additionally, a correlation between rainfall periods and the loss of suction in the unsaturated zone of the Dam might also have influenced the Dam's stability. Loss of suction occurs when the unsaturated zone of the tailings becomes saturated due to long-term rainfall. The long-term rainfall will lower the shear strength. More than this, increasing the water level will also increase the hydrostatic pressure and put more load on the tailings. By observing figure 26, it is visually possible to observe an increase in the acceleration coinciding with the periods of most precipitation.
- The chemical composition of the tailings was very high in iron and very low in quartz. Advanced laboratory testing, SEM, CPTU, and FVT data indicated that the tailings had a brittle behavior. The tests also demonstrate that the tailings were saturated, presenting loose behavior, and bonding between the particles. Studies of the soil particles indicated that the bonding derived from clay size iron oxide (Robetson et al., 2019).

With the pre-existing conditions within the Dam, only small triggering factors could potentially cause the failure of the embankment. The report emphasizes that the failure is of a brittle nature. However, creep did cause internal strain and surface deformation over time. Furthermore, the report concludes that a small amount of strain could potentially cause strength loss within the Dam. Strength loss combined with a loss of suction in the unsaturated soil (due to heavy rainfall prior to the failure date) triggered the flow liquefaction and resulted in the flow slide (Robertson et al., 2019).

4.1.2 Surface Displacement

The InSAR data for the Córrego do Feijão tailings dam was retrieved as the mean velocity from the foot of the slope.

The data show continuous displacement from June 2015 to January 2019. With an exception between May and September 2017. There are several hints of acceleration along the displacement curve, and figure 22 shows that an acceleration toward the embankment failure is visible. More than this, at least three other time periods of accelerations are also detectable along the trend line. It is interesting to understand if these hints of acceleration show similar characteristics as the final part of the graph and potentially if the inverse velocity might predict a failure, although this was not the case. Therefore, the inverse velocity will be applied. Though, to start with, the OOA is identified by applying the crossover rule presented by Carla et al. (2017a).

Figure 22: Surface displacement over time and precipitation data over time in the Córrego do Feijão tailings dam (NGI; Visual Crossin Weather, 2021).

4.1.3 Identifying crossover point

In their study, Carla et al. (2017a) suggest plotting the velocity versus time graph for the moving average values. Each plot consists of two moving averages, making it possible to identify changes in the data. The data that presented the most noticeable results for identifying the OOA and EOA was filter 2 data and filter 3 data. Both datasets plotted a c-SMA with n = 3, 4, 7, and a c-LMA with n = 9, 12, 21, and gave similar results.

The most evident moving average results were the c-LMA n= 21 and the c-SMA n=7. For both datasets, three crossover points identified an uptrend, and two crossover points identified a downtrend as demonstrated in figure 23. Therefore, the inverse velocity method was applied to three different time periods. These time periods correspond well

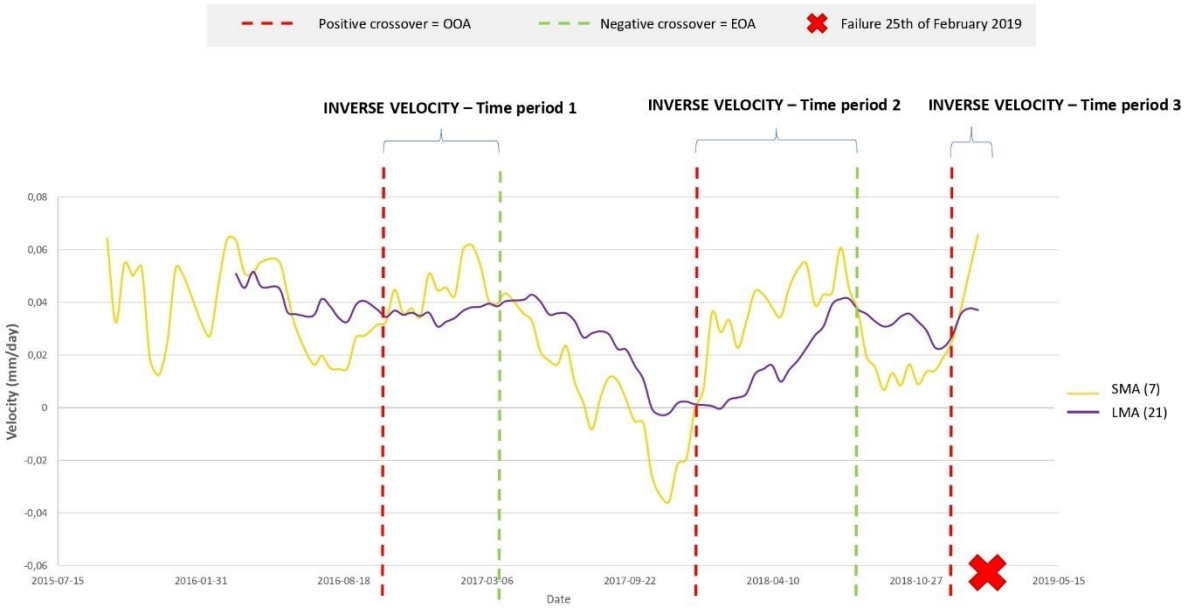

Figure 23: The moving average plot used to identify periods of acceleration in the Córrego do Feijão dam.

with the time periods of acceleration in the displacement surface displacement in figure 26. However, it seems like the OOA for the final section is detected earlier in filter 3 data when utilizing a c-SMA with n = 7, and a c-LMA with n = 21, demonstrated. Using lower MA values, e.g., c-SMA with n = 3, and a c-LMA with n = 9, makes it possible to identify the crossover point earlier. Thus, too much noise is present to retrieve significant time periods to apply the inverse velocity.

4.1.4 Applying the Inverse Velocity Method

According to the method presented by Carla et al. (2017a) the Inverse velocity of the moving average should be applied to the measured points between two crossover points. Furthermore, the inverse velocity linear regression should be plotted for the whole period between two crossover points (see figure 28 – above). However, Carla et al. (2017a) also suggest updating the trendlines and the data based on the best fit to the regression line, which will differ from case to case. The following analysis steps give a complete analytical overview of predicting a potential failure.

- The inverse velocity of the moving average has been plotted within the time period between an OOA and an EOA to predict an eventual failure;
- The regression line of the inverse velocity of the moving average has been updated by removing some outlier values to understand if the indication of failure would be more explicit;
- The regression line of the inverse velocity of the moving average has been plotted as different segments between the OOA and EOA, because multiply regression lines decline towards failures within the same time period;
- Instead of using the inverse velocity of the moving average, the inverse velocity of the different filtered datasets has also been plotted at different sections within the

time periods. By reducing the amount of filtering to the data, it is possible to analyze the best indication of failure.

The following chapter divides into three parts based on the time period (see figure 27) identified for applying the inverse velocity. Filter 1 data had too much noise though this dataset was disregarded. Filter 2 data and filter 3 data show similar results when plotting the inverse velocity of the moving average. Therefore, the description will generally refer to filter 2 data during the analysis of the inverse velocity of the moving average. When notable differences between the different filters, this will be highlighted. All the data is available in Annex 2.

TIME PERIOD 1 - JULY 2016 TO MARCH 2017

First, the inverse velocity linear regression was plotted for the whole period between two crossover points. The trendlines incline towards zero. However, the R2 values are very low, and there is no clear correlation between the points towards failure. As at least four points in the c-LMA (21) time series show some correlation and an inclining trend line, these could be further studied. However, as the smoothening on these points are high, they will show a coherency as demonstrated in figue 24 (bottom left). When plotting only this segment of the time period 1, the predicted failure is about half a year later, and the acceleration could be considered low. To further analyze this section, the data was also plotted with the inverse velocity of filter 4 data as illustrated in figure 24 (bottom right) This section showed two trendlines that predict a potential failure on the 1st of January 2017 and the 5th of May 2017.

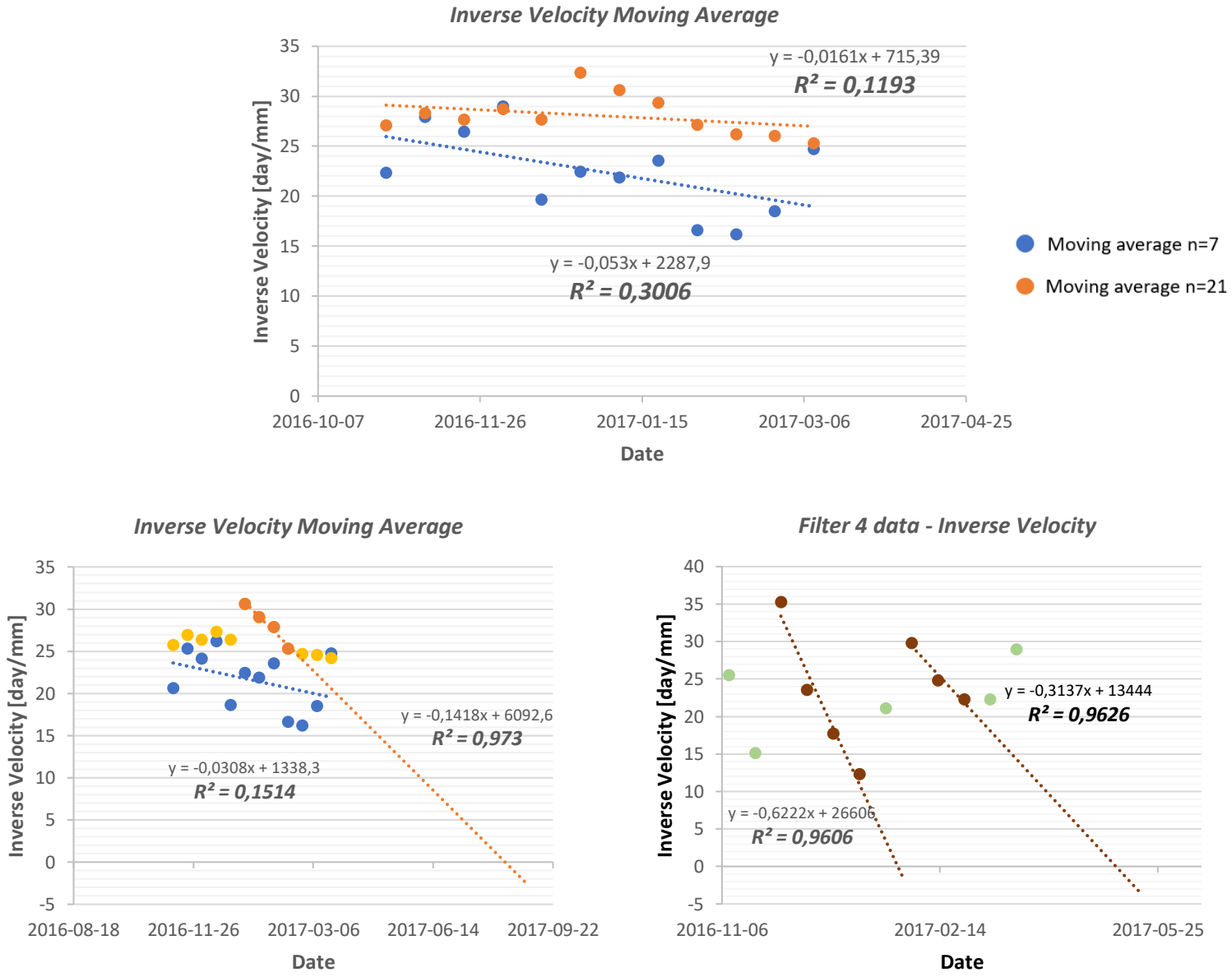

Figure 24: Top graph demonstrate the inverse velocity of the moving average during time period 1. Bottom left corresponds to the updated trendline of the iverse velocity of the moving average during time period 1. Bottom right shows the inverse velocity of filter 4 data during time period 1.

TIME PERIOD 2 - NOVEMBER 2017 TO THE 2ND OF AUGUST 018

When plotting the inverse velocity for the whole time period, the data does not show any significant correlation towards failure, as demonstrated in figure 25 (left). The R^2 is low, and it is not possible to draw a linear trend to predict the failure. However, some of the initial values of the plot are very high and low, which makes it challenging to observe a linear trend within the same range of values when compared to time period 1 or time period 3. Figue 25 (rigth) shows that by excluding the first measurement points, which corresponds to these extreme values (outliers), the updated regression lines towards zero are visible. Though, the R^2 is not considered high.

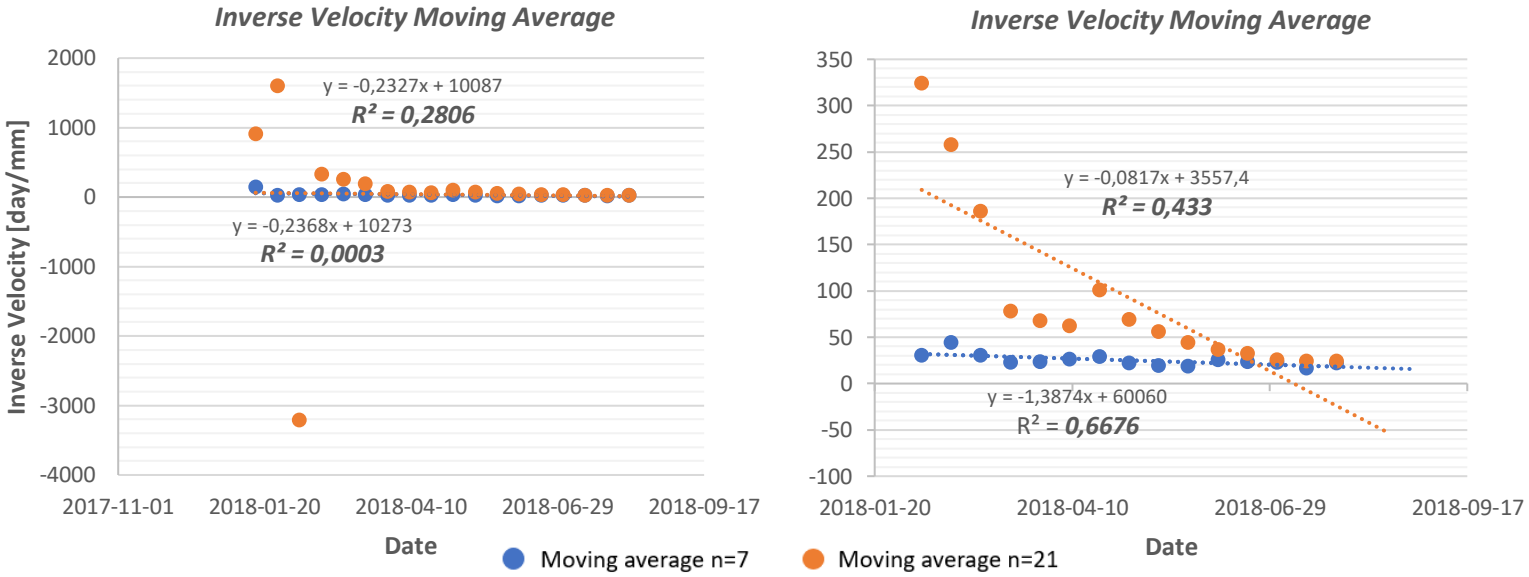

Figure 25: To the left, the inverse velocity of the moving average during the whole time period 2. To the right, the updated inverse velocity by removing the outlier values during time period 2.

When observing the updated trendline in figure 26, it is possible to observe two potential regression lines towards zero. When plotting these two intervals as different segments,

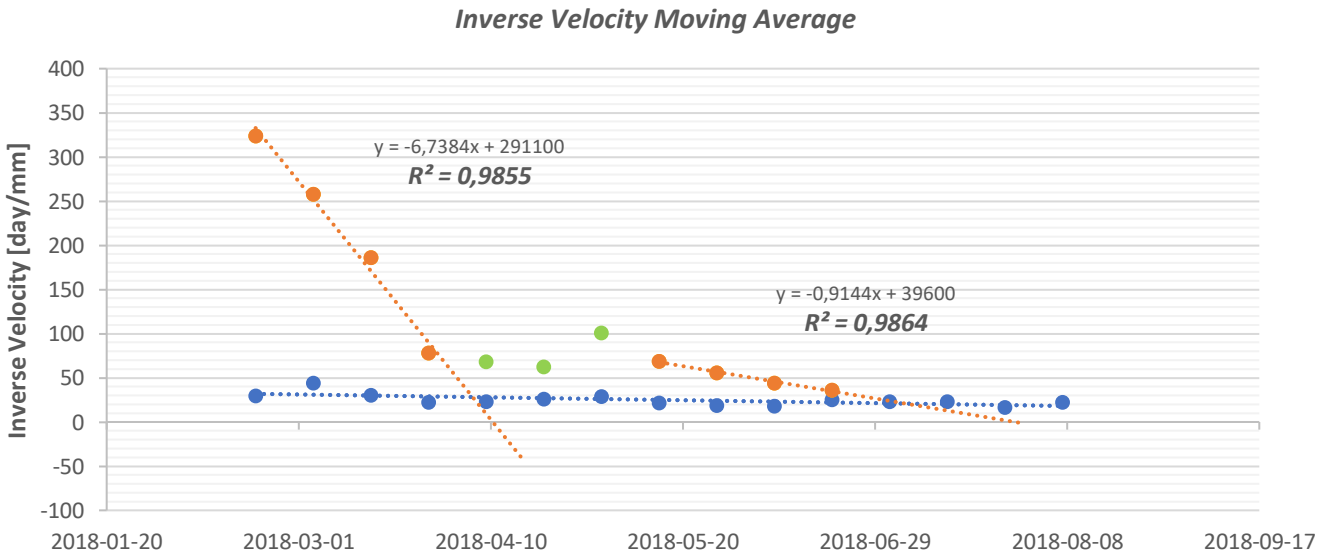

Figure 26: The updated trendline of the inverse velocity with two identified trendlines during time period 2.

two trendlines towards zero becomes evident. As demonstrated in figure 30 the trendlines intersect with the x-axis on the 10th of April 2018 and the 29th of July 2018. More than this, the coherence of the measurement points is high, as the R^2 is 0,98 for both segments. However, it should be kept in mind that this data has the most smoothening applied, resulting in a high coherence.

Furthermore, the inverse velocity of the filter 2 data, the filter 3 data, and the filter 4 data were also plotted. As these contained less filter (smoothing), several trendlines towards zero were also identified within period 2, as shown in Figures 27. Even though the filter 4 data does not have the highest R^2 value between the measurement points, it has several and a clear regression line towards zero. The filter 2 data and filter 3 data had similar results. For filter 2 data, the highest coherence, with a respective R^2 of 0,94, can be found at the first regression line, containing a few points. Thus, three measurement points could be considered too few for a valid indication with little smoothening applied. The other regression lines have a low R^2, with 0,16 and 0,55.

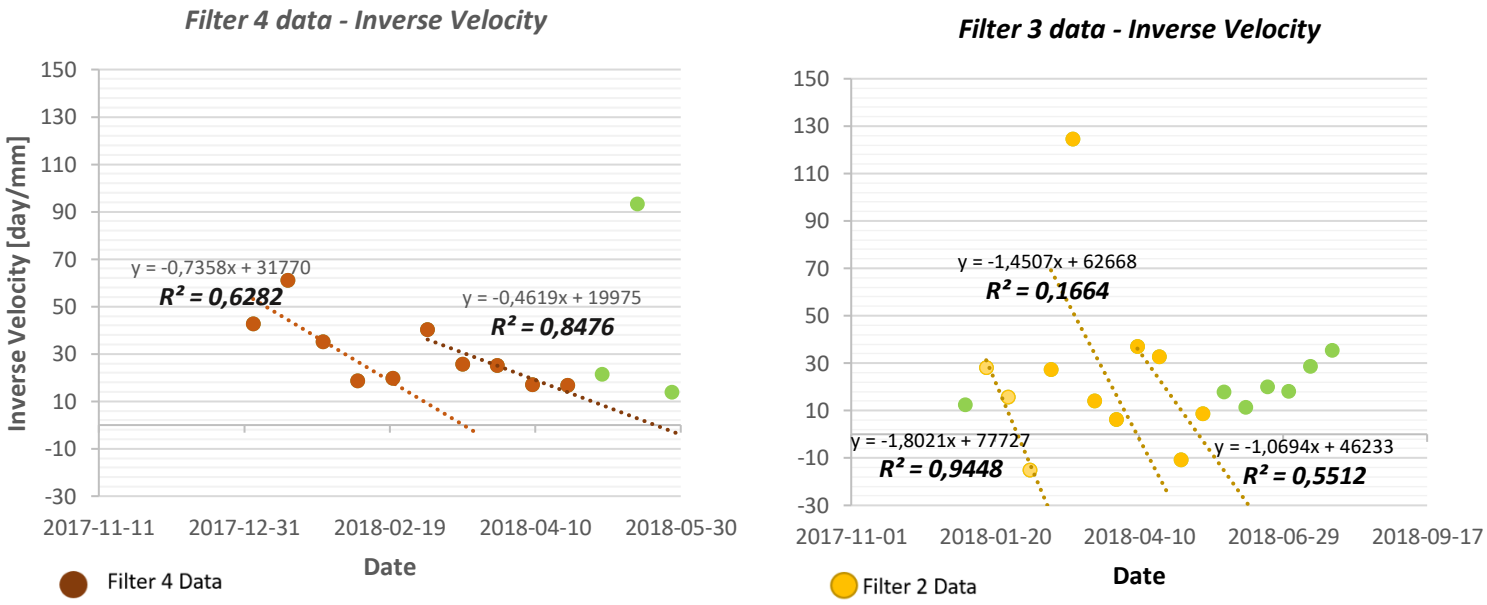

Figure 27: To the left, the inverse velocity of the filter 4 during time period 2. To the right, the inverse velocity of filter 2 data.

TIME PERIOD 3 - DECEMBER 2018 TO JANUARY 2019

The final time period shows a clear regression line towards failure. However, the prediction overestimates the time of failure (13th of February 2019) when using the inverse velocity of the moving average values. It does not coincide close to the real-time failure (25th of January 2019.) There is a slight difference between the filter 2 data and the filter 3 data as the filter 3 data detected the OOA earlier, something that can be seen in figue 28. The inverse velocity can include one more measurement point when applied. Due to high smoothening, there is a delay in detecting the OOA, and few measurement points are plotted before the actual failure. However, none of the data gives a safe estimation of the

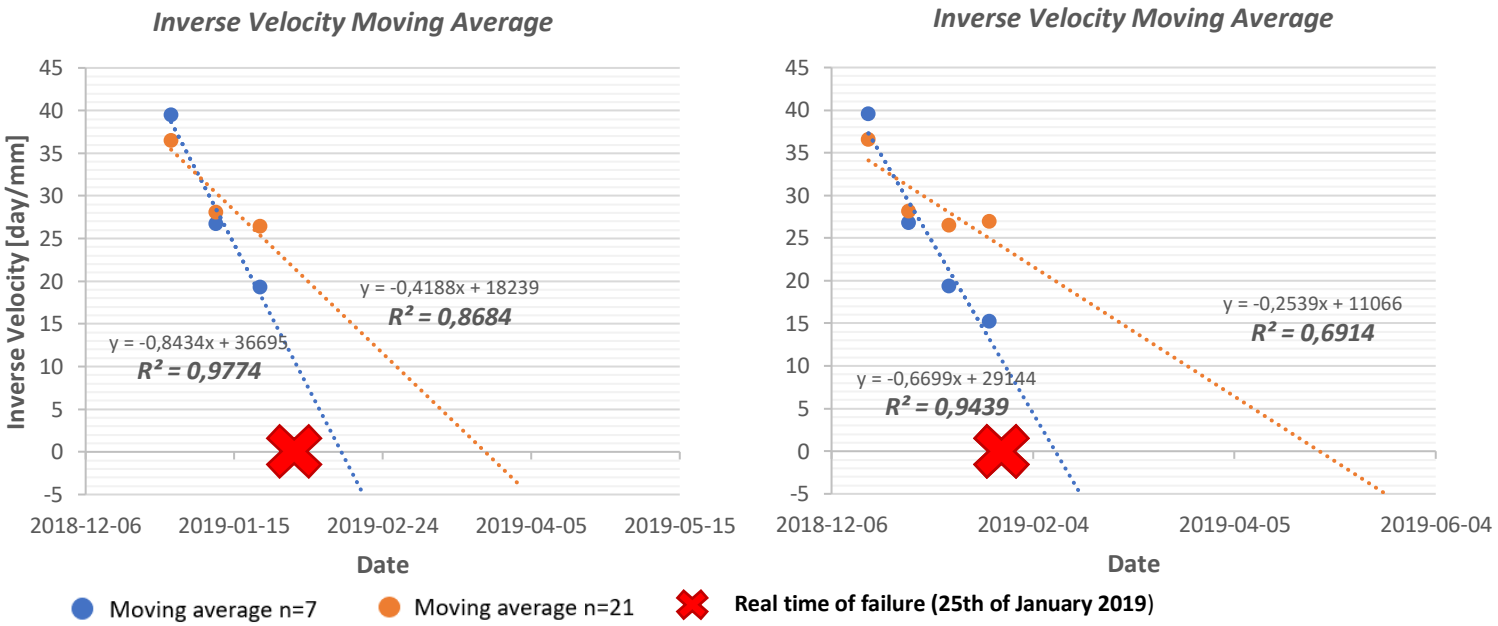

Figure 28: To the left, the inverse velocity of the moving average, calculated with filter 2 data, during time period 3. To the right, the inverse velocity of the moving average, calculated with filter 3 data, during time period 3.

predicted time of failure.

As suggested by Carla et al. (2017a), if the movement rates are low, the time of failure should be predicted while constantly updating c-SMA and c-LMA in accordance with changes in the trend line. For time period 3, coherent results to the real-time failure are observed for the smoothening of the velocity with n=3 and n=9 (figure 34). Using less smoothening on the data, the regression line intersects zero on the x-axis in coherency with the real-time failure.

The results are also apparent when using the inverse velocity of filter 2 data, filter 3 data, and filter 4 data. All the filter data intersect with zero at the exact failure date, the 25th of January 2019. Figure 29 and 30 demonstrate how the less filtered data predict the correct date of failure.

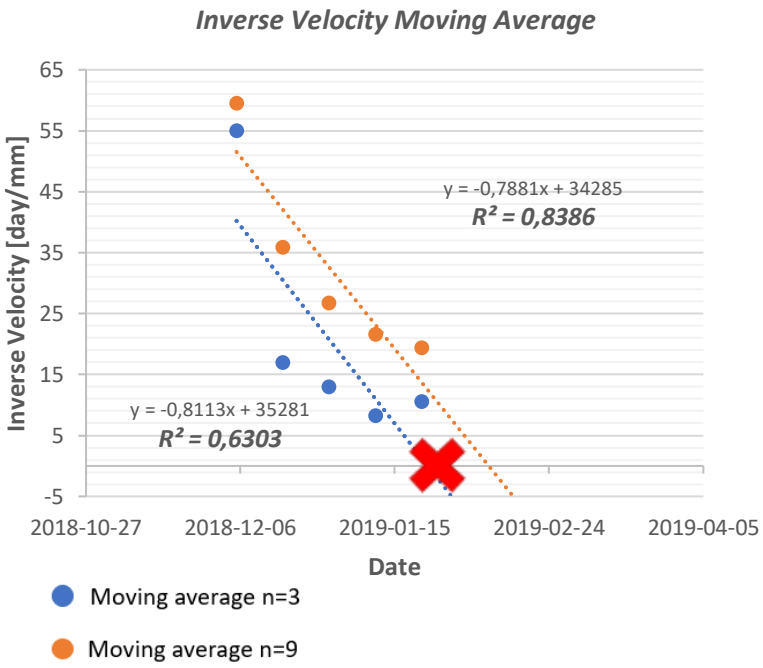

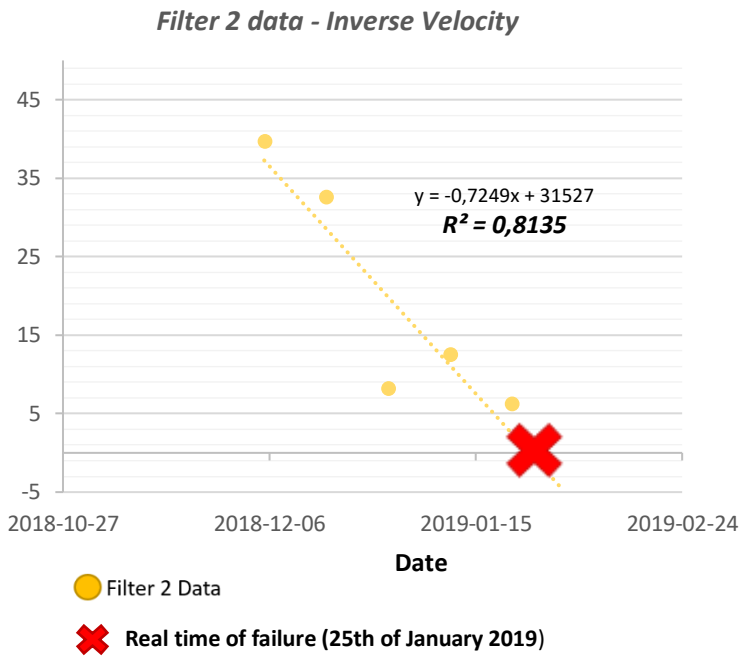

Figure 29: To the left, the inverse velocity of the moving average, during time period 3. To the right, the inverse velocity of Filter 2 data.

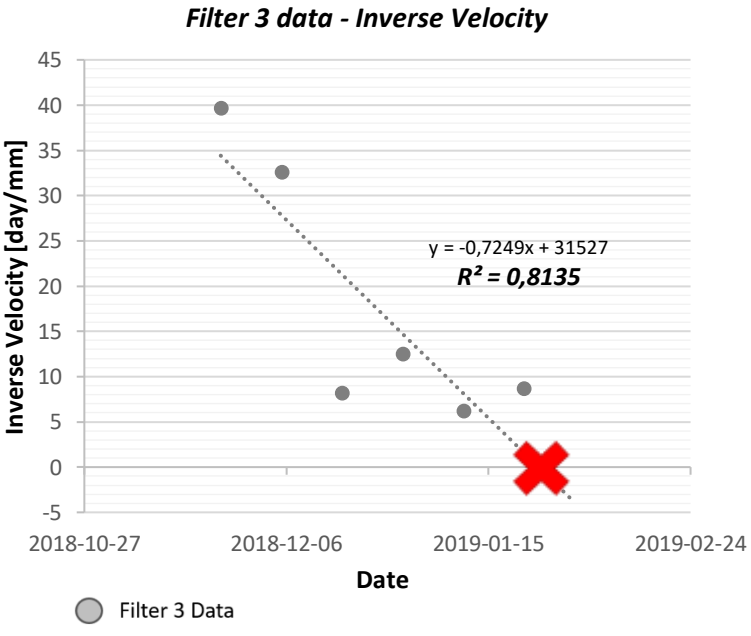

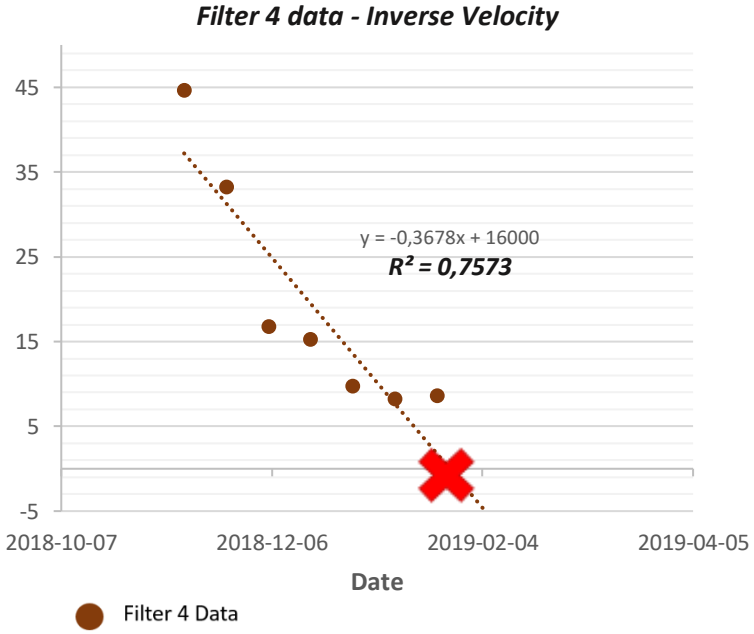

Figure 30: To the left, the inverse velocity of filter 3 data. To the reight, the inverse velocity of filter 4 data.

4.2 The Cadia tailings dam case study

The Cadia Valley Operation is located in the western part of Australia, about 20 kilometers south of Orange. The mine has been in operations since 1998 and is extracting gold and copper. Cadia Valley Operation consists of three mines and two tailings dams, namely the Northern tailings storage facility (NTSF) and the Southern tailings storage facility (STSF). The NTSF is located upstream in Roods Creek, while the STSF is located downstream.

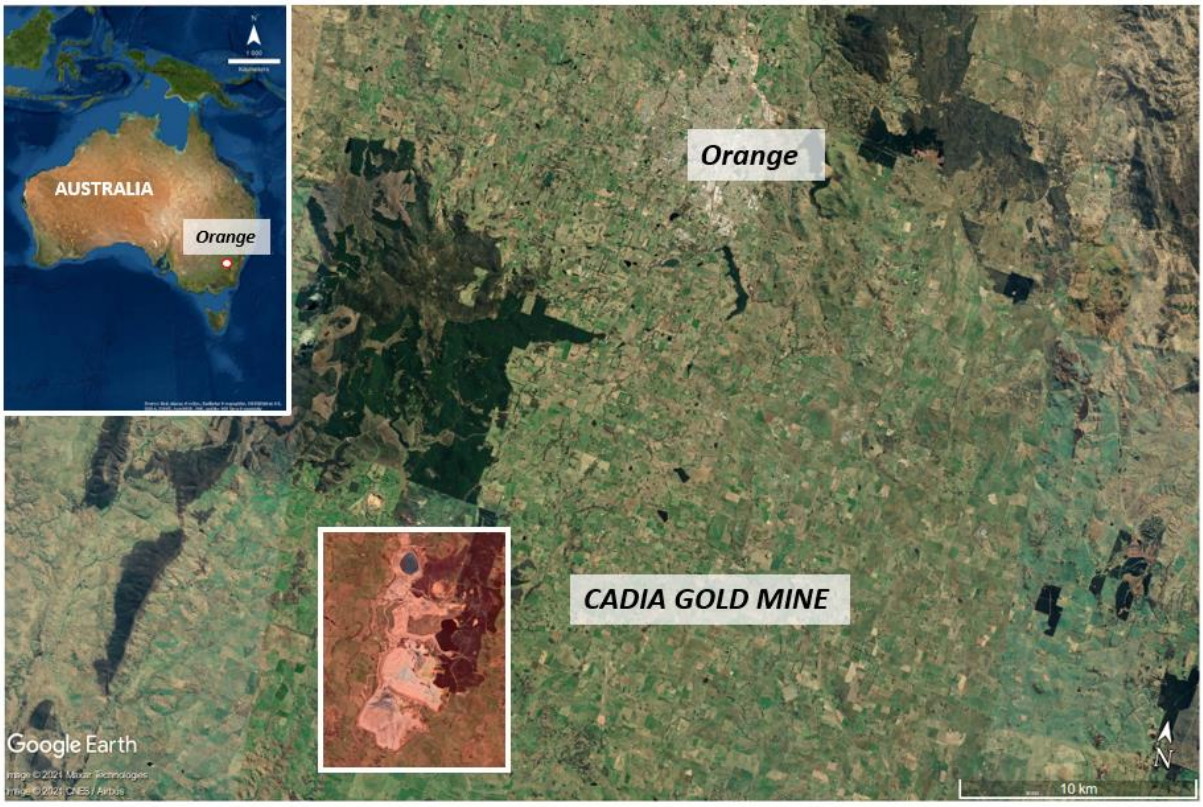

Figure 31: Geographical location of the Cadia Gold mine.

The dam failures progressed on the 8th of March 2018, as the southern wall of the NTSF collapsed into the STSF and contaminated the downstream dam (figure 32). The southern wall bordered the STFS was about 1250 meters long and 95 meters high. The failure resulted in a translational slide, also called a slum. The movement involved a 300 meters wide breach and a 170-meter lateral displacement. In total, more than 1.3 million m^3 of tailings were released during the failure. There were no people harmed during the event, as workers and a few people living downstream were evacuated prior to the failure (Chua et al., 2019; Jefferies et al., 2019).

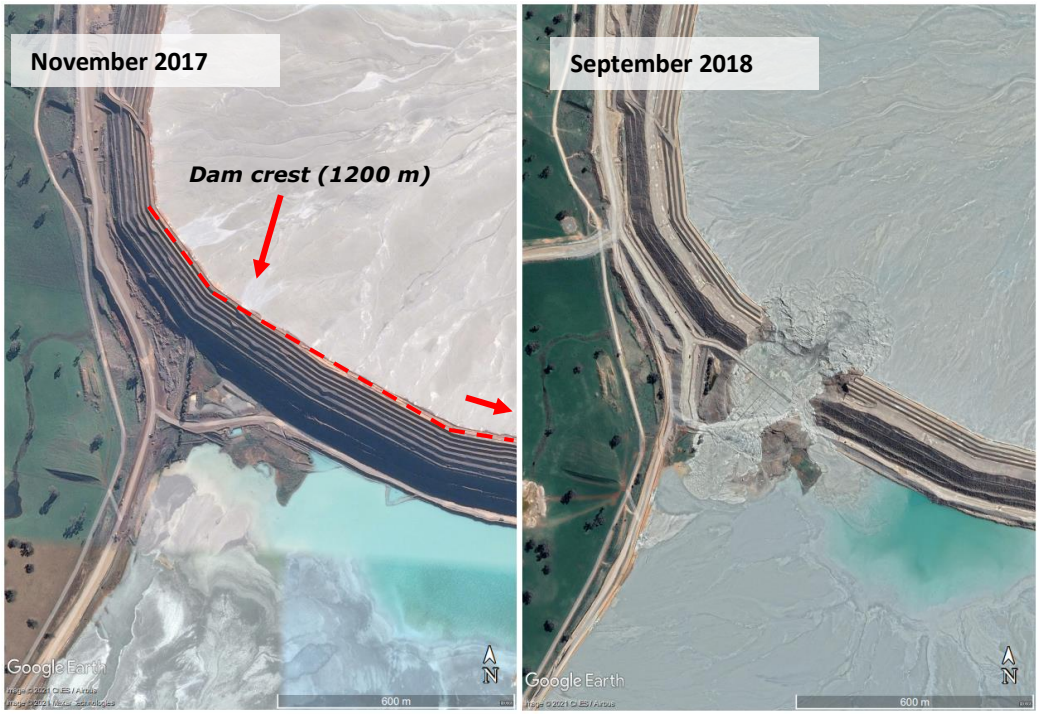

Figure 32: Cadia tailings dam before and after failure.

4.2.1 Potential triggering factors

In April 2019 the Independently Technical Review Board (ITRB) released a comprehensive report on the NTSF embankment failure. They performed a thorough study was about the tailings dam's structural, geological, geotechnical, and tailings components. In the aftermath of the failure, several authors pointed out significant surface displacement on the northern wall of the NTSF in the months prior to failure. Therefore, a progressive failure with slow deformation was considered one of the failure mechanisms. However, the ITRB concluded that the triggering of the failure was due to multiple failure mechanisms, identified as two subsequent events. Below follows a short description of the failure mechanism distinguished by ITRB.

- After the failure, geological investigations found a weak layer in the foundation below the failure zone. This weak layer consisted of Forest Reef Volcanics[3], with low-density materials. The layer was considered weak and highly compressible. When subjected to load, the layer weakens due to strain. Thus, the embankment was built with the upstream method, and the weak layer made the section of the southern wall vulnerable to static load. The foundation became unstable, which caused a horizontal movement outward (figure 33, step 1). The weak layer was located about 1 meter below the foundation level. This weak foundation layer can be considered the most controlling factor that caused the event. The movement of the foundation reduced the support to the tailings, and consequently, the movement increased the stress on the tailings (see figure 33, step 2). When the maximum stress applied to the tailings (or soil) reaches its limit, the strength of the material cannot stand the stress applied and will start to deform permanently. As

[3] The Forest Reef Volcanics originate from the Late Ordovician to Early Silurian. The layer consist "of mafic to intermediate volcanic derived sedimentary breccias and sandstones intercalated with basaltic andesite and andesitic lavas" (Jeffries et al., 2019)

the material is loaded and deformed, it will contract and develop a rise in poor pressure; hence, undrained conditions are suddenly present in the tailings. The undrained condition will again lower the shear strength of the tailings significantly, and consequently, the structure between the soil particles will collapse, and the tailings will turn liquid. Though, liquefaction occurred.

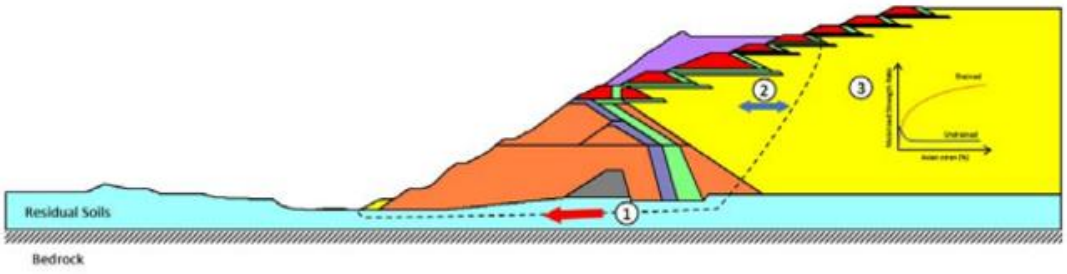

Figure 33: Failure mechanism of the Cadia mine modified by Jeffries et al. (2019).

- The second phase of the failure consisted of displacing a large portion of the embankment—an increase in the loading on the embankment explains the displacement. The liquefaction of the tailings causes the loading. As mentioned in chapter 2.2, two processes might cause liquefaction, namely static loading or earthquake. The movement of the weak foundation layer lowered the shear strength of the loose tailings and induced static liquefaction. More than this, the day before the failure, two small earthquakes occurred at the NTSF. However, in ITRB concluding remark, they disregard the hypotheses of the earthquakes inducing the liquefaction, as they indicate that the first phase of the failure mechanism was quite advanced before the earthquakes occurred.

Additionally, to the different mechanisms of failure, several other factors contributed to the destabilization of the slope. The dam's height decreased to the west. At the same time, the embankment to the east had been stabilized by a buttressed. This imbalances distribution of stability measurement on the dam structure implied that the western part of the embankment where the failure occurred had fewer stabilization measurements and consequently was more susceptible to failure than the eastern side of the embankment. Furthermore, the phreatic level was at its highest level. There was also an ongoing excavation on the toe of the slope to construct a buttressed at this part of the embankment. Though, the excavations generated instability to the slope.

In general, a combination of all these causes generated a low-resistant foundation. At the same time, the liquefaction and the increase in the hydrostatic pressure imposed loading on the structure. Eventually, it is clear that the resisting forces did not stand the driving forces, and with the liquefaction of the tailings, the dam breached.

4.2.2 Surface Displacement

The InSAR data for the Cadia tailings dam was retrieved as the mean velocity from a single point on the top of the slope.

The InSAR data shows some surface deformation of around 18 mm at the beginning of the period, and then the surface displacement is evident from September and onward. The surface displacement was constant until the dam's wall failed, indicated by a significant acceleration and notable displacement (figure 34). There was a surface displacement of 100 mm from January 2017 to March 2018. The crossover rule identified the onset of acceleration and made it possible to understand where the inverse velocity method should be applied.

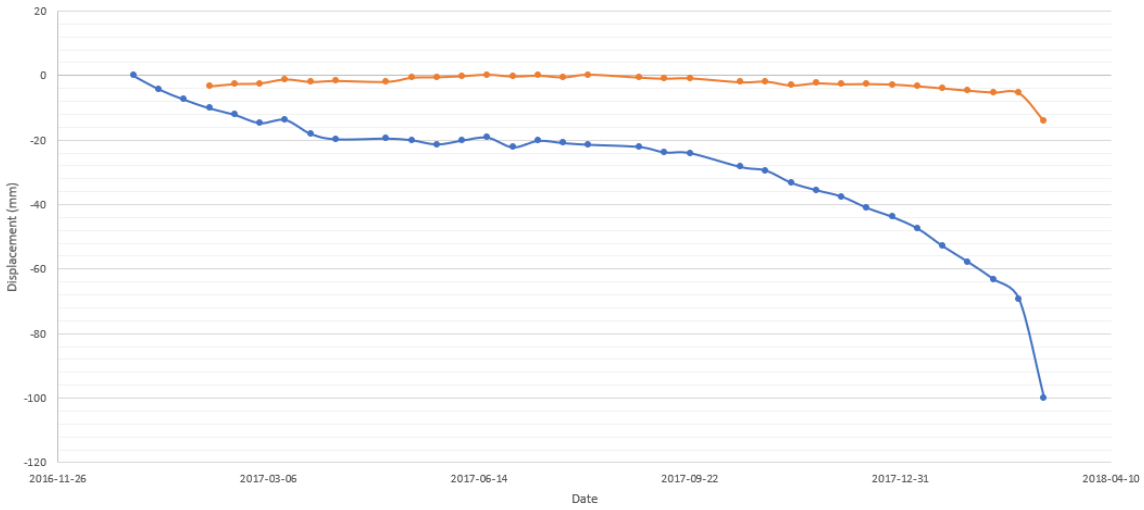

Figure 34: Surface displacement over time (NGI).

4.2.3 Identifying crossover points

The Cadia Dam's filter 1 data (the raw data) demonstrated precise results. Several moving averages evaluated the filter 1 data, where c-SMA was plotted with n = 1, 2, 3, 4, and 7, and c-LMA with n = 3, 6, 9, 12, and 21. A second dataset of the averaged difference of displacement (dataset 2) was also used to compare different moving averages. However, the raw data presented the most coherent result, and dataset 2 will not be presented here.

One OOA point was identified as most significant and was found by using different moving average plots c-SMA with n = 3, 4 or 7 and c-LMA with n = 9, 12 or 21. From c-SMA with n = 1 or 2 and c-LMA with n = 3 or 6 there were several OOAs and EOAs. However, as these points are changing fast, they are not considered as any long-term trend changes and are therefore not of significant importance. The moving average with the most evident result was the c-SMA with n = 4 and c-LMA with n = 12 as demonstrated in figure 35.

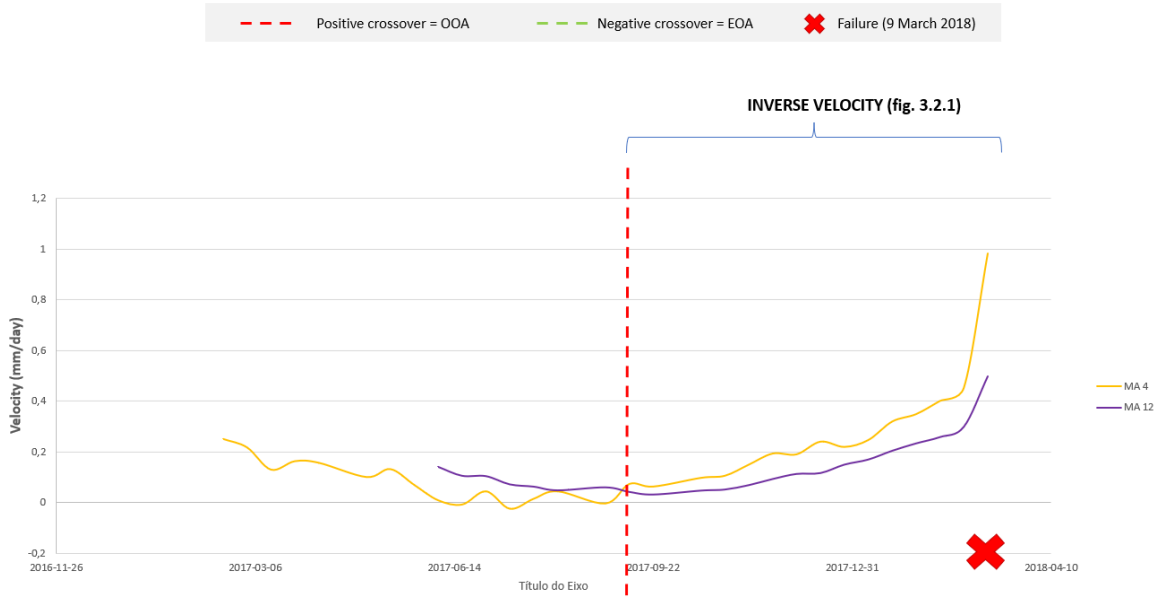

Figure 35: The moving average plot used to identify periods of acceleration in the Cadia dam.

4.2.4 The inverse velocity method

The inverse velocity data was plotted between the OOA until failure. Firstly, the inverse velocity was plotted with the moving average data. The results show that the c-LMA predicts a failure some days before the real failure, and the c-SMA predicts a failure upon the day of real failure as demonstrated in figure 36 (top). The R^2 can be considered high, and there is a relatively good correlation between the points. The inverse velocity was also plotted with the raw data and the filter 3 data. Even though the correlation between the points is low, the trendline still predicts a failure before the real date of failure with both these datasets, as shown in figure 36 (bottom).

Figure 36: On the top, the inverse velocity of the moving average. On the bottom, the inverse velocity of filter 1 data and filter 2 data.

5 Discussion

Even though the inverse velocity method is widely used for slope failure prediction, the method is relatively new to the field. Already published articles on the concept mainly consider tailings dam failures from the last decade. This study has tried to widen the understanding of how the inverse velocity method can predict tailings dam failures.

5.1 How can the Inverse Velocity method be applied to predict Tailings Dam failures?

According to the conclusion by the Expert Panel (Robertson, 2019), the stiff tailings in the Córrego do Feijão Dam provoked a sudden collapse of the soil structure. As Gama et al. (2020) point out in their conclusion, satellite data might not capture the fast acceleration prior to failure; thus, the revisiting time of the satellite does not apply to sudden collapses. Even though the InSAR data do not provide detailed information about the Córrego do Feijão Dam, Gama et al. (2020) highlight that the data would provide decision-makers with information about stability issues on the dam. Grebby et al. (2021) accentuate the same benefits of using InSAR data prior to the failure of the Córrego do Feijão Dam. However, the results in this study indicate that the acceleration of the deformation rate prior to the failure might not be anomalous behavior for the dam. Instead, by analyzing the Córrego do Feijão dam back to 2015, it is possible to observe that a similar behavior prior to the failure is observable in two other time periods. There is a clear relationship between the rainfall pattern and the acceleration of the deformation. Thus, this raises an evident challenge of using the inverse velocity on tailings dams; it might be challenging to differentiate the cyclic behavior in a tailings dam from failure behavior, especially if the data does not cover a long enough time period.

Several filters were applied to experiment how the inverse velocity method could be applied to the Córrego do Feijão dam. Using the crossover method presented by Carla et al. (2017a), the most prominent moving average plot detects the onset of acceleration three measurement points before failure. Applying the inverse velocity on these few measurement points results in an overestimation of the real-time of failure in accordance with the results presented by Gama et al. (2020). When using less filtered data, which other authors also have done (Grebby et al., 2021; Voge et al., 2021), more measurement points are plotted, and the regression line is more coherent as it intersects with the x-axis at the same date as the failure. However, assuming that the reliability of the less filtered data is more coherent with the real-time of failure, it is of interest to observe other time periods of accelerations in 2017 and 2018 (time series 1 and time series 2). Within these periods, several regression lines towards failure are plotted, and there are indications of failure (even though it did not occur) in January 2017, May 2017, April 2018, and July 2018. The Córrego do Feijão case study demonstrates that the prediction of the tailings dam failure is conditioned by the filters applied to the velocity and the numbers of measurement points included in the inverse velocity analysis.

For the Cadia tailings dam the situation is quite different. There was only one significant period of acceleration for the time studied. The results of this study are in accordance with the results presented by Chua et al. (2019) and Thomas et al. (2019). The onset of

acceleration was identified using the crossover method. When plotting the inverse velocity of the moving average, the c-LMA trendline intersected the x-axis prior to the failure. The c-SMA trendline intersected the x-axis upon the day of failure. Conclusively, the crossover rule and the inverse velocity method's application gave reliable results that could be used to predict a failure.

The Inverse Velocity method has been widely used for early warning of slope instability. In general, the velocity curve increases exponentially, as demonstrated by Fukozona (1985) and Carla et al. (2017a). The data used in this study shows that the deformation curve in the Cadia dam indicates an acceleration in line with what has been presented by Fukozona (1985) and Carla et al. (2017a). Concerning the Córrego do Feijão failure Grebby et al. (2021) highlights that a clear acceleration rate of deformation is visible from October 2018 until failure in January 2019. Oppositely, this study indicates that even though an acceleration rate is accentuated, the acceleration rate towards failure is not very significant and similar periods of acceleration rates are present when analyzing data back to 2015. When comparing the Córrego do Feijão case to the Cadia case the acceleration of deformation rate becomes evident. For a visual understanding, figure 37 illustrates how the dams differ in acceleration. The red squares correspond to the time periods of acceleration identified from the moving average.

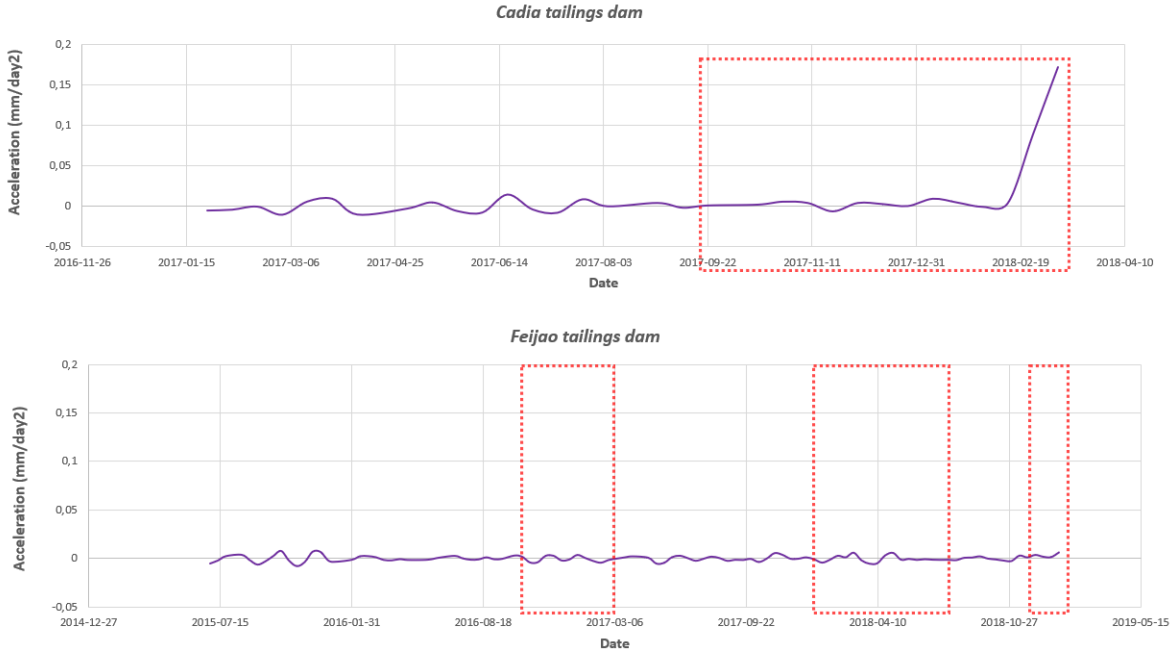

Figure 37: Illustration of the acceleration in the Cadia tailings dam and the Córrego do Feijão tailings dam.

5.2 What are the limitations of the Inverse Velocity Method when using InSAR data in a tailings dam context?

Chapter 2.4.2 refers to the main limitations regarding the inverse velocity method itself. However, some of the main limitations of applying the method to tailings dams will be briefly mentioned here.

The inverse velocity remains subjective. The number of measurement points used when applying the inverse velocity may differ between cases and authors. The studies presented by Gama et al. (2020) use a moving average of 21 measurement points, while Grebby et

al. (2021) applied a 3-point moving average, and Voge et al. (2021) based their predictions on a 7-point moving average. All authors studied the Córrego do Feijão tailings dam over approximate time periods. Knowing the real-time of failure, the data can be filtered in the best way to obtain reliable results. In the Córrego do Feijão case, the moving average with elevated smoothening identified the acceleration periods. However, less filtering showed to be much more adequate when predicting the failure when referencing the data to the real-time of failure. In the Cadia dam case, the filter used to identify the periods of acceleration gave a reliable result when predicting the failure with the inverse velocity method. The moving average of c-SMA n=4 and c-LMA n=12 gave the best results for identifying periods of acceleration. When applying the inverse velocity method, the c-SMA predicted failure coincides with the failure's real-time. Additionally, the c-LMA predicted the failure before the real-time of failure. Less filtered data also gave coherent indications of the real-time of failure; thus, the more smoothened data presented a more reliable inverse trendline. Even though the subjectivity of the method is a limitation that Carla et al. (2017a) aims to overcome with the crossover rule, the Córrego do Feijão case confirms that by aiming to obtain the most coherent results, the processing and filtering remain subjective.

As pointed out by several authors (Carla et al., 2017a; Gama et al., 2020; Grebby et al., 2021; Voge et al., 2021) the method is limited to be applied to the case studies where deformation occurs over time. Hence, this method will not monitor brittle tailings dam failure. However, as this study demonstrates, it is crucial to understand the reason for failure correctly. Relying too much on the InSAR data might make the monitoring "overlook" other reasons for failure. In the case of the Córrego do Feijão dam, the InSAR data shows deformation since 2015, which the expert panel concludes is coherent with the long-term settlement of the dam (Robertson et al., 2019). However, the total displacement of the dam was about 40-50 mm, which from a geotechnical perspective is relatively little settlement for a structure of this dimension over a 4-year period. Thus, this is not necessarily coherent with a long-term settlement of typical tailings that consist of loose granular material. The Cadia dam deformed 80 mm in a time period of 2 months hence the settlement in the Córrego do Feijão dam can be considered a low settlement rate, probably conditioned by the tailings' brittle behavior with a stiff structure. The low settlement rates prior to the failure could in itself raise specific alerts about the stiff structure of the tailings and the susceptibility to brittle failure. Even though none of these factors were displayed prior to the failure of the Córrego do Feijão mine this study emphasizes the importance of correctly interpret the geotechnical conditions in coherence with the InSAR data..

5.3 Is the inverse velocity method reliable when predicting tailings dam failure?

Several authors have investigated the use of the inverse velocity method based on InSAR data to predict tailings dams failure (Chua et al., 2019; Gama et al., 2020; Grebby et al., 2021; Voge et al., 2021). It is important to consider that tailings dams have a much more unpredictable behavior than water dams or slopes. The tailings consist of loose granular material, differing in composition and properties, which make the tailings behave unexpectedly. The unpredictable behavior is undoubtedly a factor contributing to a large amount of failures. However, it also implies that it is difficult to have a monitoring system to predict eventual failures that should work equally well for all tailings dams. This study has demonstrated that the inverse velocity can be of great advantage when predicting

tailings dam failures, for example, with the case of Cadia tailings dam. However, the method might also be subjective and not necessarily coherent with the real-time of failure as for the Córrego do Feijão tailings dam. It is noteworthy that the reliability of the inverse velocity method to a great extent depend upon the failure mechanism of the tailings dam.

This study shows that the inverse velocity method might give reasonable indications on deformation and potential failures and can definitely serve as a complementary monitoring tool in tailings dams. The same argument is put forward of all the authors that conducted studies over the same area (Chua et al., 2019; Gama et al., 2020; Grebby et al., 2021; Voge et al., 2021). Two findings were retrieved from this study as suggestions for a more reliable usage of the inverse velocity method. First, to apply the inverse velocity method, the user needs to consider tailings dams' long-time behavior. Cyclic behavior might influence the surface displacement in a tailings dam. Only considering the behavior in the year/month prior to failure will exclude information about the dam's long-term behavior, which might be crucial to understand the dam's failing mechanism. Second, Grebby et al. (2021) emphasize the benefits of using InSAR data to monitor tailings dams remote and cost-effectively, and additionally the precise achievement of applying the inverse velocity method to the Córrego do Feijão tailings dam. The results of the current study differs from what Grebby at al. (2021) presented, as they underscores that caution needs to be taken when using InSAR data as a monitoring tool. Even though there are signs of surface displacement and acceleration in the InSAR data, this is not necessarily what will lead to failure. A sudden collapse caused by another failure mechanism might occur and relying too much on the InSAR data might cause a lack of attention to other plausible causes. Thus, in-situ monitoring tools should always complement the satellite data.

6 Conclusion

The main objective of this research has been to understand the reliability of using the inverse velocity method in the context of tailings dams failures. The method presented by Carla et al., (2017a) was used as guidance to apply the inverse velocity method to the InSAR data.

The following conclusions have been retrieved through this investigation:

- The InSAR method provides valuable information when observing surface deformation in Tailings Dams. Both case studies demonstrate how the InSAR technique manages to give access data covering the whole area of the tailings dams.
- The InSAR monitoring should be complemented with precise in-situ monitoring. Failure might be triggered by other causes such as a sudden loss of strength, structural anomalies, or seismic activity. Relying solely on measurements from displacement data can take away the attention from other relevant failure mechanisms.
- The InSAR data provides reliable data for the inverse velocity method, and the method seems to be useful to indicate a failure e.g. in the Cadia tailings dam. In such cases, integrating the inverse velocity method to an early-warning system would provide adequate data to predict and mitigate future tailings dams failure.
- Even though the method presented by Carla et al. (2017a) gives a good indication of where and how to apply the inverse velocity method, the method remains subjective. By using different filters on the data, the predicted failure time will vary. The case study of Córrego do Feijão tailings dam exemplifies how several authors have predicted different dates of failure by using different filtering on the same case study.
- Using the method over a more extended time period seems to give a more comprehensive understanding of the long-term behavior of the dam. Cyclic behavior or settlement might cause an increase in the displacement rate during different time periods.

This study has identified numerous fields that are of interest to investigate further.

- To better understand how to interpret the acceleration trends prior to failure, additional studies on surface displacement in tailings dams where failures have not yet occurred should be conducted. Observing the displacement curve over more extended periods of time might indicate significant failure precursors.
- Further studies on the relationship between surface deformation and the tailings properties would map out what kind of movement could be expected from the different types of tailings. This would facilitate the deformation curve interpretation and help distinguish cyclic behavior or settlement from the acceleration prior to failure.
- The guidelines provided by Carla et al. (2017a) could be applied to more tailings dams case studies to know if the method on a general basis is as useful for tailings dams failures as for slope failures. Additionally, comparing the results of the different applications could help specify how to improve the method.

7 References

Adamo, N., Al-Ansari, N., Sissakian, V., Laue, J., & Knutsson, S. (2020). Dam Safety: Monitoring of Tailings Dams and Safety Reviews. Journal of Earth Sciences and Geotechnical Engineering, 11, 249-289. doi:10.47260/jesge/1117

BHP, Broken Hill Proprietary Company Limited (2019). ESG briefing: Tailings dams. Retrieved from https://www.bhp.com/sustainability/tailings-storage-facilities/what-are-tailings-storage-facilities

Biggs, J., & Wright, T. J. (2020). How satellite InSAR has grown from opportunistic science to routine monitoring over the last decade. Nature Communications, 11(1), 3863. doi:10.1038/s41467-020-17587-6

Bowker, L. N., & Chambers, D. M. (2017). In the dark shadow of the supercycle tailings failure risk & public liability reach all time highs. Environments (Basel, Switzerland), 4(4), 1-21. doi:10.3390/environments4040075

Bowker, L. N., & Chambers, D. M. (2015). The Risk Public Liability & Economics of Tailings Facility Failures.

Calvo, G., Mudd, G., Valero, A., & Valero, A. (2016). Decreasing Ore Grades in Global Metallic Mining: A Theoretical Issue or a Global Reality? Resources, 5(4). doi:10.3390/resources5040036

Carlà, T., Intrieri, E., Di Traglia, F., Nolesini, T., Gigli, G., & Casagli, N. (2017a). Guidelines on the use of inverse velocity method as a tool for setting alarm thresholds and forecasting landslides and structure collapses. Landslides, 14(2), 517-534. doi:10.1007/s10346-016-0731-5

Carlà, T., Intrieri, E., Farina, P., & Casagli, N. (2017b). A new method to identify impending failure in rock slopes. International Journal of Rock Mechanics and Mining Sciences, 93, 76-81. doi:10.1016/j.ijrmms.2017.01.015

Chua, S., Fuhrmann, T., & Garthwaite, M. (2019). Leveraging open-access remote sensing imagery to monitor dam infrastructure: Case study of the Cadia tailings dam collapse, Australia.

Cigna, F., & Tapete, D. (2021). Present-day land subsidence rates, surface faulting hazard and risk in Mexico City with 2014–2020 Sentinel-1 IW InSAR. Remote sensing of environment, 253, 112161. doi:https://doi.org/10.1016/j.rse.2020.112161

Davies, M. P. (2002). Tailings impoundment failures Are geotechnical engineers listening? GEOTECHNICAL NEWS-VANCOUVER-, 20(3), 31-36.

Jefferies, M., Morgenstern, R, N., Zyl, V, D., and Wales, J., (2019). Report on NTSF Embankment Failure, Cadia Valley Operation for Ashurts Australia. Retrieved from https://www.newcrest.com/sites/default/files/2019-10/190417_Report%20on%20NTSF%20Embankment%20Failure%20at%20Cadia%20for%20Ashurst.pdf

Ferretti, A., Monti-Guarnieri, A., Prati, C., Rocca, F., & Massonet, D. (2007). InSAR Principles - Guidelines for SAR Interferometry Processing and Interpretation. ESA Training Manual, 19.

Fundao Tailings Dam Review Panel. (2016). Report on the Immediate Causes of the Failure of the Fundão Dam Retrieved from https://www.resolutionmineeis.us/sites/default/files/references/fundao-2016.pdf

Fukuzono, T. (1985). A Method to Predict the Time of Slope Failure Caused by Rainfall Using the Inverse Number of Velocity of Surface Displacement. Landslides, 22(2), 8-13_11. doi:10.3313/jls1964.22.2_8

Gama, F., Mura, J., Paradella, W., & Oliveira, C. (2020). Deformations Prior to the Brumadinho Dam Collapse Revealed by Sentinel-1 InSAR Data Using SBAS and PSI Techniques. Remote Sensing, 12, 3664. doi:10.3390/rs12213664

Global Tailings Portal. (2019). Retrieved from https://tailing.grida.no/#header.

Global Tailings Review (2020). Retrieved from https://globaltailingsreview.org/?lang

Grebby, S., Sowter, A., Gluyas, J., Toll, D., Gee, D., Athab, A., & Girindran, R. (2021). Advanced analysis of satellite data reveals ground deformation precursors to the Brumadinho Tailings Dam collapse. Communications Earth & Environment, 2(1). doi:10.1038/s43247-020-00079-2

Klohn, E. J. (1979a). Seepage Control for Tailings Dam In Tailings and Waste Dispostal - Seepage, Contamination, Regulations and Control.

Hussain, E., Novellino, A., Jordan, C., & Bateson, L. (2021). Offline-Online Change Detection for Sentinel-1 InSAR Time Series. Remote Sensing, 13(9), 1656. Retrieved from https://www.mdpi.com/2072-4292/13/9/1656

ICOLD, The International Comission on Large Dams (2001). Tailings Dams Risk of Dangerous Occurrences, Bulletin 121. Retrieved from https://ussdams.wildapricot.org/resources/Documents/ICOLD%202001%20Bulletin%20121.pdf

Intrieri, E., Carlà, T., & Gigli, G. (2019). Forecasting the time of failure of landslides at slope-scale: A literature review. Earth-science reviews, 193, 333-349. doi:10.1016/j.earscirev.2019.03.019

Klohn, E. J. (1979a). Seepage Control for Tailings Dam In Tailings and Waste Dispostal - Seepage, Contamination, Regulations and Control.

Kossoff, D., Dubbin, W. E., Alfredsson, M., Edwards, S. J., Macklin, M. G., & Hudson-Edwards, K. A. (2014). Mine tailings dams: Characteristics, failure, environmental impacts, and remediation. Applied geochemistry, 51, 229-245. doi:10.1016/j.apgeochem.2014.09.010

Lauknes, T. R., Shanker, A., Dehls, J., Zebker, H., Henderson, I., & Larsen, Y. (2010). Detailed rockslide mapping in northern Norway with small baseline and persistent scatterer interferometric SAR time series methods. Remote sensing of environment, 114, 2097-2109. doi:10.1016/j.rse.2010.04.015

Lin, Y. N., Park, E., Wang, Y., Quek, Y. P., Lim, J., Alcantara, E., & Loc, H. H. (2021). The 2020 Hpakant Jade Mine Disaster, Myanmar: A multi-sensor investigation for slope failure. ISPRS Journal of Photogrammetry and Remote Sensing, 177, 291-305. doi:https://doi.org/10.1016/j.isprsjprs.2021.05.015

Lyu, Z., Chai, J., Xu, Z., Qin, Y., & Cao, J. (2019). A Comprehensive Review on Reasons for Tailings Dam Failures Based on Case History. Advances in Civil Engineering, 2019, 4159306. doi:10.1155/2019/4159306

Morgenstern, N. R. (2018). Geotechnical risk, regulation, and public policy.

NASA, National Aeronautics and Space Administration (2022). What is Synthetic Aperture Radar? Retrieved from https://earthdata.nasa.gov/learn/backgrounders/what-is-sar

Owen, J. R., Kemp, D., Lèbre, É., Svobodova, K., & Pérez Murillo, G. (2020). Catastrophic tailings dam failures and disaster risk disclosure. International journal of disaster risk reduction, 42, 101361. doi:10.1016/j.ijdrr.2019.101361

Pettorelli, N., Schulte to Buehne, H., Shapiro, A., & Glover-Kapfer, P. (2018). Conservation Technology Series Issue 4: SATELLITE REMOTE SENSING FOR CONSERVATION.

Rana, N. M., Ghahramani, N., Evans, S. G., McDougall, S., Small, A., & Take, W. A. (2021). Catastrophic mass flows resulting from tailings impoundment failures. Engineering Geology, 292, 106262. doi:https://doi.org/10.1016/j.enggeo.2021.106262

Rico, M., Benito, G., Salgueiro, A. R., Díez-Herrero, A., & Pereira, H. G. (2008). Reported tailings dam failures. A review of the European incidents in the worldwide context. J Hazard Mater, 152(2), 846-852. doi:10.1016/j.jhazmat.2007.07.050

Robertson, P. K., L.d. Melo, D.J. Williams, and G.W. Wilson. (2019). Report of the Expert Panel on the Technical Causes of the Failure of Feijão Dam I. Retrieved from https://www.resolutionmineeis.us/documents/robertson-et-al-2019

Roche, C., Thygesen, K., and Baker, E., . (2017). Mine Tailings Storage: Safety Is no Accident. UN Environment. Retrieved from GRID-Arendal:

Rose, N. D., & Hungr, O. (2007). Forecasting potential rock slope failure in open pit mines using the inverse-velocity method. International Journal of Rock Mechanics and Mining Sciences, 44, 308–320. doi:10.1016/j.ijrmms.2006.07.014

Rosen., J. (2021). Fleets of radar satellites are measuring movements on Earth like never before. Science. doi:doi: 10.1126/science.abh2435

Rouyet, L., Lauknes, Tom Rune., Høgda, Kjell-Arild. (2015). Satellittbasert radarinterferometri (InSAR) for naturfare, skred og infrastruktur. Retrieved from Norges Vassdrags- og Energidirektorat

Silva Rotta, L. H., Alcântara, E., Park, E., Negri, R. G., Lin, Y. N., Bernardo, N., . . . Souza Filho, C. R. (2020). The 2019 Brumadinho tailings dam collapse: Possible

cause and impacts of the worst human and environmental disaster in Brazil. International Journal of Applied Earth Observation and Geoinformation, 90, 102119. doi:https://doi.org/10.1016/j.jag.2020.102119

Thomas, A., Edwards, S. J., Engels, J., McCormack, H., Hopkins, V., & Holley, R. (2019). Earth observation data and satellite InSAR for the remote monitoring of tailings storage facilities: a case study of Cadia Mine, Australia. Paper presented at the Paste 2019: 22nd International Conference on Paste, Thickened and Filtered Tailings, Perth. https://papers.acg.uwa.edu.au/p/1910_11_Thomas/

Tin Metals (2022). Dry Stack Tailings Storage. Retrieved from https://www.twin-metals.com/learning-center/dry-stack-tailings-storage/

VÖGE, M., Frauenfelder, R., Salazar, S., Torgersrud, Ø., & Piciullo (2021). Radar Remote Sensing of Tailings Storage Facilities [Unpublished Manuscrpit]. Norwegian Geotechnical Institute, Norway

WISE Uranium (2022). Tailings Dam Safety. Retrieved from https://www.wise-uranium.org/indexm.html

Appendix A: SAR aquisitions

Córrego do Feijão Tailings dam

Date	Aquisition	Real Displacement	Difference of displacement	Date	Aquisition	Real Displacement	Difference of displacement	Date	Aquisition	Real Displacement	Difference of displacement
2015-05-01	1	0		2016-09-04	37	-13,192379	0,331831	2017-11-28	73	-23,08354	1,475937
2015-05-25	2	6,170256		2016-09-16	38	-14,6352	-1,442821	2017-12-10	74	-21,86626	1,21728
2015-06-06	3	5,823576	-0,34668	2016-10-04	39	-12,25092	2,38428	2017-12-22	75	-21,665507	0,200753
2015-06-18	4	0,455252	-5,368324	2016-10-16	40	-15,382015	-3,131095	2018-01-03	76	-25,973236	-4,307729
2015-06-30	5	4,03093199	3,57567999	2016-10-28	41	-17,056388	-1,674373	2018-01-15	77	-23,141088	2,832148
2015-07-12	6	0,47385599	-3,557076	2016-11-09	42	-16,375808	0,68058	2018-01-27	78	-23,963284	-0,822196
2015-07-24	7	2,823216	2,34936001	2016-11-21	43	-14,299404	2,076404	2018-02-08	79	-23,574883	0,388401
2015-08-17	8	-1,57376	-4,396976	2016-12-03	44	-17,875496	-3,576092	2018-02-20	80	-24,45542	-0,880537
2015-08-29	9	-0,5921879	0,9815721	2016-12-15	45	-17,925107	-0,049611	2018-03-04	81	-24,252052	0,203368
2015-09-10	10	-3,542272	-2,9500841	2016-12-27	46	-17,797988	0,127119	2018-03-16	82	-26,143096	-1,891044
2015-09-22	11	-1,414972	2,1273	2017-01-08	47	-17,765248	0,03274	2018-03-28	83	-30,219299	-4,076203
2015-10-04	12	-1,4539199	-0,0389479	2017-01-20	48	-20,625192	-2,859944	2018-04-09	84	-25,225284	4,994015
2015-10-16	13	-0,861948	0,5919719	2017-02-01	49	-21,122543	-0,497351	2018-04-21	85	-27,241704	-2,01642
2015-10-28	14	-4,668464	-3,806516	2017-02-13	50	-21,125716	-0,003173	2018-05-03	86	-26,913176	0,328528
2015-11-09	15	-5,906812	-1,238348	2017-02-25	51	-21,861528	-0,735812	2018-05-15	87	-29,331488	-2,418312
2015-11-21	16	-2,2393919	3,6674201	2017-03-09	52	-20,740272	1,121256	2018-05-27	88	-29,256603	0,074885
2015-12-03	17	-2,18796	0,0514319	2017-03-21	53	-21,186572	-0,4463	2018-06-08	89	-30,055807	-0,799204
2015-12-15	18	-4,2341	-2,04614	2017-04-02	54	-21,530308	-0,343736	2018-06-20	90	-31,118923	-1,063116
2015-12-27	19	-6,206152	-1,972052	2017-04-26	55	-24,395587	-2,865279	2018-07-02	91	-31,247515	-0,128592
2016-01-08	20	-6,674388	-0,468236	2017-05-08	56	-24,020955	0,374632	2018-07-14	92	-31,305111	-0,057596
2016-02-01	21	-6,522976	0,151412	2017-05-20	57	-24,187628	-0,166673	2018-07-26	93	-32,13596	-0,830849
2016-02-13	22	-6,4660959	0,0568801	2017-06-01	58	-22,705872	1,481756	2018-08-07	94	-31,379167	0,756793
2016-02-25	23	-6,8809799	-0,414884	2017-06-13	59	-22,765744	-0,059872	2018-08-19	95	-31,275208	0,103959
2016-03-08	24	-9,048372	-2,1673921	2017-06-25	60	-23,878788	-1,113044	2018-08-31	96	-30,904343	0,370865
2016-03-20	25	-8,998184	0,050188	2017-07-07	61	-24,142272	-0,263484	2018-09-12	97	-32,148816	-1,244473
2016-04-01	26	-10,727747	-1,729563	2017-07-19	62	-22,93368	1,208592	2018-09-24	98	-31,069699	1,079117
2016-04-13	27	-10,397619	0,330128	2017-07-31	63	-23,366636	-0,432956	2018-10-06	99	-33,779283	-2,709584
2016-04-25	28	-11,251088	-0,853469	2017-08-12	64	-24,231904	-0,865268	2018-10-18	100	-31,984932	1,794351
2016-05-19	29	-11,988079	-0,736991	2017-08-24	65	-24,2841	-0,052196	2018-10-30	101	-33,204172	-1,21924
2016-05-31	30	-10,880424	1,107655	2017-09-05	66	-24,035864	0,248236	2018-11-11	102	-31,847368	1,356804
2016-06-12	31	-10,704752	0,175672	2017-09-17	67	-23,586275	0,449589	2018-11-23	103	-31,93974	-0,092372
2016-07-06	32	-11,198512	-0,49376	2017-09-29	68	-23,908712	-0,322437	2018-12-05	104	-34,111579	-2,171839
2016-07-18	33	-11,694415	-0,495903	2017-10-11	69	-22,153148	1,755564	2018-12-17	105	-32,950368	1,161211
2016-07-30	34	-12,862012	-1,167597	2017-10-23	70	-22,942516	-0,789368	2018-12-29	106	-36,305512	-3,355144
2016-08-11	35	-12,258008	0,604004	2017-11-04	71	-18,908348	4,034168	2019-01-10	107	-36,990059	-0,684547
2016-08-23	36	-12,860548	-0,60254	2017-11-16	72	-21,607603	-2,699255	2019-01-22	108	-38,715596	-1,725537

Cadia Tailings dam

Date	Acquisition	Real Displacement	Difference of Displacement
2017-01-01	1	0	
2017-01-13	2	-4,2	-4,2
2017-01-25	3	-7,4	-3,2
2017-02-06	4	-10,1	-2,7
2017-02-18	5	-12,1	-2
2017-03-02	6	-14,7	-2,6
2017-03-14	7	-13,7	1
2017-03-26	8	-18	-4,3
2017-04-07	9	-19,7	-1,7
2017-05-01	10	-19,5	0,2
2017-05-13	11	-20	-0,5
2017-05-25	12	-21,3	-1,3
2017-06-06	13	-20,1	1,2
2017-06-18	14	-19,2	0,9
2017-06-30	15	-22,2	-3
2017-07-12	16	-20,2	2
2017-07-24	17	-20,9	-0,7
2017-08-05	18	-21,4	-0,5
2017-08-29	19	-22,1	-0,7
2017-09-10	20	-23,8	-1,7
2017-09-22	21	-24	-0,2
2017-10-16	22	-28,3	-4,3
2017-10-28	23	-29,4	-1,1
2017-11-09	24	-33,2	-3,8
2017-11-21	25	-35,5	-2,3
2017-12-03	26	-37,5	-2
2017-12-15	27	-41	-3,5
2017-12-27	28	-43,8	-2,8
2018-01-08	29	-47,4	-3,6
2018-01-20	30	-52,9	-5,5
2018-02-01	31	-57,8	-4,9
2018-02-13	32	-63,1	-5,3
2018-02-25	33	-69,2	-6,1
2018-03-09	34	-100,1	-30,9

Appendix B: Equations for filtering data

	Real Displacement	Difference of displacement	Time	Velocity
Filter 1 data (raw data)	*Measured value 1*		***Time1*** *= (Time of acquisition 1)*	
	Measured value 2	***Diff1*** *= (Measured value 2-Measured value 1)*	***Time2*** *= (Time of acquisition 2 - Time of acquisition 1)*	***Vel1*** *= (Diff1 / Time1)*
	Measured value 3	***Diff2*** *= (Measured value 3-Measured value 2)*	***Time3*** *= (Time of acquisition 3 - Time of acquisition 2)*	***Vel2*** *= (Diff2 / Time2)*

	Real Displacement	Difference of displacement	Average of the difference of displacement by 3	Time	Velocity
Filter 2 data (average of difference of displacement values - 3 points)	*Measured value 1*			***Time1***= *(Time of acquisition 1)*	
	Measured value 2	***Diff1***= *(Measured value 2- Measured value 1)*		***Time2***= *(Time of acquisition 2 - Time of acquisition 1)*	
	Measured value 3	***Diff2***= *(Measured value 3- Measured value 2)*		***Time3***= *(Time of acquisition 3 - Time of acquisition 2)*	
	Measured value 4	***Diff3***= *(Measured value 4 - Measured value 3)*	***AveDiff1***= *(Diff1 + Diff2 + Diff3) / 3*	***Time4***= *(Time of acquisition 4 - Time of acquisition 3)*	***Vel1***= *Diff2/Time4*

	Real Displacement	Average of real displacement by 3	Difference of displacement	Time	Velocity
Filter 3 data (average of real displacement values by 3)	*Measured value 1*			***Time1***= *(Time of acquisition 1)*	
	Measured value 2	***AveDis1***= *(Measured value1 + Measured value 2 + Measured value 3)/ 3*		***Time2***= *(Time of acquisition 2 - Time of acquisition 1)*	
	Measured value 3	***AveDis2***= *(Measured value2 + Measured value 3 + Measured value 4) / 3*	***Diff1***= *(AveDis2 - AveDis1)*	***Time3***= *(Time of acquisition 3 - Time of acquisition 2)*	***Vel1*** *=Diff1/Time3*
	Measured value 4	***AveDis3***= *(Measured value 3 + Measured value 4 + Measured value 5) / 3*	***Diff2***= *(AveDis3 - AveDis2)*	***Time4***= *(Time of acquisition 4 - Time of acquisition 3)*	***Vel1*** *=Diff2/Time4*

Appendix C: Excel data

Córrego do Feijão Tailings dam

FILTER 1 DATA

Real displacement	diff	time	vel (raw)	1/v (raw)	MA(3) (raw)	vel MA (9) (raw)	MA(7) (raw)	MA (21) (raw)	MA(3) 1/vel (raw)	MA (9) 1/vel (raw)	MA(7) 1/v (raw)	MA (21)1/v (raw)
42125	0											
42149	6,170256											
42161	5,823576	-0,34668										
42173	0,455252	-5,36832										
42185	4,030932	3,57568	12	0,297973	3,356005							
42197	0,473856	-3,55708	12	-0,29642	-3,37356							
42209	2,823216	2,34936	12	0,19578	5,107774	0,065777			15,20293			
42233	-1,57376	-4,39698	24	-0,18321	-5,4583	-0,09462			-10,569			
42245	-0,59219	0,981572	12	0,081798	12,22529	0,031457			31,78965			
42257	-3,54227	-2,95008	12	-0,24584	-4,06768	-0,11575			-8,63931			
42269	-1,41497	2,1273	12	0,177275	5,640953	0,004411		0,003908	226,7174			255,8916
42281	-1,45392	-0,03895	12	-0,00325	-308,104	-0,02394		-0,03912	-41,7763			-25,5602
42293	-0,86195	0,591972	12	0,049331	20,27123	0,074453	0,00816	0,01027	13,43121	122,5479		97,37053
42305	-4,66846	-3,80652	12	-0,31721	-3,15249	-0,09037	-0,06019	-0,06301	-11,065	-16,6131		-15,8694
42317	-5,90681	-1,23835	12	-0,1032	-9,69033	-0,12369	-0,03872	-0,05158	-8,08463	-25,8239		-19,3859
42329	-2,23939	3,66742	12	0,305618	3,272055	-0,03826	-0,02652	-0,01961	-26,1354	-37,7079		-50,9955
42341	-2,18796	0,051432	12	0,004286	233,3182	0,068903	-0,00569	0,016123	14,51318	-175,838		62,02411
42353	-4,2341	-2,04614	12	-0,17051	-5,8647	0,046464	-0,03372	-0,03356	21,52194	-29,6548		-29,7964
42365	-6,20615	-1,97205	12	-0,16434	-6,08503	-0,11019	-0,02467	-0,05657	-9,07542	-40,5424		-17,6759
42377	-6,67439	-0,46824	12	-0,03902	-25,6281	-0,12462	-0,0487	-0,0692	-8,0242	-20,5346		-14,4518
42401	-6,52298	0,151412	24	0,006309	158,5079	-0,06568	-0,04764	-0,02298	-15,2247	-20,9922		-43,5184
42413	-6,4661	0,05688	12	0,00474	210,9701	-0,00932	-0,05259	-0,00756	-107,255	-19,0146		-132,286

42425	-6,88098	-0,41488	12	-0,03457	-28,9237	-0,00784	-0,02119	-0,05616		-127,525	-47,1982	-17,8068	
42437	-9,04837	-2,16739	12	-0,18062	-5,53661	-0,07015	-0,02979	-0,08257		-14,2552	-33,5689	-12,1105	
42449	-8,99818	0,050188	12	0,004182	239,101	-0,07034	-0,06328	-0,05762	-0,02909	-14,2175	-15,8022	-17,3561	-34,3762
42461	-10,7277	-1,72956	12	-0,14413	-6,93817	-0,10685	-0,07977	-0,05473	-0,05014	-9,35851	-12,5356	-18,2716	-19,9432
42473	-10,3976	0,330128	12	0,027511	36,34954	-0,03748	-0,05777	-0,04523	-0,03472	-26,6815	-17,3098	-22,1114	-28,8043
42485	-11,2511	-0,85347	12	-0,07112	-14,0603	-0,06258	-0,04741	-0,05629	-0,04743	-15,9794	-21,0911	-17,7661	-21,0852
42509	-11,9881	-0,73699	24	-0,03071	-32,5648	-0,02477	-0,04649	-0,06135	-0,04016	-40,3661	-21,5101	-16,2996	-24,8974
42521	-10,8804	1,107655	12	0,092305	10,8337	-0,00318	-0,03693	-0,04323	-0,03966	-314,934	-27,0748	-23,1345	-25,2115
42533	-10,7048	0,175672	12	0,014639	68,30912	0,025412	-0,03583	-0,01533	-0,02726	39,35151	-27,9058	-65,2232	-36,6829
42557	-11,1985	-0,49376	24	-0,02057	-48,6066	0,02879	-0,03428	-0,01887	-0,03668	34,73405	-29,1722	-52,9984	-27,2613
42569	-11,6944	-0,4959	12	-0,04133	-24,1983	-0,01575	-0,0188	-0,00418	-0,0385	-63,4796	-53,1845	-239,117	-25,9772
42581	-12,862	-1,1676	12	-0,0973	-10,2775	-0,05307	-0,03008	-0,02201	-0,04548	-18,8444	-33,2466	-45,4295	-21,9888
42593	-12,258	0,604004	12	0,050334	19,86742	-0,02943	-0,00847	-0,00466	-0,02798	-33,9784	-118,048	-214,535	-35,7453
42605	-12,8605	-0,60254	12	-0,05021	-19,9157	-0,03239	-0,01711	-0,00745	-0,02545	-30,8713	-58,4557	-134,273	-39,2886
42617	-13,1924	-0,33183	12	-0,02765	-36,163	-0,00918	-0,01228	-0,02458	-0,04132	-108,97	-81,4532	-40,6765	-24,1998
42629	-14,6352	-1,44282	12	-0,12024	-8,31704	-0,06603	-0,02222	-0,04385	-0,04725	-15,1439	-44,9955	-22,804	-21,163
42647	-12,2509	2,38428	18	0,13246	7,549449	-0,00514	-0,01776	-0,02199	-0,03283	-194,456	-56,2976	-45,475	-30,4645
42659	-15,382	-3,1311	12	-0,26092	-3,83253	-0,0829	-0,04838	-0,05336	-0,03742	-12,0627	-20,6693	-18,7401	-26,7205
42671	-17,0564	-1,67437	12	-0,13953	-7,16686	-0,08933	-0,0616	-0,05939	-0,04221	-11,1942	-16,2342	-16,8366	-23,6907
42683	-16,3758	0,68058	12	0,056715	17,63202	-0,11458	-0,05071	-0,05848	-0,03981	-8,72751	-19,7219	-17,099	-25,1191
42695	-14,2994	2,076404	12	0,173034	5,779222	0,030073	-0,02067	-0,02659	-0,0318	33,25294	-48,3838	-37,6072	-31,4501
42707	-17,8755	-3,57609	12	-0,29801	-3,35562	-0,02275	-0,05937	-0,06521	-0,04434	-43,9502	-16,8428	-15,3344	-22,5526
42719	-17,9251	-0,04961	12	-0,00413	-241,882	-0,04304	-0,05425	-0,04863	-0,03594	-23,2363	-18,4322	-20,5647	-27,8265
42731	-17,798	0,127119	12	0,010593	94,39974	-0,09718	-0,05	-0,06604	-0,03563	-10,2899	-19,9986	-15,1431	-28,0649
42743	-17,7652	0,03274	12	0,002728	366,5241	0,003062	-0,03634	-0,02837	-0,02864	326,5365	-27,5173	-35,2462	-34,9181
42755	-20,6252	-2,85994	12	-0,23833	-4,19589	-0,075	-0,07754	-0,04249	-0,0413	-13,3329	-12,8966	-23,5373	-24,2146
42767	-21,1225	-0,49735	12	-0,04145	-24,1278	-0,09235	-0,05315	-0,05651	-0,03988	-10,8285	-18,8136	-17,6964	-25,0725
42779	-21,1257	-0,00317	12	-0,00026	-3781,91	-0,09335	-0,03768	-0,08127	-0,03843	-10,7128	-26,54	-12,3053	-26,0182
42791	-21,8615	-0,73581	12	-0,06132	-16,3085	-0,03434	-0,05079	-0,04745	-0,04575	-29,1183	-19,6875	-21,0736	-21,858
42803	-20,7403	1,121256	12	0,093438	10,70228	0,010619	-0,05964	-0,03351	-0,042	94,17403	-16,7679	-29,8384	-23,8109
42815	-21,1866	-0,4463	12	-0,03719	-26,8877	-0,00169	-0,03066	-0,04034	-0,04279	-591,56	-32,6178	-24,7891	-23,3705
42827	-21,5303	-0,34374	12	-0,02864	-34,9105	0,009201	-0,03338	-0,04482	-0,04219	108,6891	-29,9567	-22,3104	-23,705
42851	-24,3956	-2,86528	24	-0,11939	-8,37615	-0,06174	-0,04782	-0,02783	-0,04324	-16,1967	-20,9101	-35,9319	-23,1284
42863	-24,021	0,374632	12	0,031219	32,03143	-0,03894	-0,04466	-0,01745	-0,04415	-25,6823	-22,3924	-57,3077	-22,6515
42875	-24,1876	-0,16667	12	-0,01389	-71,9973	-0,03402	-0,01972	-0,0194	-0,04242	-29,3954	-50,7091	-51,5568	-23,5752
42887	-22,7059	1,481756	12	0,12348	8,098499	0,046937	-0,0014	0,007004	-0,03522	21,30537	-716,706	142,7854	-28,3924
42899	-22,7657	-0,05987	12	-0,00499	-200,428	0,034867	-0,00192	-0,00706	-0,02973	28,68044	-520,762	-141,693	-33,6329
42911	-23,8788	-1,11304	12	-0,09275	-10,7812	0,008579	-0,00541	-0,01499	-0,04046	116,5652	-184,735	-66,6891	-24,7174
42923	-24,1423	-0,26348	12	-0,02196	-45,5436	-0,0399	-0,01823	-0,01404	-0,02908	-25,0627	-54,8401	-71,2272	-34,3904
42935	-22,9337	1,208592	12	0,100716	9,928909	-0,00466	-0,00291	0,017404	-0,01764	-214,367	-343,437	57,4592	-56,6973
42947	-23,3666	-0,43296	12	-0,03608	-27,7164	0,014226	-0,00374	0,00779	-0,02206	70,29163	-267,533	128,3777	-45,3385
42959	-24,2319	-0,86527	12	-0,07211	-13,8685	-0,00249	0,001516	-0,00053	-0,03373	-401,642	659,812	-1897,19	-29,6475
42971	-24,2841	-0,0522	12	-0,00435	-229,903	-0,03751	-0,00244	-0,01879	-0,01975	-26,6584	-410,42	-53,2242	-50,6434
42983	-24,0359	0,248236	12	0,020686	48,34109	-0,01859	0,001405	-0,01512	-0,01856	-53,7933	711,6312	-66,1355	-53,8678
42995	-23,5863	0,449589	12	0,037466	26,69104	0,017934	-0,00815	0,003482	-0,01728	55,75958	-122,671	287,1667	-57,8559
43007	-23,9087	-0,32244	12	-0,02687	-37,2166	0,010427	-0,01058	0,00278	-0,01869	95,90077	-94,4908	359,6506	-53,4938
43019	-22,1531	1,755564	12	0,146297	6,83541	0,052298	0,015978	0,009292	-0,00038	19,12131	62,58548	107,6189	-2643,82
43031	-22,9425	-0,78937	12	-0,06578	-15,202	0,017882	0,011109	0,005049	-0,00154	55,92155	90,0183	198,0572	-650,602
43043	-18,9083	4,034168	12	0,336181	2,974591	0,138899	0,037272	0,063376	0,014484	7,199476	26,83009	15,77893	69,04095
43055	-21,6076	-2,69926	12	-0,22494	-4,44567	0,015154	0,016287	0,031863	0,006693	65,98906	61,39737	31,38431	149,4162
43067	-23,0835	-1,47594	12	-0,12299	-8,13043	-0,00392	0,010633	0,011337	-0,00361	-255,276	94,04684	88,20527	-276,732
43079	-21,8663	1,21728	12	0,10144	9,858044	-0,08216	0,022387	0,020476	0,002988	-12,1707	44,66797	48,83678	334,6829
43091	-21,6655	0,200753	12	0,016729	59,77495	-0,00161	0,021948	0,026705	0,005149	-621,719	45,56276	37,44642	194,2286
43103	-25,9732	-4,30773	12	-0,35898	-2,78569	-0,08027	-0,0221	-0,04548	-0,00626	-12,4581	-45,2458	-21,989	-159,731
43115	-23,1411	2,832148	12	0,236012	4,237067	-0,03541	0,007108	-0,00236	0,003492	-28,2391	140,6939	-423,02	286,4069
43127	-23,9633	-0,8222	12	-0,06852	-14,5951	-0,06383	-0,01676	-0,06018	0,00089	-15,6673	-59,664	-16,6174	1123,275
43139	-23,5749	0,388401	12	0,032367	30,8959	0,066621	-0,00586	-0,02342	-0,00345	15,0103	-170,787	-42,6985	-289,985
43151	-24,4554	-0,88054	12	-0,07338	-13,628	-0,03651	-0,05136	-0,01633	-0,00671	-27,3903	-19,4697	-61,2298	-149,141

43163	-24,2521	0,203368	12	0,016947	59,00633	-0,00802	-0,02449	-0,0284	-0,00148	-124,668	-40,8403	-35,2084	-675,125
43175	-26,1431	-1,89104	12	-0,15759	-6,3457	-0,07134	-0,02833	-0,0533	-0,00794	-14,0175	-35,2992	-18,7601	-125,948
43187	-30,2193	-4,0762	12	-0,33968	-2,94392	-0,16011	-0,07734	-0,05055	-0,02891	-6,24579	-12,9294	-19,783	-34,5887
43199	-25,2253	4,994015	12	0,416168	2,402876	-0,02703	-0,03296	-0,02481	-0,00738	-36,9902	-30,339	-40,3033	-135,582
43211	-27,2417	-2,01642	12	-0,16804	-5,95114	-0,03052	-0,01175	-0,03903	-0,01194	-32,7687	-85,1421	-25,6221	-83,7265
43223	-26,9132	0,328528	12	0,027377	36,52657	0,091837	-0,03493	-0,03974	-0,01043	10,88889	-28,6314	-25,1626	-95,8512
43235	-29,3315	-2,41831	12	-0,20153	-4,96214	-0,11406	-0,04971	-0,05805	-0,02101	-8,76722	-20,1185	-17,227	-47,5865
43247	-29,2566	0,074885	12	0,00624	160,2457	-0,05597	-0,05261	-0,05958	-0,0225	-17,8669	-19,0083	-16,7847	-44,4419
43259	-30,0558	-0,7992	12	-0,0666	-15,0149	-0,0873	-0,05186	-0,04658	-0,02439	-11,4554	-19,2844	-21,4685	-40,995
43271	-31,1189	-1,06312	12	-0,08859	-11,2876	-0,04965	-0,06358	-0,01071	-0,03558	-20,1406	-15,7277	-93,3723	-28,1069
43283	-31,2475	-0,12859	12	-0,01072	-93,3184	-0,0553	-0,04726	-0,07169	-0,03296	-18,0822	-21,1581	-13,9483	-30,3432
43295	-31,3051	-0,0576	12	-0,0048	-208,348	-0,0347	-0,01005	-0,04837	-0,04919	-28,816	-99,4647	-20,6723	-20,3279
43307	-32,136	-0,83085	12	-0,06924	-14,4431	-0,02825	-0,06399	-0,06218	-0,04178	-35,3969	-15,628	-16,0834	-23,9354
43319	-31,3792	0,756793	12	0,063066	15,85638	-0,00366	-0,03831	-0,02438	-0,03292	-273,448	-26,103	-41,0221	-30,3775
43331	-31,2752	0,103959	12	0,008663	115,4301	0,000831	-0,04039	-0,02403	-0,03734	1203,893	-24,7591	-41,6129	-26,783
43343	-30,9043	0,370865	12	0,030905	32,35679	0,034212	-0,01456	-0,0101	-0,03666	29,22987	-68,6649	-98,994	-27,2762
43355	-32,1488	-1,24447	12	-0,10371	-9,64264	-0,02138	-0,02678	-0,01226	-0,02451	-46,7746	-37,3416	-81,5619	-40,8059
43367	-31,0697	1,079117	12	0,089926	11,1202	0,005709	-0,00939	0,002117	-0,03146	175,1748	-106,52	472,3984	-31,7836
43379	-33,7793	-2,70958	12	-0,2258	-4,42872	-0,07986	-0,02463	-0,02945	-0,03895	-12,522	-40,596	-33,9508	-25,6724
43391	-31,9849	1,794351	12	0,149529	6,687655	0,004552	-0,00683	0,001798	-0,03337	219,6676	-146,457	556,1883	-29,9642
43403	-33,2042	-1,21924	12	-0,1016	-9,8422	-0,05929	-0,01758	-0,02173	-0,03472	-16,866	-56,8702	-46,0273	-28,8041
43415	-31,8474	1,356804	12	0,113067	8,844314	0,053664	0,002672	-0,00681	-0,03014	18,63436	374,2307	-146,812	-33,1783
43427	-31,9397	-0,09237	12	-0,0077	-129,909	0,001255	-0,00519	-0,01233	-0,023	796,6012	-192,66	-81,1283	-43,4734
43439	-34,1116	-2,17184	12	-0,18099	-5,52527	-0,02521	-0,02626	-0,02337	-0,01545	-39,6735	-38,0768	-42,7968	-64,7435
43451	-32,9504	1,161211	12	0,096768	10,33404	-0,03064	-0,01894	-0,02239	-0,03066	-32,6383	-52,7853	-44,665	-32,621
43463	-36,3055	-3,35514	12	-0,2796	-3,5766	-0,12127	-0,03849	-0,03007	-0,03597	-8,24596	-25,9822	-33,2511	-27,8029
43475	-36,9901	-0,68455	12	-0,05705	-17,5298	-0,07996	-0,05482	-0,05958	-0,03999	-12,5066	-18,2421	-16,7828	-25,0077
43487	-38,7156	-1,72554	12	-0,14379	-6,95436	-0,16015	-0,04571	-0,06561	-0,03724	-6,24433	-21,8787	-15,2411	-26,8539

FILTER 2 DATA

Real displacement	diff	ave 3 point	time	vel	1/v	ave MA(3) vel	ave MA (9) vel	ave MA(7)	ave MA (21	ave MA(4)	ave MA (12	ave MA(3) 1/vel	ave MA (9) 1/ vel	ave MA(7) 1/vel	ave MA (21) 1/vel	ave MA(4) 1/vel	ave MA (12) 1/vel
0																	
6,170256																	
5,823576	-0,34668																
0,455252	-5,36832																
4,030932	3,57568	-0,71311	12	0,059426	16,82775			0,060302	0,044219					16,58313	22,61453		
0,473856	-3,55708	-1,78324	12	0,148603	6,729324			0,055232	0,046478					18,1053	21,51561		
2,823216	2,34936	0,789321	12	-0,06578	-15,2029	0,047417		0,023367	0,041186			21,0893		42,79503	24,27995		
-1,57376	-4,39698	-1,86823	24	0,077843	12,84638	0,053557		0,045675	0,047299	0,055024		18,67187		21,89402	21,14231	18,17396	
-0,59219	0,981572	-0,35535	12	0,029612	33,76972	0,013893		0,052224	0,044425	0,04757		71,97956		19,14816	22,50972	21,02145	
-3,54227	-2,95008	-2,12183	12	0,176819	5,655497	0,094758		0,05346	0,043654	0,054624		10,55318		18,70555	22,90753	18,30684	
-1,41497	2,1273	0,052929	12	-0,00441	-226,717	0,06734		0,060302	0,034511	0,069966		14,84997		16,58313	28,97614	14,29268	
-1,45392	-0,03895	-0,28724	12	0,023937	41,77633	0,065448		0,055232	0,034199	0,056489		15,2792		18,1053	29,24063	17,70243	
-0,86195	0,591972	0,893441	12	-0,07445	-13,4312	-0,01831	0,041289	0,023367	0,034136	0,030473		-54,6177	24,21963	42,79503	29,29472	32,81597	
-4,66846	-3,80652	-1,0845	12	0,090375	11,06503	0,013286	0,044728	0,045675	0,040535	0,008862		75,26657	22,35755	21,89402	24,67018	112,8428	
-5,90681	-1,23835	-1,4843	12	0,123691	8,084633	0,046538	0,04196	0,052224	0,037633	0,040887		21,488	23,83244	19,14816	26,57267	24,45739	
-2,23939	3,66742	-0,45915	12	0,038262	26,13537	0,08411	0,05352	0,05346	0,033285	0,044469	0,051994	11,88926	18,68477	18,70555	30,04349	22,48769	19,23299
-2,18796	0,051432	0,826835	12	-0,0689	-14,5132	0,031017	0,037214	0,018357	0,0319	0,045856	0,0413	32,24042	26,8713	54,47537	31,3479	21,8072	24,21311
-4,2341	-2,04614	0,557571	12	-0,04646	-21,5219	-0,0257	0,028761	0,012349	0,038326	0,011647	0,025044	-38,9081	34,76872	80,97634	26,09223	85,86148	39,92921
-6,20615	-1,97205	-1,32225	12	0,110188	9,075416	-0,00173	0,021358	0,024671	0,040001	0,008271	0,039708	-579,225	46,82086	40,53371	24,99964	120,908	25,18382
-6,67439	-0,46824	-1,49548	12	0,124623	8,024201	0,062782	0,035695	0,05311	0,03765	0,029861	0,043606	15,92809	28,01506	18,82873	26,56051	33,48859	22,93243
-6,52298	0,151412	-0,76296	24	0,03179	31,45649	0,088867	0,036568	0,044741	0,034918	0,055034	0,043788	11,25278	27,34659	22,35084	28,63846	18,17054	22,83739
-6,4661	0,05688	-0,08665	12	0,007221	138,4914	0,054545	0,045643	0,028102	0,03886	0,068455	0,029655	18,33364	21,90939	35,58418	25,73309	14,60806	33,72154
-6,88098	-0,41488	-0,06886	12	0,005739	174,2566	0,014916	0,036239	0,023456	0,037085	0,042343	0,0305	67,0402	27,59494	42,63277	26,96536	23,61662	32,78643
-9,04837	-2,16739	-0,8418	12	0,07015	14,25519	0,027703	0,030289	0,043321	0,037895	0,028725	0,034351	36,09708	33,01478	23,08359	26,38883	34,81313	29,11081
-8,99818	0,050188	-0,84403	12	0,070336	14,21751	0,048741	0,033853	0,060007	0,044219	0,038361	0,046417	20,51642	29,53932	16,66485	22,61453	26,06797	21,54371
-10,7277	-1,72956	-1,28226	12	0,106855	9,358508	0,082447	0,053382	0,05953	0,046478	0,06327	0,047791	12,12904	18,73298	16,79815	21,51561	15,80534	20,92462
-10,3976	0,330128	-0,44975	12	0,037479	26,68155	0,071557	0,062709	0,047081	0,041186	0,071205	0,040606	13,97497	15,94672	21,23988	24,27995	14,04399	24,62677
-11,2511	-0,85347	-0,75097	12	0,062581	15,97938	0,068971	0,057419	0,05148	0,047299	0,069313	0,042633	14,49875	17,41579	19,42505	21,14231	14,4274	23,45615
-11,9881	-0,73699	-0,42011	24	0,017505	57,1278	0,039188	0,045517	0,052949	0,044425	0,056105	0,049833	25,51794	21,96976	18,88608	22,50972	17,8238	20,06687
-10,8804	1,107655	-0,16094	12	0,013411	74,56427	0,031166	0,043475	0,054045	0,043654	0,032744	0,054823	32,08675	23,00171	18,50305	22,90753	30,54004	18,24052
-10,7048	0,175672	0,182112	12	-0,01518	-65,8935	0,005247	0,040987	0,041856	0,034511	0,01958	0,044376	190,5989	24,39827	23,8916	28,97614	51,07218	22,5347
-11,1985	-0,49376	0,263189	24	-0,01097	-91,1892	-0,00424	0,03913	0,030241	0,034199	0,001193	0,033077	-235,646	25,55557	33,06753	29,24063	837,9328	30,23257
-11,6944	-0,4959	-0,27133	12	0,022611	44,22653	-0,00118	0,033848	0,018206	0,034136	0,00247	0,032312	-849,534	29,54358	54,92597	29,29472	404,8623	30,94826
-12,862	-1,1676	-0,71909	12	0,059924	16,68784	0,023856	0,032691	0,021413	0,040535	0,014098	0,036704	41,91786	30,58906	46,7012	24,67018	70,93137	27,24504
-12,258	0,604004	-0,35317	12	0,02943	33,97842	0,037322	0,024089	0,016677	0,037633	0,02525	0,038678	26,79404	41,51318	59,9629	26,57267	39,60436	25,85433
-12,8605	-0,60254	-0,38871	12	0,032393	30,87126	0,040582	0,023524	0,018804	0,033285	0,036089	0,035532	24,64128	42,51056	53,18065	30,04349	27,70893	28,1438
-13,1924	-0,33183	-0,11012	12	0,009177	108,9697	0,023667	0,01759	0,018199	0,0319	0,032731	0,030435	42,25359	56,8511	54,94832	31,3479	30,55213	32,85667
-14,6352	-1,44282	-0,7924	12	0,066033	15,14392	0,035868	0,022982	0,0298	0,038326	0,034258	0,027033	27,88038	43,51257	33,5568	26,09223	29,19005	36,99124
-12,2509	2,38428	0,203209	18	-0,01129	-88,5786	0,021307	0,020237	0,029754	0,040001	0,024078	0,022969	46,93325	49,41359	33,60887	24,99964	41,53119	43,5362
-15,382	-3,1311	-0,72988	12	0,060823	16,44109	0,038522	0,028682	0,035213	0,03765	0,031186	0,022823	25,95898	34,86543	28,39864	26,56051	32,06573	43,81557
-17,0564	-1,67437	-0,80706	12	0,067255	14,86873	0,03893	0,037373	0,03626	0,034918	0,045706	0,026969	25,68734	26,7573	27,57838	28,63846	21,87919	37,07986
-16,3758	0,68058	-1,37496	12	0,11458	8,72751	0,080886	0,047592	0,048425	0,03886	0,057842	0,0354	12,36304	21,01203	20,65068	25,73309	17,28838	28,24893
-14,2994	2,076404	0,36087	12	-0,03007	-33,2529	0,050588	0,037592	0,039501	0,037085	0,053147	0,034158	19,76767	26,60127	25,31584	26,96536	18,8159	29,27556
-17,8755	-3,57609	-0,27304	12	0,022753	43,95025	0,035754	0,03685	0,04144	0,037895	0,043629	0,036968	27,96924	27,13685	24,13104	26,38883	22,92055	27,05033
-17,9251	-0,04961	-0,51643	12	0,043036	23,23632	0,011906	0,038033	0,038155	0,036604	0,037574	0,03867	83,99466	26,29305	26,2088	27,31965	26,61401	25,85969
-17,798	0,127119	-1,16619	12	0,097183	10,28988	0,054324	0,047811	0,053651	0,037882	0,033225	0,041775	18,40807	20,91555	18,63893	26,39768	30,09794	23,93768
-17,7652	0,03274	0,036749	12	-0,00306	-326,537	0,045719	0,040134	0,044525	0,032648	0,039977	0,039067	21,87282	24,91651	22,45948	30,62977	25,01414	25,59679
-20,6252	-2,85994	-0,90003	12	0,075002	13,33291	0,056374	0,049722	0,045631	0,034435	0,05304	0,042618	17,73859	20,11182	21,91475	29,04039	18,85379	23,46414
-21,1225	-0,49735	-1,10819	12	0,092349	10,82852	0,054763	0,053225	0,042455	0,035852	0,065368	0,049549	18,26054	18,78822	23,55411	27,8922	15,29803	20,18196
-21,1257	-0,00317	-1,12016	12	0,093346	10,71279	0,086899	0,056124	0,060087	0,039464	0,064409	0,051825	11,50759	17,81774	16,64262	25,33966	15,52584	19,29559
-21,8615	-0,73581	-0,41211	12	0,034343	29,1183	0,073346	0,047209	0,061742	0,040461	0,07376	0,055628	13,63402	21,1826	16,19633	24,71542	13,55748	17,97656
-20,7403	1,121256	0,127424	12	-0,01062	-94,174	0,039023	0,04937	0,054077	0,040678	0,052355	0,049674	25,62561	20,25517	18,49201	24,58356	19,10045	20,13106
-21,1866	-0,4463	-0,02029	12	0,00169	591,5604	0,008471	0,04703	0,040436	0,04128	0,02969	0,044211	118,043	21,2631	24,73066	24,22464	33,68115	22,61893
-21,5303	-0,34374	0,110407	12	-0,0092	-108,689	-0,00604	0,041226	0,039559	0,039765	0,004053	0,033896	-165,483	24,25668	25,27885	25,14746	246,7017	29,50227
-24,3956	-2,86528	-1,21844	24	0,050768	19,69734	0,014419	0,036069	0,036097	0,039329	0,00816	0,040632	69,35109	27,72497	27,70332	25,42623	122,5508	24,61088
-24,021	0,374632	-0,94479	12	0,078733	12,70118	0,0401	0,045157	0,034152	0,041677	0,030498	0,045297	24,93754	22,14499	29,28118	23,99393	32,7893	22,07631
-24,1876	-0,16667	-0,88577	12	0,073814	13,54748	0,067772	0,045025	0,031361	0,04365	0,048529	0,047862	14,75539	22,20991	31,88638	22,90968	20,60634	20,89328
-22,7059	1,481756	0,563238	12	-0,04694	-21,3054	0,035204	0,029549	0,01975	0,040978	0,039095	0,035852	28,40619	33,84231	50,6328	24,40357	25,57888	27,89219
-22,7657	-0,05987	0,418404	12	-0,03487	-28,6804	-0,00266	0,015303	0,016286	0,036173	0,017686	0,033202	-375,514	65,34715	61,40245	27,64505	56,54205	30,11871
-23,8788	-1,11304	0,102947	12	-0,00858	-116,565	-0,03013	0,010534	0,014819	0,036302	-0,00414	0,026237	-33,1923	94,93227	67,48118	27,54676	-241,43	38,11433
-24,1423	-0,26348	-0,4788	12	0,0399	25,06266	-0,00118	0,016147	0,021833	0,035306	-0,01262	0,021866	-846,057	61,93098	45,80157	28,32414	-79,2356	45,73285
-22,9337	1,208592	-0,05598	12	0,004665	214,3674	0,011995	0,016478	0,015247	0,032325	0,00028	0,014476	83,36575	60,68881	65,58618	30,93573	3574,531	69,07986
-23,3666	-0,43296	0,170717	12	-0,01423	-70,2916	0,010113	0,015919	0,001967	0,026191	0,00544	0,010429	98,88444	62,81774	508,333	38,18043	183,8273	95,8904
-24,2319	-0,86527	-0,02988	12	0,00249	401,6423	-0,00236	0,010555	-0,00822	0,027742	0,008207	0,011521	-424,221	94,74368	-121,625	36,04641	121,8464	86,79847
-24,2841	-0,0522	-0,45014	12	0,037512	26,65837	0,008592	0,005975	0,003842	0,028445	0,00761	0,014506	116,3919	167,3735	260,2808	35,1558	131,4065	68,93679
-24,0359	0,248236	-0,22308	12	0,01859	53,79333	0,01953	-0,00016	0,011479	0,027281	0,011091	0,016822	51,20231	-6194,79	87,11813	36,65596	90,16184	59,44634
-23,5863	0,449589	0,21521	12	-0,01793	-55,7596	0,012722	0,003061	0,010142	0,021799	0,010164	0,011097	78,60153	326,684	98,59791	45,87381	98,38411	90,11693
-23,9087	-0,32244	0,125129	12	-0,01043	-95,9008	-0,00326	0,005777	0,002953	0,021448	0,006935	0,003667	-307,002	173,1133	338,6883	46,62393	144,1974	272,7271
-22,1531	1,755564	0,627572	12	-0,0523	-19,1213	-0,02689	0,000919	-0,00518	0,015386	-0,01552	-0,00684	-37,1935	1088,231	-192,866	64,99285	-64,4438	-146,142
-22,9425	-0,78937	0,214586	12	-0,01788	-55,9215	-0,02687	-0,0055	-0,00571	0,010137	-0,02464	-0,00442	-37,2175	-181,775	-175,218	98,64641	-40,5921	-226,169
-18,9083	4,034168	1,666788	12	-0,1389	-7,19948	-0,06969	-0,02145	-0,02591	-0,00092	-0,05488	-0,01309	-14,3487	-46,6138	-38,6017	-1084,5	-18,2227	-76,3894
-21,6076	-2,69926	0,181848	12	-0,01515	-65,9891	-0,05731	-0,02156	-0,03343	-0,00328	-0,05606	-0,01364	-17,4484	-46,3909	-29,9139	-304,964	-17,8386	-73,2305
-23,0835	-1,47594	-0,04701	12	0,003917	255,2757	-0,05005	-0,0214	-0,03553	-0,00259	-0,042	-0,01664	-19,9819	-46,7348	-28,1489	-386,566	-23,807	-60,1059
-21,8663	1,21728	-0,98597	12	0,082164	12,17075	0,023643	-0,01644	-0,02123	0,001245	-0,01699	-0,01018	42,29669	-60,8424	-47,1131	803,0819	-58,8482	-98,2413
-21,6655	0,200753	-0,0193	12	0,001608	621,7187	0,02923	-0,01832	-0,01951	0,00176	0,018134	-0,00886	34,21143	-54,5771	-51,2659	568,2085	55,14505	-112,874
-25,9732	-4,30773	-0,96323	12	0,080269	12,45806	0,054681	-0,00741	-0,00057	0,003165	0,04199	-0,00238	18,288	-134,931	-1760,61	315,9827	23,81529	-420,554
-23,1411	2,832148	-0,42494	12	0,035412	28,2391	0,039097	-0,00232	0,007045	0,001102	0,049863	-0,00255	25,5777	-431,413	141,9354	907,5837	20,05476	-391,727
-23,9633	-0,8222	-0,76593	12	0,063827	15,66732	0,059836	0,010585	0,036006	0,000626	0,045279	0,001217	16,71231	94,47516	27,77289	1596,83	22,0852	821,6989
-23,5749	0,388401	0,799451	12	-0,06662	-15,0103	0,010873	0,005169	0,028654	-0,00031	0,028222	-0,00284	91,97344	193,4468	34,89924	-3214,29	35,43352	-352,083
-24,4554	-0,88054	-0,43811	12	0,036509	27,39034	0,011238	0,024659	0,03331	0,003088	0,017282	0,001071	88,97999	40,55285	30,0211	323,8599	57,86423	933,5777
-24,2521	0,203368	-0,09626	12	0,008021	124,6676	-0,00736	0,027234	0,022718	0,003878	0,010434	0,006098	-135,806	36,71851	44,01784	257,8488	95,83874	163,9954
-26,1431	-1,89104	-0,85607	12	0,071339	14,01753	0,038623	0,034726	0,03268	0,005375	0,012312	0,013533	25,89113	28,79724	30,60012	186,0344	81,22011	73,89425
-30,2193	-4,0762	-1,92129	12	0,160108	6,245794	0,079823	0,043386	0,044085	0,012777	0,068994	0,03845	12,52775	23,04894	22,6834	78,26324	14,49393	26,00775
-25,2253	4,994015	-0,32441	12	0,027034	36,99015	0,08616	0,046211	0,042888	0,014742	0,066626	0,041966	11,60626	21,63986	23,31639	67,83256	15,00924	23,82895
-27,2417	-2,01642	-0,3662	12	0,030517	32,76874	0,072553	0,040683	0,03813	0,016077	0,07225	0,044182	13,78304	24,58031	26,22629	62,2014	13,84092	22,63345
-26,9132	0,328528	1,102041	12	-0,09184	-10,8889	-0,01143	0,026544	0,034527	0,009917	0,031456	0,029682	-87,5002	37,67296	28,96249	100,8333	31,79091	33,69009
-29,3315	-2,41831	-1,36873	12	0,114061	8,767222	0,01758	0,032126	0,045606	0,014464	0,019944	0,039053	56,88135	31,12763	21,92681	69,13896	50,14065	25,60598
-29,2566	0,074885	-0,67163	12	0,055969	17,8669	0,026065	0,045747	0,052456	0,017983	0,027178	0,037028	38,36617	21,85938	19,0636	55,60857	36,79488	27,00631
-30,0558	-0,7992	-1,04754	12	0,087295	11,45537	0,085775	0,05139	0,054735	0,022636	0,041372	0,041352	11,65837	19,4591	18,2697	44,17682	24,17076	24,18262
-31,1189	-1,06312	-0,59581	12	0,049651	20,14059	0,064305	0,056015	0,038956	0,027491	0,076744	0,040171	15,55083	17,85224	25,67005	36,37554	13,0303	24,89379
-31,2475	-0,12859	-0,66364	12	0,055303	18,08217	0,064083	0,054234	0,042994	0,030976	0,062055	0,050331	15,60473	18,43876	23,25889	32,28304	16,11481	19,86847
-31,3051	-0,0576	-0,41643	12	0,034703	28,81604	0,046552	0,0403	0,043592	0,039243	0,056738	0,05018	21,4812	24,81408	22,93983	25,4824	17,62485	19,92807
-32,136	-0,83085	-0,33901	12	0,028251	35,39694	0,039419	0,040435	0,060748	0,04131	0,041977	0,051866	25,36847	24,73111	16,46153	24,2074	23,82257	19,28035
-31,3792	0,756793	-0,04388	12	0,003657	273,4482	0,022204	0,03745	0,044976	0,041297	0,030479	0,046226	45,03766	26,70194	22,23424	24,21467	32,81001	21,63281
-31,2752	0,103959	0,009968	12	-0,00083	-1203,89	0,010359	0,047562	0,036861	0,037345	0,016445	0,032815	96,53321	21,02507	27,12866	26,77724	60,8085	30,47428
-30,9043	0,370865	0,410539	12	-0,03421	-29,2299	-0,01046	0,031088	0,019503	0,035639	-0,00078	0,027711	-95,5864	32,16727	51,2735	28,05881	-1276,25	36,08709
-32,1488	-1,24447	-0,25655	12	0,021379	46,77457	-0,00455	0,027244	0,015464	0,032835	-0,0025	0,026949	-219,57	36,70515	64,66456	30,45518	-399,757	37,10677
-31,0697	1,079117	0,068503	12	-0,00571	-175,175	-0,00618	0,01691	0,006748	0,030877	-0,00484	0,034127	-161,803	59,13531	148,1819	32,38655	-206,487	29,30265

-33,7793	-2,70958	-0,95831	12	0,079859	12,522	0,031843	0,020267	0,013199	0,03164	0,01533	0,031276	31,40375	49,34162	75,76101	31,6051	65,23326	31,97293
-31,9849	1,794351	0,054628	12	-0,00455	-219,668	0,0232	0,013616	0,008513	0,034596	0,022744	0,026233	43,10436	73,44159	117,4646	28,90498	43,96683	38,11996
-33,2042	-1,21924	-0,71149	12	0,059291	16,86599	0,044866	0,016348	0,016461	0,035681	0,032222	0,023899	22,28859	61,16857	60,74999	28,02616	31,03435	41,84226
-31,8474	1,356804	0,643972	12	-0,05366	-18,6344	0,000358	0,007247	0,008913	0,032744	0,020233	0,01529	2792,574	137,9965	112,1926	30,54037	49,42316	65,40362
-31,9397	-0,09237	0,015064	12	-0,00126	-796,601	0,001457	0,006701	0,013621	0,029287	-4,5E-05	0,010576	686,2982	149,2371	73,41455	34,14524	-22092,7	94,54951
-34,1116	-2,17184	-0,30247	12	0,025206	39,67349	-0,0099	0,009594	0,014168	0,022863	0,007394	0,009785	-100,963	104,2353	70,58191	43,73927	135,2401	102,1968
-32,9504	1,161211	-0,36767	12	0,030639	32,63826	0,018196	0,016799	0,01936	0,023034	0,000231	0,009984	54,95582	59,52634	51,65174	43,41333	4324,324	100,16
-36,3055	-3,35514	-1,45526	12	0,121271	8,245964	0,059039	0,027898	0,025276	0,027356	0,043965	0,019785	16,93804	35,84431	39,56255	36,55499	22,74527	50,54274
-36,9901	-0,68455	-0,95949	12	0,079958	12,5066	0,077289	0,037417	0,037349	0,035537	0,064268	0,026518	12,93839	26,72588	26,77426	28,13989	15,55973	37,7108
-38,7156	-1,72554	-1,92174	12	0,160145	6,244332	0,120458	0,046338	0,051757	0,037731	0,098003	0,042714	8,301638	21,58077	19,32103	26,50325	10,20373	23,41153

FILTER 3 DATA

Mean displacement (3-points)	diff	time	vel	1/v	mean MA(3) vel	mean MA (9) vel	ave MA(7) vel	mean MA (21) vel	mean MA(4) vel	mean (12) vel	mean MA 1/vel	MA(3)	mean MA (9) 1/ vel	mean MA 1/vel	mean MA (21) 1/vel	mean MA 1/vel	mean MA (12) 1/vel
3,997944																	
4,149695	0,151751																
3,436587	-0,71311																
1,653347	-1,78324	12	0,148603	6,729324													
2,442668	0,789321	12	-0,06578	-15,2029													
0,574437	-1,86823	12	0,155686	6,42319	0,079504						12,57796						
0,219089	-0,35535	24	0,014806	67,53943	0,034905				0,06333		28,64912				15,79039		
-1,90274	-2,12183	12	0,176819	5,655497	0,11577				0,070384		8,637787				14,20786		
-1,84981	0,052929	12	-0,00441	-226,717	0,062405				0,085725		16,0244				11,6652		
-2,13705	-0,28724	12	0,023937	41,77633	0,065448		0,064238		0,052788		15,2792		15,56718		18,94374		
-1,24361	0,893441	12	-0,07445	-13,4312	-0,01831		0,032372		0,030473		-54,6177		30,89046		32,81597		
-2,32811	-1,0845	12	0,090375	11,06503	0,013286	0,051732	0,05468		0,008862		75,26657	19,33051	18,28828		112,8428		
-3,81241	-1,4843	12	0,123691	8,084633	0,046538	0,048964	0,050109		0,040887		21,488	20,42329	19,95642		24,45739		
-4,27156	-0,45915	12	0,038262	26,13537	0,08411	0,060524	0,05346		0,044469		11,88926	16,52248	18,70555		22,48769		
-3,44472	0,826835	12	-0,0689	-14,5132	0,031017	0,035569	0,018357		0,045856	0,046553	32,24042	28,11413	54,47537		21,8072	21,48089	
-2,88715	0,557571	12	-0,04646	-21,5219	-0,0257	0,028761	0,012349		0,011647	0,030297	-38,9081	34,76872	80,97634		85,86148	33,00615	
-4,2094	-1,32225	12	0,110188	9,075416	-0,00173	0,021358	0,024671		0,008271	0,044961	-579,225	46,82086	40,53371		120,908	22,24145	
-5,70488	-1,49548	12	0,124623	8,024201	0,062782	0,035695	0,05311		0,029861	0,042373	15,92809	28,01506	18,82873		33,48859	23,6002	
-6,46784	-0,76296	12	0,06358	15,72824	0,099464	0,0401	0,049282		0,062982	0,046437	10,05393	24,93775	20,29119		15,87765	21,53455	
-6,55449	-0,08665	24	0,00361	276,9828	0,063938	0,048774	0,032128		0,0755	0,032003	15,64021	20,50289	31,12547		13,24499	31,24713	
-6,62335	-0,06886	12	0,005739	174,2566	0,02431	0,03937	0,027482		0,049388	0,032849	41,13596	25,40031	36,38773		20,24785	30,44258	
-7,46515	-0,8418	12	0,07015	14,25519	0,0265	0,033421	0,047346		0,03577	0,0367	37,73638	29,92173	21,1209		27,95663	27,24811	
-8,30918	-0,84403	12	0,070336	14,21751	0,048741	0,036984	0,064032		0,037459	0,048766	20,51642	27,03854	15,61714		26,69609	20,50627	
-9,59143	-1,28226	12	0,106855	9,358508	0,082447	0,056513	0,063556	0,050822	0,06327	0,050139	12,12904	17,69509	15,73415	19,6767	15,80534	19,9446	
-10,0412	-0,44975	12	0,037479	26,68155	0,071557	0,06584	0,051107	0,04553	0,071205	0,042955	13,97497	15,18836	19,56683	21,96359	14,04399	23,28044	
-10,7922	-0,75097	12	0,062581	15,97938	0,068971	0,06055	0,050964	0,051642	0,069313	0,044981	14,49875	16,51522	19,62164	19,36403	14,4274	22,23158	
-11,2123	-0,42011	12	0,035009	28,5639	0,045023	0,050593	0,05545	0,045896	0,060481	0,05364	22,21087	19,76553	18,03436	21,78856	16,53414	18,64267	
-11,3732	-0,16093	24	0,006706	149,1285	0,034765	0,044274	0,055588	0,04551	0,035444	0,058071	28,76442	22,58674	17,98954	21,97324	28,2138	17,22024	
-11,1911	0,182112	12	-0,01518	-65,8935	0,008846	0,042186	0,043398	0,036367	0,02228	0,047624	113,0418	23,70432	23,04231	27,49725	44,88355	20,99771	
-10,9279	0,263189	12	-0,02193	-45,5946	-0,01013	0,039112	0,030217	0,035533	0,001152	0,035411	-98,6751	25,56771	33,09367	28,14292	868,3513	28,23959	
-11,1992	-0,27133	24	0,011305	88,45307	-0,0086	0,032574	0,016567	0,034931	-0,00477	0,031055	-116,266	30,69975	60,3596	28,62753	-209,453	32,20085	
-11,9183	-0,71909	12	0,059924	16,68784	0,016432	0,031417	0,019774	0,04133	0,00853	0,035748	60,85575	31,83022	50,57204	24,19531	117,2302	27,97369	
-12,2715	-0,35317	12	0,02943	33,97842	0,033553	0,022814	0,015038	0,038428	0,019682	0,037722	29,80337	43,83275	66,49808	26,02254	50,80827	26,5096	
-12,6602	-0,38871	12	0,032393	30,87126	0,040582	0,022249	0,014664	0,034081	0,033263	0,034576	24,64128	44,94619	68,19318	29,34216	30,06336	28,92201	
-12,7703	-0,11012	12	0,009177	108,9697	0,023667	0,016315	0,015017	0,032696	0,032731	0,029479	42,25359	61,29302	66,59006	30,58513	30,55213	33,92226	
-13,5627	-0,7924	12	0,066033	15,14392	0,035868	0,019762	0,026619	0,039121	0,034258	0,026077	27,88038	50,60173	37,56778	25,56162	29,19005	38,34742	
-13,3595	0,203209	12	-0,01693	-59,0524	0,019425	0,017136	0,027333	0,040527	0,022667	0,021543	51,47929	58,35827	36,58635	24,67469	44,11678	46,41892	
-14,0894	-0,72988	18	0,040549	24,66163	0,029883	0,023327	0,03151	0,037211	0,024706	0,019707	33,46428	42,86845	31,73573	26,87362	40,47572	50,74351	
-14,8964	-0,80706	12	0,067255	14,86873	0,03029	0,033237	0,032558	0,034479	0,039226	0,022394	33,01422	30,08703	30,71483	29,00282	25,49345	44,65458	
-16,2714	-1,37496	12	0,11458	8,72751	0,074128	0,044712	0,044722	0,036908	0,051363	0,031384	13,49016	22,36541	22,36045	27,0944	19,46944	31,8637	
-15,9105	0,36087	12	-0,03007	-33,2529	0,050588	0,034712	0,035798	0,035304	0,048078	0,030142	19,76767	28,80824	27,93434	28,32536	20,79956	33,17598	
-16,1836	-0,27304	12	0,022753	43,95025	0,035754	0,03397	0,037738	0,036114	0,043629	0,033866	27,96924	29,43743	26,49872	27,68989	22,92055	29,52807	
-16,7	-0,51643	12	0,043036	23,23632	0,011906	0,035153	0,034452	0,034823	0,037574	0,03651	83,99466	28,4471	29,02557	28,71655	26,61401	27,38953	
-17,8662	-1,16619	12	0,097183	10,28988	0,054324	0,044931	0,050755	0,036102	0,033225	0,039615	18,40807	22,25614	19,70256	27,69963	30,09794	25,24283	

-17,8294	0,036749	12	-0,00306	-326,537	0,045719	0,037254	0,044525	0,030867	0,039977	0,036907	21,87282	26,84266	22,45948	32,39663	25,01414	27,09478
-18,7295	-0,90003	12	0,075002	13,33291	0,056374	0,047469	0,045631	0,032654	0,05304	0,040458	17,73859	21,06625	21,91475	30,6239	18,85379	24,71681
-19,8377	-1,10819	12	0,092349	10,82852	0,054763	0,053225	0,042455	0,034072	0,065368	0,047389	18,26054	18,78822	23,55411	29,34982	15,29803	21,10182
-20,9578	-1,12016	12	0,093346	10,71279	0,086899	0,056124	0,060087	0,03685	0,064409	0,049665	11,50759	17,81774	16,64262	27,13725	15,52584	20,13475
-21,3699	-0,41211	12	0,034343	29,1183	0,073346	0,047209	0,061742	0,038166	0,07376	0,053938	13,63402	21,1826	16,19633	26,20149	13,55748	18,53965
-21,2425	0,127424	12	-0,01062	-94,174	0,039023	0,04937	0,054077	0,038383	0,052355	0,049674	25,62561	20,25517	18,49201	26,05335	19,10045	20,13106
-21,2628	-0,02029	12	0,00169	591,5604	0,008471	0,04703	0,040436	0,039508	0,02969	0,044211	118,043	21,2631	24,73066	25,31153	33,68115	22,61893
-21,1524	0,110407	12	-0,0092	-108,689	-0,00604	0,041226	0,039559	0,038531	0,004053	0,033896	-165,483	24,25668	25,27885	25,95299	246,7017	29,50227
-22,3708	-1,21844	12	0,101537	9,848672	0,031342	0,041709	0,043349	0,040513	0,020852	0,044863	31,90593	23,97536	23,06839	24,68358	47,95716	22,29002
-23,3156	-0,94479	24	0,039366	25,40235	0,043901	0,046424	0,03578	0,040986	0,033348	0,046248	22,77863	21,54067	27,94822	24,39863	29,98662	21,62276
-24,2014	-0,88577	12	0,073814	13,54748	0,071572	0,046292	0,03299	0,042958	0,051379	0,048812	13,97185	21,60209	30,31204	23,27835	19,46312	20,48658
-23,6382	0,563238	12	-0,04694	-21,3054	0,022081	0,030816	0,021379	0,040286	0,041945	0,036802	45,28688	32,45101	46,77515	24,82233	23,84062	27,17208
-23,2197	0,418404	12	-0,03487	-28,6804	-0,00266	0,01657	0,017915	0,035482	0,007844	0,034152	-375,514	60,35091	55,81968	28,18367	127,4804	29,28077
-23,1168	0,102947	12	-0,00858	-116,565	-0,03013	0,011801	0,016448	0,035879	-0,00414	0,027187	-33,1923	84,74076	60,79848	27,87114	-241,43	36,78228
-23,5956	-0,4788	12	0,0399	25,06266	-0,00118	0,017414	0,023462	0,035849	-0,01262	0,022816	-846,057	57,42546	42,62185	27,89516	-79,2356	43,82837
-23,6516	-0,05598	12	0,004665	214,3674	0,011995	0,017744	0,009623	0,032868	0,00028	0,015426	83,36575	56,3559	103,914	30,42471	3574,531	64,82498
-23,4809	0,170717	12	-0,01423	-70,2916	0,010113	0,017186	0,001967	0,026734	0,00544	0,011379	98,88444	58,1871	508,333	37,40503	183,8273	87,8833
-23,5107	-0,02988	12	0,00249	401,6423	-0,00236	0,006181	-0,00822	0,028285	0,008207	0,012471	-424,221	161,7928	-121,625	35,35448	121,8464	80,18543
-23,9609	-0,45014	12	0,037512	26,65837	0,008592	0,005975	0,003842	0,028988	0,00761	0,015456	116,3919	167,3735	260,2808	34,49733	131,4065	64,69897
-24,184	-0,22308	12	0,01859	53,79333	0,01953	-0,00016	0,011479	0,027824	0,011091	0,017772	51,20231	-6194,79	87,11813	35,94066	90,16184	56,26814
-23,9687	0,21521	12	-0,01793	-55,7596	0,012722	0,003061	0,010142	0,022342	0,010164	0,007816	78,60153	326,684	98,59791	44,759	98,38411	127,9401
-23,8436	0,125129	12	-0,01043	-95,9008	-0,00326	0,005777	0,002953	0,021991	0,006935	0,003667	-307,002	173,1133	338,6883	45,47282	144,1974	272,7271
-23,216	0,627572	12	-0,0523	-19,1213	-0,02689	0,000919	-0,00518	0,015929	-0,01552	-0,00684	-37,1935	1088,231	-192,866	62,77758	-64,4438	-146,142
-23,0015	0,214586	12	-0,01788	-55,9215	-0,02687	-0,0055	-0,00571	0,01068	-0,02464	-0,00442	-37,2175	-181,775	-175,218	93,63155	-40,5921	-226,169
-21,3347	1,666788	12	-0,1389	-7,19948	-0,06969	-0,02145	-0,02591	-0,00038	-0,05488	-0,01309	-14,3487	-46,6138	-38,6017	-2637,54	-18,2227	-76,3894
-21,1528	0,181848	12	-0,01515	-65,9891	-0,05731	-0,02156	-0,03343	-0,00274	-0,05606	-0,01364	-17,4484	-46,3909	-29,9139	-365,48	-17,8386	-73,3205
-21,1998	-0,04701	12	0,003917	255,2757	-0,05005	-0,0214	-0,03553	-0,00204	-0,042	-0,01664	-19,9819	-46,7348	-28,1489	-489,252	-23,807	-60,1059
-22,1858	-0,98597	12	0,082164	12,17075	0,023643	-0,01644	-0,02123	0,001788	-0,01699	-0,01018	42,29669	-60,8424	-47,1131	559,238	-58,8482	-98,2413
-22,2051	-0,0193	12	0,001608	621,7187	0,02923	-0,01832	-0,01951	0,002303	0,018134	-0,00886	34,21143	-54,5771	-51,2659	434,2423	55,14505	-112,874
-23,1683	-0,96323	12	0,080269	12,45806	0,054681	-0,00741	-0,00057	0,00129	0,04199	-0,00238	18,288	-134,931	-1760,61	775,1107	23,81529	-420,554
-23,5933	-0,42494	12	0,035412	28,2391	0,039097	-0,00232	0,007045	0,001102	0,049863	-0,00255	25,5777	-431,413	141,9354	907,5837	20,05476	-391,727
-24,3592	-0,76593	12	0,063827	15,66732	0,059836	0,010585	0,036006	0,000626	0,045279	0,001217	16,71231	94,47516	27,77289	1596,83	22,0852	821,6989
-23,5598	0,799451	12	-0,06662	-15,0103	0,010873	0,005169	0,028654	-0,00031	0,028222	-0,00284	91,97344	193,4468	34,89924	-3214,29	35,43352	-352,083
-23,9979	-0,43811	12	0,036509	27,39034	0,011238	0,024659	0,03331	0,003088	0,017282	0,001071	88,97999	40,55285	30,0211	323,8599	57,86423	933,5777
-24,0941	-0,09626	12	0,008021	124,6676	-0,00736	0,027234	0,022718	0,003878	0,010434	0,006098	-135,806	36,71851	44,01784	257,8488	95,83874	163,9954
-24,9502	-0,85607	12	0,071339	14,01753	0,038623	0,034726	0,03268	0,005375	0,012312	0,013533	25,89113	28,79724	30,60012	186,0344	81,22011	73,89425
-26,8715	-1,92129	12	0,160108	6,245794	0,079823	0,043386	0,044085	0,012777	0,068994	0,03845	12,52775	23,04894	22,6834	78,26324	14,49393	26,00775
-27,1959	-0,32441	12	0,027034	36,99015	0,08616	0,046211	0,042888	0,014742	0,066626	0,041966	11,60626	21,63986	23,31639	67,83256	15,00924	23,82895
-27,5621	-0,3662	12	0,030517	32,76874	0,072553	0,040683	0,03813	0,016077	0,07225	0,044182	13,78304	24,58031	26,22629	62,2014	13,84092	22,63345
-26,4601	1,102041	12	-0,09184	-10,8889	-0,01143	0,026544	0,034527	0,009917	0,031456	0,029682	-87,5002	37,67296	28,96249	100,8333	31,79091	33,69009
-27,8288	-1,36873	12	0,114061	8,767222	0,01758	0,032126	0,045606	0,014464	0,019944	0,039053	56,88135	31,12763	21,92681	69,13896	50,14065	25,60598
-28,5004	-0,67163	12	0,055969	17,8669	0,026065	0,045747	0,052456	0,017983	0,027178	0,037028	38,36617	21,85938	19,0636	55,60857	36,79488	27,00631
-29,548	-1,04754	12	0,087295	11,45537	0,085775	0,05139	0,054735	0,022636	0,041372	0,041352	11,65837	19,4591	18,2697	44,17682	24,17076	24,18262
-30,1438	-0,59581	12	0,049651	20,14059	0,064305	0,056015	0,038956	0,027491	0,076744	0,040171	15,55083	17,85224	25,67005	36,37554	13,0303	24,89379
-30,8074	-0,66364	12	0,055303	18,08217	0,064083	0,054234	0,042994	0,030976	0,062055	0,050331	15,60473	18,43876	23,25889	32,28304	16,11481	19,86847
-31,2238	-0,41643	12	0,034703	28,81604	0,046552	0,0403	0,043592	0,039243	0,056738	0,05018	21,4812	24,81408	22,93983	25,4824	17,62485	19,92807
-31,5629	-0,33901	12	0,028251	35,39694	0,039419	0,040435	0,060748	0,04131	0,041977	0,051866	25,36847	24,73111	16,46153	24,2074	23,82257	19,28035
-31,6067	-0,04388	12	0,003657	273,4482	0,022204	0,03745	0,044976	0,041297	0,030479	0,046226	45,03766	26,70194	22,23424	24,21467	32,81001	21,63281
-31,5968	0,009968	12	-0,00083	-1203,89	0,010359	0,047562	0,036861	0,037345	0,016445	0,032815	96,53321	21,02507	27,12866	26,77724	60,8085	30,47428
-31,1862	0,410539	12	-0,03421	-29,2299	-0,01046	0,031088	0,019503	0,035639	-0,00078	0,027711	-95,5864	32,16727	51,2735	28,05881	-1276,25	36,08709
-31,4428	-0,25655	12	0,021379	46,77457	-0,00455	0,027244	0,015464	0,032835	-0,0025	0,026949	-219,57	36,70515	64,66456	30,45518	-399,757	37,10677
-31,3743	0,068503	12	-0,00571	-175,175	-0,00618	0,01691	0,006748	0,030877	-0,00484	0,034127	-161,803	59,13531	148,1819	32,38655	-206,487	29,30265
-32,3326	-0,95831	12	0,079859	12,522	0,031843	0,020267	0,013199	0,03164	0,01533	0,031276	31,40375	49,34162	75,76101	31,6051	65,23326	31,97293
-32,278	0,054628	12	-0,00455	-219,668	0,0232	0,013616	0,008513	0,034596	0,022744	0,026233	43,10436	73,44159	117,4646	28,90498	43,96683	38,11996
-32,9895	-0,71149	12	0,059291	16,86599	0,044866	0,016348	0,016461	0,035681	0,032222	0,023899	22,28859	61,16857	60,74999	28,02616	31,03435	41,84226
-32,3455	0,643972	12	-0,05366	-18,6344	0,000358	0,007247	0,008913	0,032744	0,020233	0,01529	2792,574	137,9965	112,1926	30,54037	49,42316	65,40362
-32,3304	0,015064	12	-0,00126	-796,601	0,001457	0,006701	0,013621	0,029287	-4,5E-05	0,010576	686,2982	149,2371	73,41455	34,14524	-22092,7	94,54951
-32,6329	-0,30247	12	0,025206	39,67349	-0,0099	0,009594	0,014168	0,022863	0,007394	0,009785	-100,963	104,2353	70,58191	43,73927	135,2401	102,1968
-33,0006	-0,36767	12	0,030639	32,63826	0,018196	0,016799	0,01936	0,023034	0,000231	0,009984	54,95582	59,52634	51,65174	43,41333	4324,324	100,16
-34,4558	-1,45526	12	0,121271	8,245964	0,059039	0,027898	0,025276	0,027356	0,043965	0,019785	16,93804	35,84431	39,56255	36,55499	22,74527	50,54274
-35,4153	-0,95949	12	0,079958	12,5066	0,077289	0,037417	0,037349	0,035537	0,064268	0,026518	12,93839	26,72588	26,77426	28,13989	15,55973	37,7108
-37,3371	-1,92174	12	0,160145	6,244332	0,120458	0,046338	0,051757	0,037731	0,098003	0,042714	8,301638	21,58077	19,32103	26,50325	10,20373	23,41153
-37,8528	-0,51577	12	0,042981	23,2661	0,094361	0,051619	0,065564	0,037113	0,101089	0,044514	10,59756	19,3727	15,25238	26,94494	9,892287	22,46476

FILTER 4 DATA

mean 7 points	diff	time	vel	1/v
2,825298				
2,600475	-0,22482	12	0,018735	53,37536
1,634412	-0,96606	12	0,080505	12,42154
0,296434	-1,33798	12	0,111498	8,968755
0,029259	-0,26717	24	0,011132	89,82881
-0,75429	-0,78355	12	0,065296	15,31491
-0,94512	-0,19083	12	0,015902	62,88348
-2,01536	-1,07024	12	0,089187	11,21244
-2,63437	-0,61901	12	0,051584	19,38587
-2,86968	-0,23531	12	0,01961	50,99551
-2,67621	0,193473	12	-0,01612	-62,0241
-3,07894	-0,40273	12	0,033561	29,79645
-3,75783	-0,67889	12	0,056574	17,6759
-4,58818	-0,83035	12	0,069196	14,45176
-4,85311	-0,26493	12	0,022078	45,29493
-4,93301	-0,0799	12	0,006658	150,1921
-5,59609	-0,66308	12	0,055257	18,09725
-6,57615	-0,98006	24	0,040836	24,48833
-7,25674	-0,68058	12	0,056715	17,63193
-7,90268	-0,64594	12	0,053829	18,57752
-8,43457	-0,53189	12	0,044324	22,56105
-9,11001	-0,67544	12	0,056287	17,76608
-9,89887	-0,78885	12	0,065738	15,21193
-10,4702	-0,57135	12	0,047612	21,00292
-10,7068	-0,23663	12	0,019719	50,713
-11,0212	-0,31433	24	0,013097	76,35225
-11,1593	-0,1381	12	0,011508	86,89643
-11,5113	-0,35206	12	0,029338	34,08547
-11,6552	-0,14385	24	0,005994	166,8454
-11,7798	-0,12464	12	0,010387	96,27849
-12,1101	-0,33028	12	0,027523	36,33289
-12,6716	-0,56149	12	0,046791	21,37161
-12,8219	-0,15034	12	0,012529	79,81695
-13,3487	-0,5268	12	0,0439	22,77904
-13,9479	-0,5992	12	0,049933	20,02682
-14,5362	-0,58826	18	0,032681	30,59886
-14,7417	-0,20555	12	0,017129	58,37971
-15,4107	-0,66902	12	0,055751	17,93677
-15,8807	-0,46999	12	0,039166	25,53264
-16,6732	-0,79244	12	0,066037	15,14314
-17,0136	-0,34046	12	0,028372	35,24624
-17,5235	-0,50983	12	0,042486	23,5373
-18,2016	-0,6781	12	0,056509	17,69637
-19,1768	-0,97519	12	0,081266	12,30533
-19,7462	-0,56943	12	0,047453	21,07359
-20,1484	-0,40217	12	0,033514	29,83839
-20,6324	-0,48408	12	0,04034	24,78912
-21,1703	-0,53787	12	0,044822	22,3104
-21,7089	-0,53863	12	0,044886	22,27883
-22,123	-0,41406	12	0,034505	28,98139
-22,5604	-0,43742	12	0,036451	27,43384
-22,681	-0,12062	24	0,005026	198,971
-22,9704	-0,28935	12	0,024113	41,47181
-23,355	-0,3846	12	0,03205	31,20106
-23,7281	-0,37314	12	0,031095	32,15971
-23,5193	0,208844	12	-0,0174	-57,4592
-23,4258	0,093474	12	-0,00779	-128,378
-23,4321	-0,00633	12	0,000527	1897,19
-23,6576	-0,22546	12	0,018788	53,22425
-23,839	-0,18145	12	0,01512	66,13548
-23,7972	0,041788	12	-0,00348	-287,167
-23,7639	0,033366	12	-0,00278	-359,651
-23,6524	0,111505	12	-0,00929	-107,619
-23,5918	0,060589	12	-0,00505	-198,057
-22,8313	0,760508	12	-0,06338	-15,7789
-22,4489	0,382357	12	-0,03186	-31,3843
-22,3129	0,136046	12	-0,01134	-88,2053
-22,0672	0,245716	12	-0,02048	-48,8368
-21,7467	0,320458	12	-0,0267	-37,4464
-22,2924	-0,54573	12	0,045477	21,98902
-22,3208	-0,02837	12	0,002364	423,0204
-23,0429	-0,72213	12	0,060178	16,61742
-23,324	-0,28104	12	0,02342	42,69855
-23,52	-0,19598	12	0,016332	61,22985
-23,8608	-0,34083	12	0,028402	35,20843
-24,5004	-0,63966	12	0,053305	18,7601
-25,107	-0,60658	12	0,050548	19,78303
-25,4048	-0,29774	12	0,024812	40,30331
-25,8731	-0,46835	12	0,039029	25,6221
-26,35	-0,4769	12	0,039742	25,16256
-27,0466	-0,69658	12	0,058048	17,227
-27,7615	-0,71494	12	0,059578	16,78472
-28,3205	-0,55896	12	0,04658	21,46849
-28,449	-0,12852	12	0,01071	93,37234
-29,3093	-0,86032	12	0,071693	13,94832
-29,8898	-0,58049	12	0,048374	20,67231
-30,6359	-0,74611	12	0,062176	16,08338
-30,9284	-0,29253	12	0,024377	41,02205
-31,2168	-0,28837	12	0,024031	41,6129
-31,338	-0,12122	12	0,010102	98,99403
-31,4852	-0,14713	12	0,012261	81,56187
-31,4598	0,025402	12	-0,00212	-472,398
-31,8132	-0,35345	12	0,029454	33,95075
-31,7916	0,021575	12	-0,0018	-556,188
-32,0524	-0,26072	12	0,021726	46,02727
-32,1341	-0,08174	12	0,006811	146,8121
-32,282	-0,14791	12	0,012326	81,1283

-32,5624	-0,28039	12	0,023366	42,79681
-32,8311	-0,26867	12	0,022389	44,66496
-33,192	-0,36089	12	0,030074	33,25114
-33,907	-0,71502	12	0,059585	16,78279
-34,6943	-0,78735	12	0,065612	15,24107
-35,922	-1,22768	12	0,102307	9,774528
-37,383	-1,46099	12	0,121749	8,213609
-38,7802	-1,39723	12	0,116436	8,588406

Cadia Tailins Dam

										FILTER 1 DATA								FILTER2 DATA						
	real displacement	difference	ave 3 point	time (days)	time accumulated (days)	Vel	vel 3 ave	1/v	1/v 3 ave	MA 3	MA 9	MA 2	MA 6	MA 4	MA 12	MA 7	MA 21	MA 3 (ave 3)	MA 9 (ave 3)	MA 2 (ave 3)	MA 6 (ave 3)	MA 4 (ave 3)	MA 12 (ave 3)	1/v MA 4	1/v MA 12
2017-01-01	0																								
2017-01-13	-4,2	-4,2		12	12	0,35		2,857143																	
2017-01-25	-7,4	-3,2		12	24	0,266667		3,75																	
2017-02-06	-10,1	-2,7	-3,366666667	12	36	0,225	0,280556	4,444444	3,564356436			0,308333												3,966942	
2017-02-18	-12,1	-2	-2,633333333	12	48	0,166667	0,219444	6	4,556962025	0,280555556		0,245833			0,252083333									3,966942	
2017-03-02	-14,7	-2,6	-2,433333333	12	60	0,216667	0,202778	4,615385	4,931506849	0,219444444		0,195833			0,21875					0,25				4,571429	
2017-03-14	-13,7	1	-1,2	12	72	-0,08333	0,1	-12	10	0,202777778		0,191667	0,190277778		0,13125			0,234259259		0,211111111		0,20069444		7,619048	
2017-03-26	-18	-4,3	-1,966666667	12	84	0,358333	0,163889	2,790698	6,101694915	0,1		0,066667	0,191666667	0,164583333				0,174074074		0,151388889		0,17152778		6,075949	
2017-04-07	-19,7	-1,7	-1,666666667	12	96	0,141667	0,138889	7,058824	7,2	0,163888889		0,1375	0,170833333	0,158333333		0,214286		0,155555556		0,131944444	0,18425926	0,15138889		6,315789	
2017-05-01	-19,5	0,2	-1,933333333	24	120	-0,00833	0,080556	-120	12,4137931	0,138888889	0,181481	0,25	0,131944444	0,102083333		0,184524		0,134259259		0,151388889	0,15092593	0,12083333		9,795918	
2017-05-13	-20	-0,5	-0,666666667	12	132	0,041667	0,055556	24	18	0,163888889	0,147222	0,066667	0,111111111	0,133333333		0,145238		0,127777778		0,109722222	0,12361111	0,10972222		7,5	
2017-05-25	-21,3	-1,3	-0,533333333	12	144	0,108333	0,044444	9,230769	22,5	0,058333333	0,12963	0,016667	0,093055556	0,070833333		0,119048		0,091666667	0,142901235	0,068055556	0,09722222	0,07986111		14,11765	
2017-06-06	-20,1	1,2	-0,2	12	156	-0,1	0,016667	-10	60	0,047222222	0,093519	0,075	0,090277778	0,010416667	0,140278	0,110714		0,060185185	0,113580247	0,05	0,08333333	0,04930556		96	7,128713
2017-06-18	-19,2	0,9	0,266666667	12	168	-0,075	-0,02222	-13,3333	-45	0,016666667	0,066667	0,004167	0,018055556	-0,00625	0,104861	0,065476		0,038888889	0,086728395	0,030555556	0,05231481	0,02361111		-160	9,536424
2017-06-30	-22,2	-3	-0,3	12	180	0,25	0,025	4	40	-0,022222222	0,07037	-0,0875	0,036111111	0,045833333	0,103472	0,066667		0,012962963	0,066975309	-0,002777778	0,03333333	0,01597222		21,81818	9,66443
2017-07-12	-20,2	2	-0,033333333	12	192	-0,16667	0,002778	-6	360	0,025	0,061111	0,0875	0,009722222	-0,022916667	0,070833	0,05119		0,006481481	0,05617284	0,001388889	0,02037037	0,00555556	0,116414141	-43,6364	14,11765
2017-07-24	-20,9	-0,7	-0,566666667	12	204	0,058333	0,047222	17,14286	21,17647059	0,002777778	0,027778	0,041667	0,0125	0,016666667	0,061806	0,007143		0,001851852	0,043209877	0,013888889	0,01898148	0,01319444	0,108796296	60	16,17978
2017-08-05	-21,4	-0,5	0,266666667	12	216	0,041667	-0,02222	24	-45	0,047222222	0,016667	-0,05417	0,001388889	0,045833333	0,047222	0,016667		0,025	0,025308642	0,025	0,00787037	0,01319444	0,085648148	21,81818	21,17647
2017-08-29	-22,1	-0,7	-0,633333333	12	228	0,058333	0,052778	17,14286	18,94736842	-0,022222222	0,024074	0,05	0,027777778	-0,002083333	0,059028	0,016667		0,009259259	0,022222222	0,0125	0,01388889	0,02013889	0,071296296	-480	16,94118
2017-09-10	-23,8	-1,7	-0,966666667	12	240	0,141667	0,080556	7,058824	12,4137931	0,052777778	0,035185	0,05	0,063888889	0,075	0,040972	0,009524		0,025925926	0,025	0,015277778	0,03101852	0,03958333	0,052546296	13,33333	24,40678
2017-09-22	-24	-0,2	-0,866666667	12	252	0,016667	0,072222	60	13,84615385	0,080555556	0,025	0,1	0,025	0,064583333	0,030556	0,044048		0,037037037	0,02808642	0,066666667	0,03888889	0,04583333	0,048611111	15,48387	32,72727
2017-10-16	-28,3	-4,3	-2,066666667	24	276	0,179167	0,086111	5,581395	11,61290323	0,072222222	0,056019	0,079167	0,082638889	0,098958333	0,046181	0,057143		0,068518519	0,035802469	0,076388889	0,05277778	0,07291667	0,041666667	10,10526	21,65414
2017-10-28	-29,4	-1,1	-1,866666667	12	288	0,091667	0,155556	10,90909	6,428571429	0,1125	0,074537	0,097917	0,088194444	0,107291667	0,050347	0,047024	0,103598	0,07962963	0,055555556	0,079166667	0,07083333	0,09861111	0,036111111	9,320388	19,86207
2017-11-09	-33,2	-3,8	-3,066666667	12	300	0,316667	0,255556	3,157895	3,913043478	0,095833333	0,081944	0,135417	0,134027778	0,151041667	0,067708	0,083929	0,102083	0,10462963	0,08117284	0,120833333	0,11712963	0,14236111	0,036574074	6,62069	14,76923
2017-11-21	-35,5	-2,3	-2,4	12	312	0,191667	0,2	5,217391	5	0,195833333	0,121759	0,204167	0,15625	0,194791667	0,092014	0,120833	0,098674	0,165740741	0,10308642	0,205555556	0,14166667	0,17430556	0,044907407	5,13369	10,86792
2017-12-03	-37,5	-2	-2,7	12	324	0,166667	0,225	6	4,444444444	0,2	0,133796	0,254167	0,160416667	0,191666667	0,112153	0,142262	0,096023	0,203703704	0,122839506	0,227777778	0,16574074	0,20902778	0,0625	5,217391	8,916409
2017-12-15	-41	-3,5	-2,6	12	336	0,291667	0,216667	3,428571	4,615384615	0,225	0,161574	0,179167	0,20625	0,241666667	0,115625	0,157738	0,101705	0,226851852	0,149382716	0,2125	0,18981481	0,22430556	0,077777778	4,137931	8,648649
2017-12-27	-43,8	-2,8	-2,766666667	12	348	0,233333	0,230556	4,285714	4,337349398	0,216666667	0,181019	0,229167	0,215277778	0,220833333	0,148958	0,179167	0,102462	0,213888889	0,169135802	0,220833333	0,21388889	0,21805556	0,09837963	4,528302	6,713287
2018-01-08	-47,4	-3,6	-3,3	12	360	0,3	0,275	3,333333	3,636363636	0,230555556	0,198611	0,2625	0,25	0,247916667	0,169097	0,210119	0,119886	0,224074074	0,190740741	0,223611111	0,2337963	0,23680556	0,114351852	4,033613	5,913758
2018-01-20	-52,9	-5,5	-3,966666667	12	372	0,458333	0,330556	2,181818	3,025210084	0,275	0,247685	0,266667	0,273611111	0,320833333	0,203819	0,227381	0,124432	0,240740741	0,219444444	0,252777778	0,2462963	0,26319444	0,133333333	3,116883	4,906303
2018-02-01	-57,8	-4,9	-4,666666667	12	384	0,408333	0,388889	2,44898	2,571428571	0,330555556	0,273148	0,379167	0,309722222	0,35	0,232986	0,279762	0,136553	0,278703704	0,25308642	0,302777778	0,27777778	0,30625	0,152314815	2,857143	4,292101
2018-02-13	-63,1	-5,3	-5,233333333	12	396	0,441667	0,436111	2,264151	2,292993631	0,388888889	0,312037	0,433333	0,355555556	0,402083333	0,257986	0,292857	0,157008	0,331481481	0,284259259	0,359722222	0,31296296	0,35763889	0,181712963	2,487047	3,876178
2018-02-25	-69,2	-6,1	-5,433333333	12	408	0,508333	0,452778	1,967213	2,208588957	0,436111111	0,333333	0,425	0,391666667	0,454166667	0,298958	0,328571	0,17822	0,385185185	0,30617284	0,4125	0,35231481	0,40208333	0,209722222	2,201835	3,344948
2018-03-09	-100,1	-30,9	-14,1	12	420	2,575	1,175	0,38835	0,85106383	0,452777778	0,598148	0,475	0,781944444	0,983333333	0,498611	0,377381	0,290341	0,425925926	0,414506173	0,444444444	0,50972222	0,61319444	0,239351852	1,016949	2,005571

Appendix D: Moving average figures

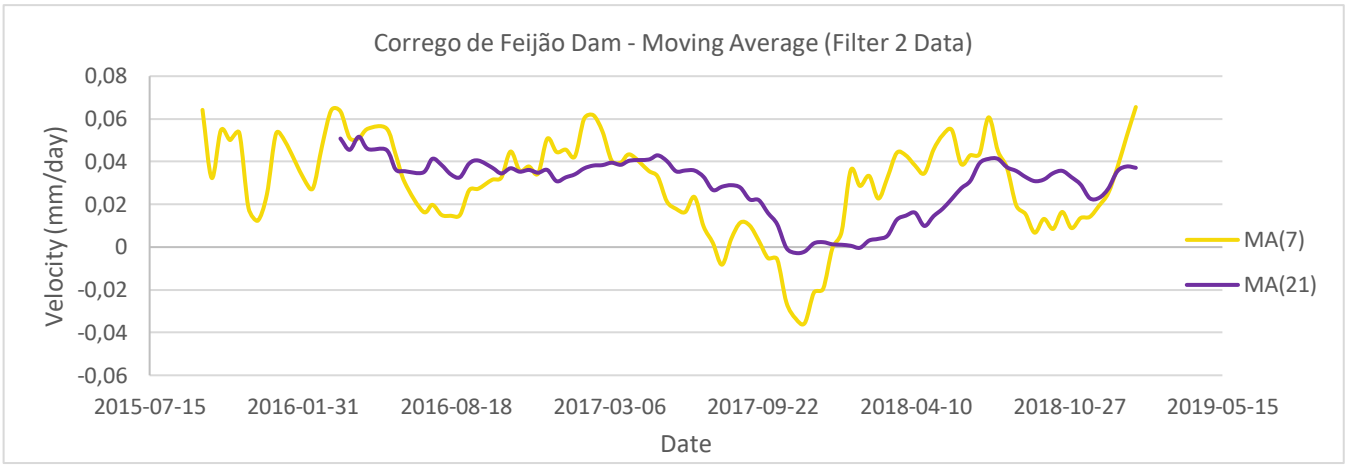

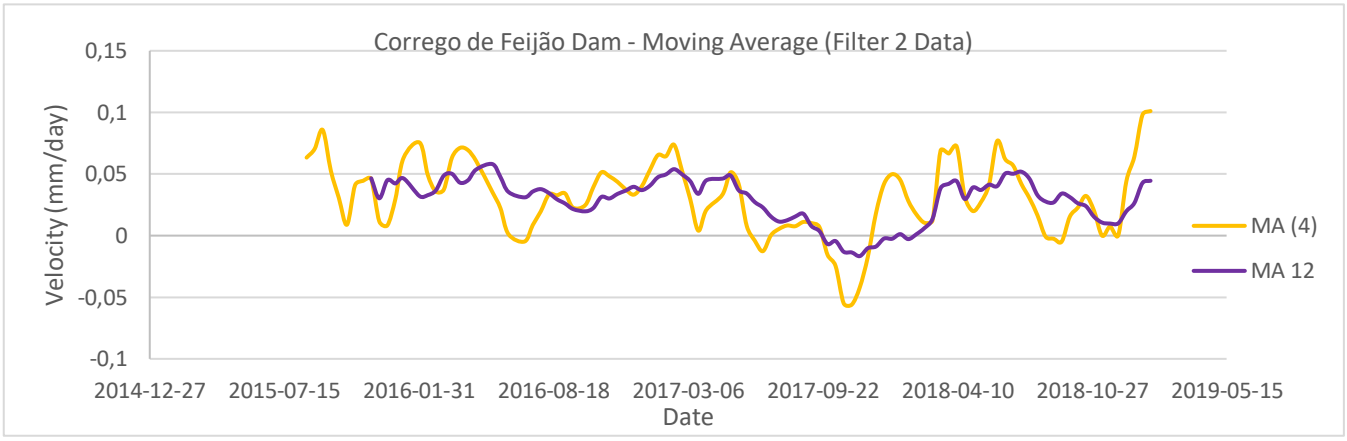

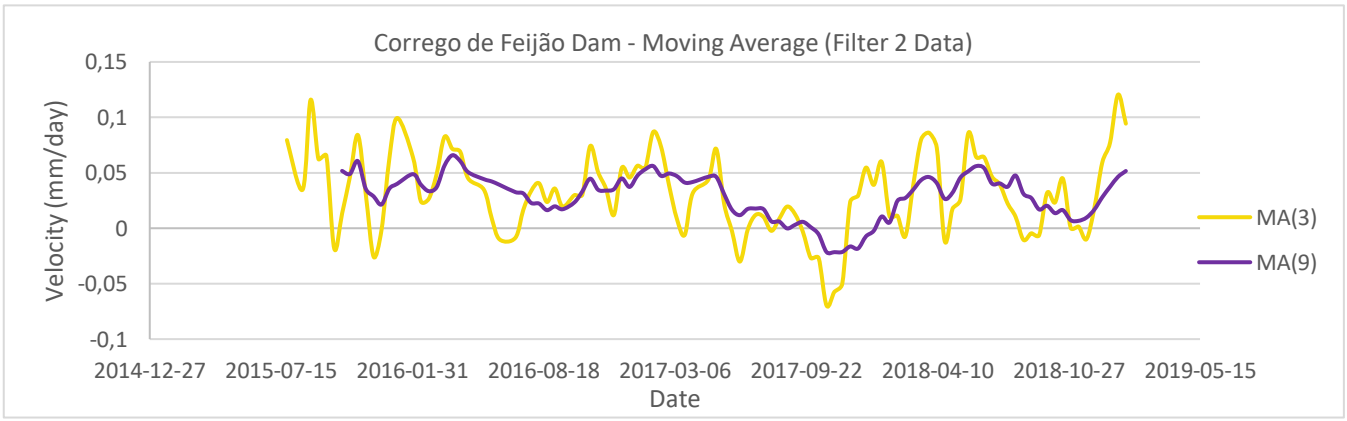

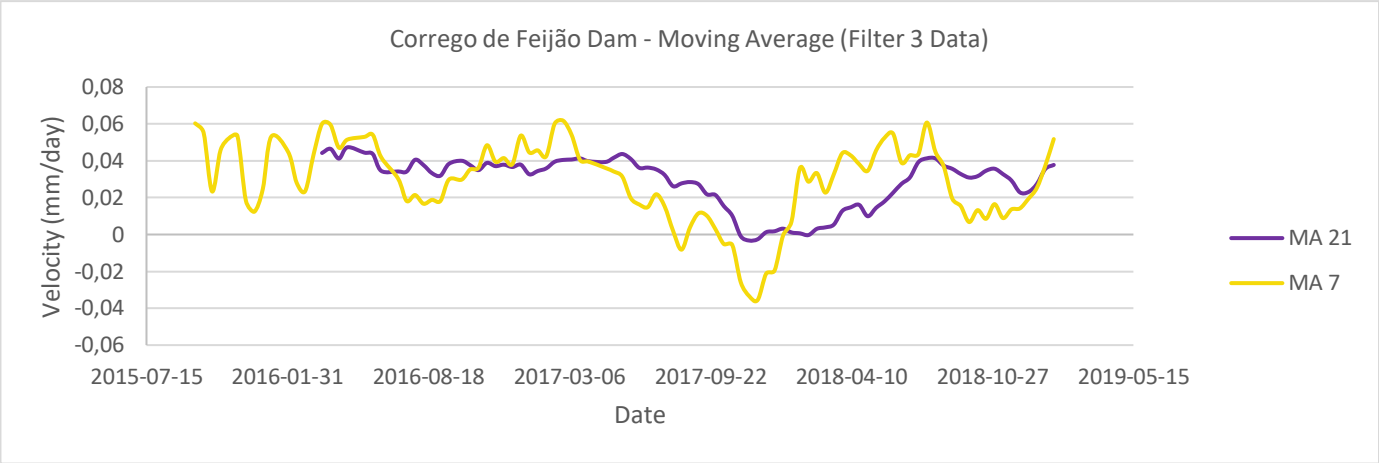
Corrego de Feijão Dam - Moving Average (Filter 3 Data)
Velocity (mm/day)
0,08
0,06
0,04
0,02
0
-0,02
-0,04
-0,06
2015-07-15
2016-01-31
2016-08-18
2017-03-06
2017-09-22
2018-04-10
2018-10-27
2019-05-15
Date
MA 21
MA 7

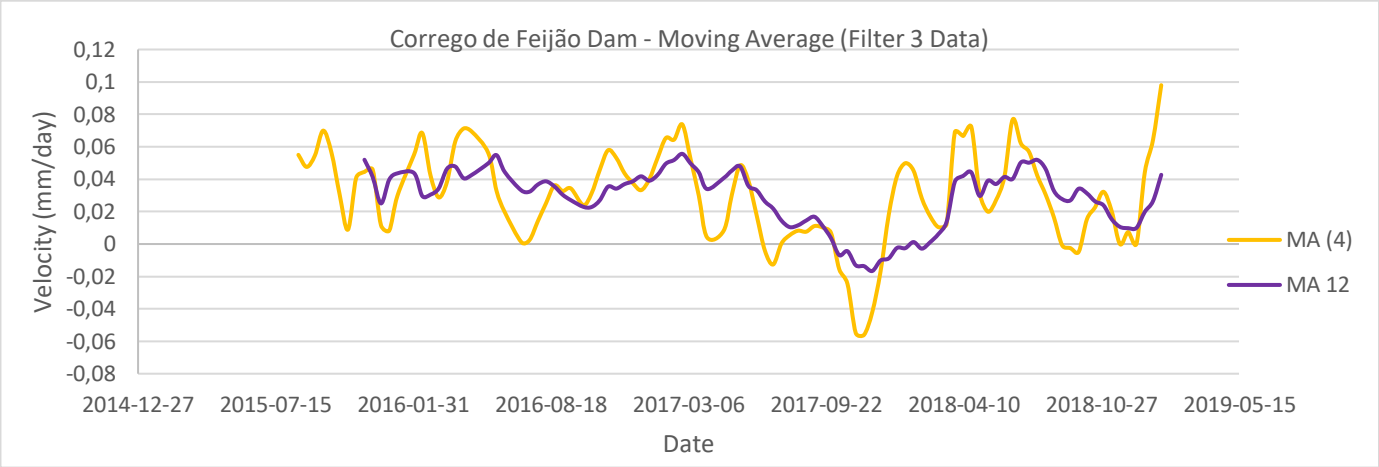
Corrego de Feijão Dam - Moving Average (Filter 3 Data)
Velocity (mm/day)
0,12
0,1
0,08
0,06
0,04
0,02
0
-0,02
-0,04
-0,06
-0,08
2014-12-27
2015-07-15
2016-01-31
2016-08-18
2017-03-06
2017-09-22
2018-04-10
2018-10-27
2019-05-15
Date
MA (4)
MA 12

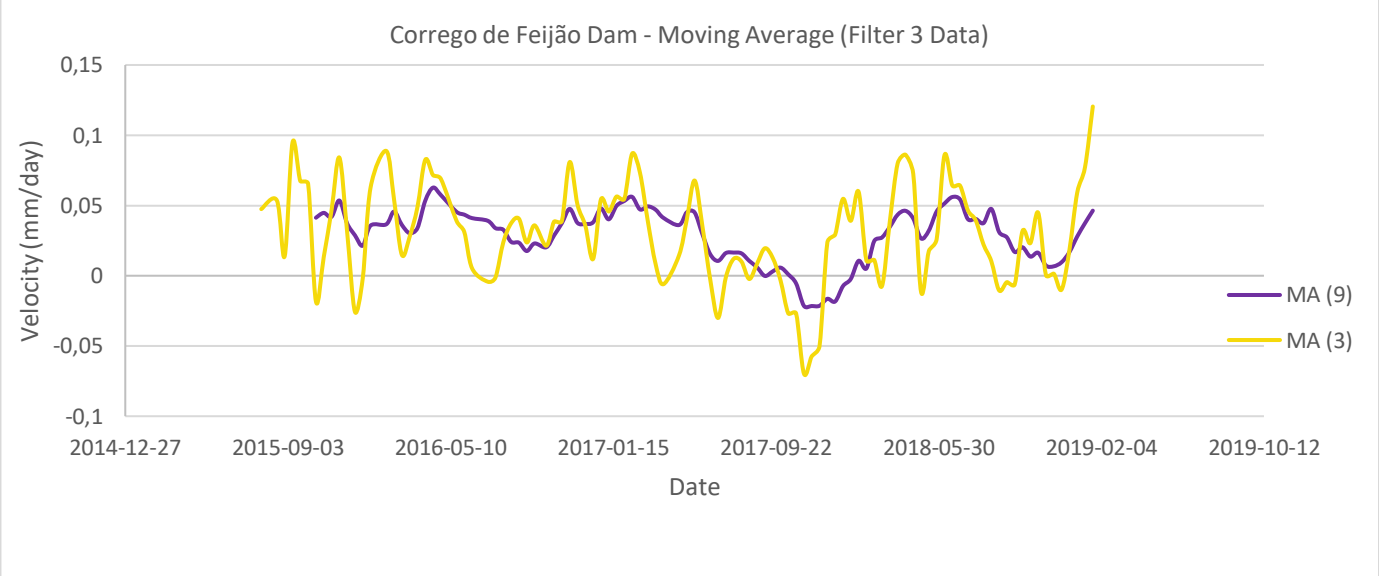
Corrego de Feijão Dam - Moving Average (Filter 3 Data)
Velocity (mm/day)
0,15
0,1
0,05
0
-0,05
-0,1
2014-12-27
2015-09-03
2016-05-10
2017-01-15
2017-09-22
2018-05-30
2019-02-04
2019-10-12
Date
MA (9)
MA (3)

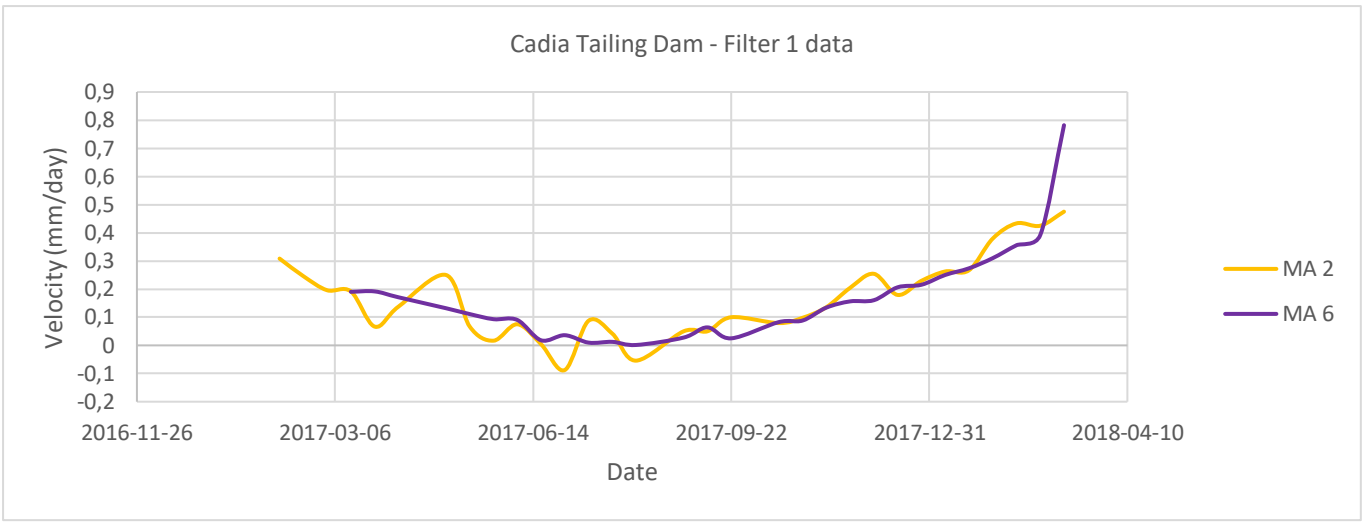
Cadia Tailing Dam - Filter 1 data
Velocity (mm/day)
0,9
0,8
0,7
0,6
0,5
0,4
0,3
0,2
0,1
0
-0,1
-0,2
2016-11-26
2017-03-06
2017-06-14
2017-09-22
2017-12-31
2018-04-10
Date
MA 2
MA 6

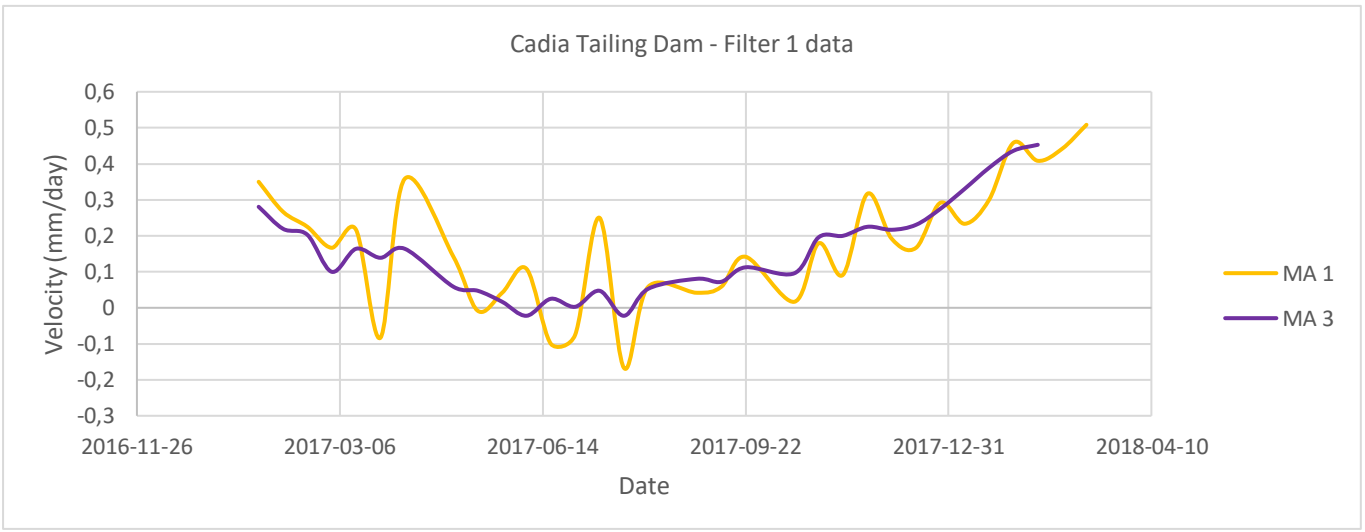
Cadia Tailing Dam - Filter 1 data
Velocity (mm/day)
0,6
0,5
0,4
0,3
0,2
0,1
0
-0,1
-0,2
-0,3
2016-11-26
2017-03-06
2017-06-14
2017-09-22
2017-12-31
2018-04-10
Date
MA 1
MA 3

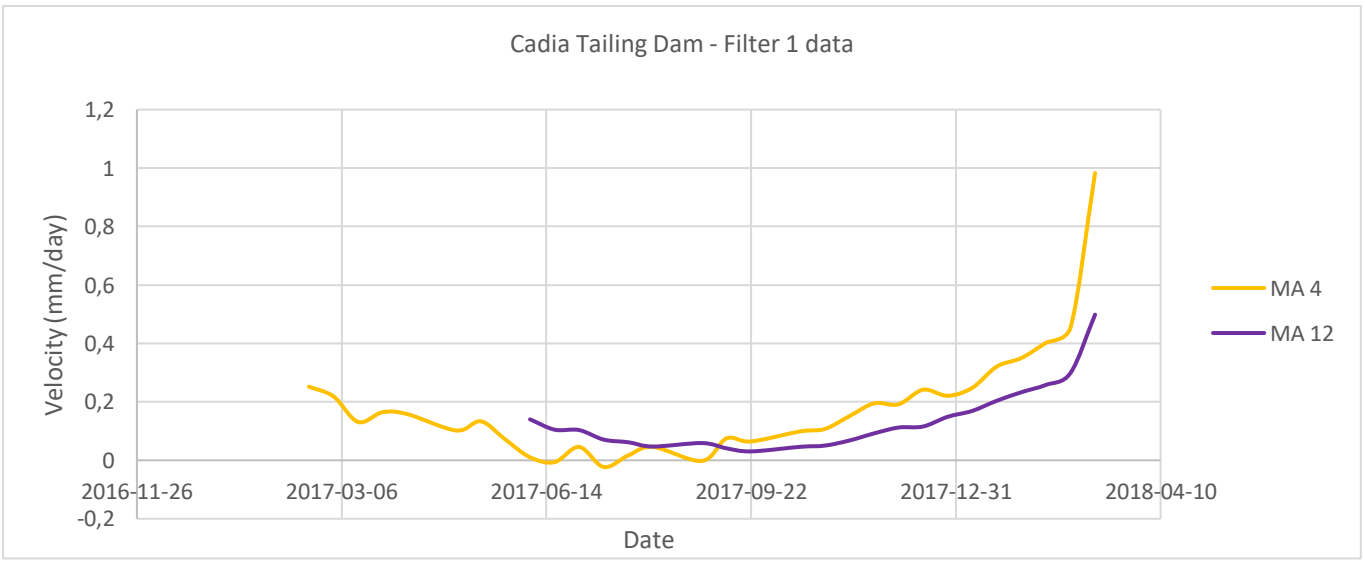
Cadia Tailing Dam - Filter 1 data
Velocity (mm/day)
1,2
1
0,8
0,6
0,4
0,2
0
-0,2
2016-11-26
2017-03-06
2017-06-14
2017-09-22
2017-12-31
2018-04-10
Date
MA 4
MA 12

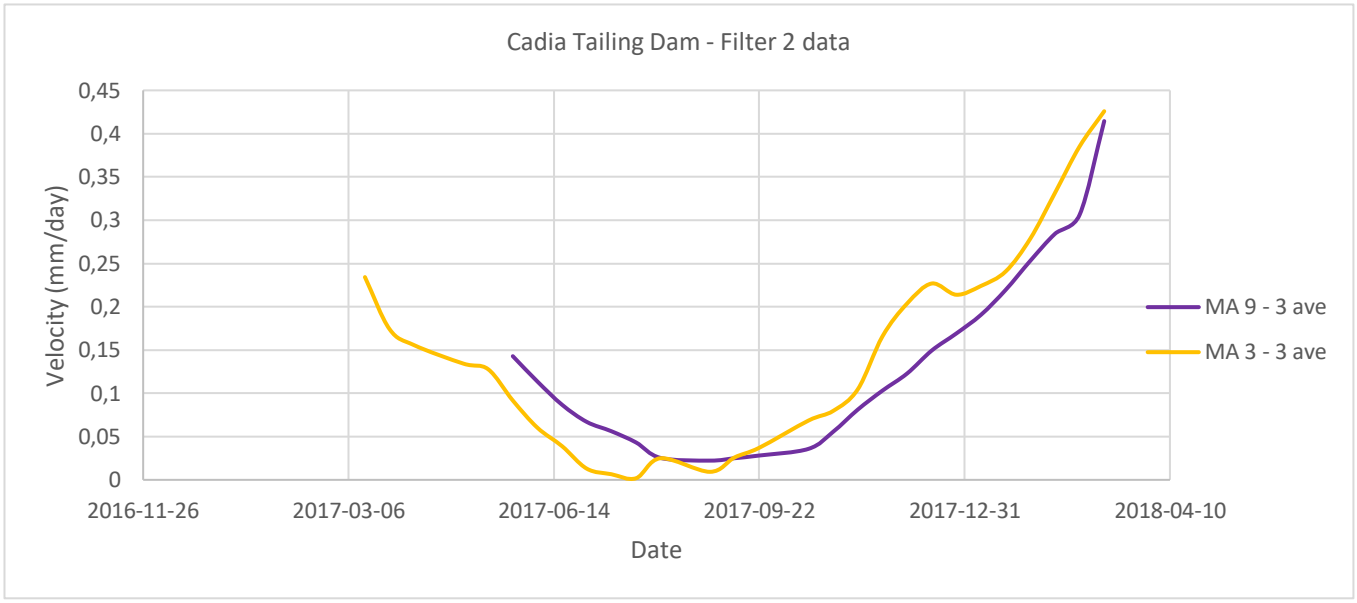
Cadia Tailing Dam - Filter 2 data
0,45
0,4
0,35
0,3
0,25
0,2
0,15
0,1
0,05
0
Velocity (mm/day)
2016-11-26
2017-03-06
2017-06-14
2017-09-22
2017-12-31
2018-04-10
Date
MA 9 - 3 ave
MA 3 - 3 ave

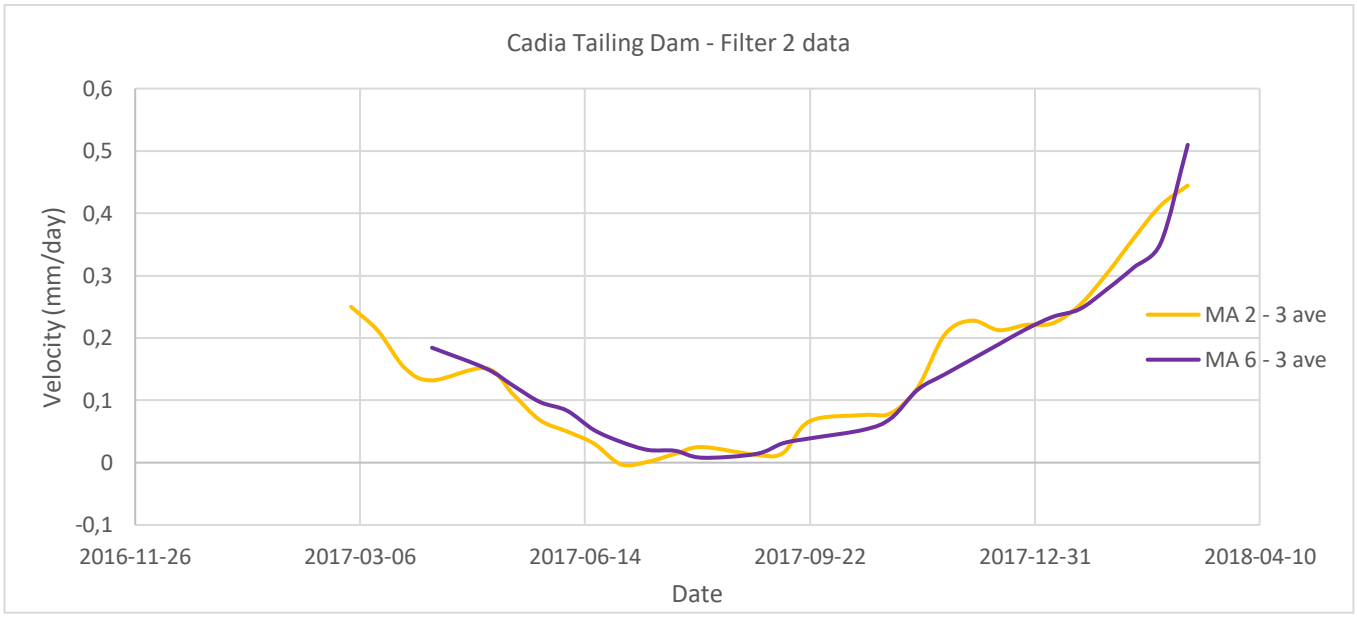
Cadia Tailing Dam - Filter 2 data
0,6
0,5
0,4
0,3
0,2
0,1
0
-0,1
Velocity (mm/day)
2016-11-26
2017-03-06
2017-06-14
2017-09-22
2017-12-31
2018-04-10
Date
MA 2 - 3 ave
MA 6 - 3 ave